



**UNIVERSITÀ DEGLI STUDI DI PARMA**

Dipartimento di Chimica

Ph.D. in Science and Technology of

Innovative Materials

XXVI Cycle

**Self-Assembly  
of Supramolecular  
Architectures  
in Solution and on Surfaces**

Kasjan Misztal



Coordinator: **Prof. Enrico Dalcanale**

Supervisor: **Prof. Enrico Dalcanale**

Author: **Kasjan Marek Misztal**





*Dedykuję Rodzicom i Innie*

*(...)*

*Success in my only (...) option*

*Failure's not!*

*You can do anything you set your mind to*

*(...)*

Eminem, Loose Yourself

# Contents

## CHAPTER 1

### A General Introduction to Supramolecular Chemistry

1.1 The “chemistry beyond the molecule” .....	1
1.2 Secondary Interactions: a “glue” to assemble supramolecular architectures.....	2
• Hydrogen Bonding .....	2
• Metal-Ligand Coordination .....	5
• Ion-Dipole Interactions .....	6
• CH- $\pi$ Interactions.....	7
• $\pi$ - $\pi$ Interactions .....	8
• Halogen Bonding.....	9
• Hydrophobic effect .....	10
• Host-Guest Complexation .....	11
1.3 Structural Subunits to build Supramolecular Frameworks .....	12
• Cavitands .....	12
Tetraphosphonate-bridged Cavitands.....	12
Tetramethylene-bridged Cavitands.....	14
• Phthalocyanines.....	14
1.4 References and Notes .....	17

## **CHAPTER 2**

### ***Design and synthesis of a cavitated pillar for MOF***

2.1 Introduction .....	23
2.2 Results and Discussion .....	24
2.3 Conclusions .....	28
2.4 Experimental Section.....	28
2.5 Acknowledgements .....	32
2.6 References and Notes.....	33

## **CHAPTER 3**

### **Hierarchical Self-Assembly**

#### **of Luminescent Eu(III) Complexes on Silicon**

3.1 Introduction .....	35
3.2 Results and Discussion .....	37
3.2.1 Design and strategy .....	37
3.2.2 Self-assembly in solution.....	38
3.2.3 Absorption and luminescence spectra in solution.....	39
3.2.4 Self-assembly on the Tiii functionalized Si surface .....	41
3.2.5 Step-by-step monitoring of the self-assembly process via XPS ...	42

3.2.6 Photophysical measurements on the surface .....	45
3.3 Conclusions .....	47
3.4 Experimental Section.....	47
3.5 Acknowledgements .....	51
3.5 References and Notes.....	51

## **CHAPTER 4**

### **Cavitand-based luminescent dopants for liquid crystals cells**

4.1 Introduction .....	55
4.2 Results and Discussion .....	58
4.3 Conclusions .....	62
4.4 Experimental Section.....	63
4.5 Acknowledgements .....	64
4.6 References and Notes .....	64

## **CHAPTER 5**

### **Phthalocyanines for Applications in Organic Photovoltaic Solar Cells**

5.1 Introduction .....	67
------------------------	----

5.1.1 General design.....	72
5.2 Results and discussion .....	72
5.3 Conclusions .....	79
5.4 Experimental Section.....	80
5.5 Acknowledgements.....	85
5.6 References and Notes .....	86

## **CHAPTER 6**

### **Towards UPY-decorated Terbium Phthalocyanine Double Deckers Single Molecule Magnets**

6.1 Introduction .....	89
6.2 Results and Discussion .....	91
6.2.1 Design of system .....	91
6.2.2 Monomer functionalization.....	93
6.2.3 TbDD post-functionalization.....	94
6.3 Conclusions .....	98
6.4 Experimental Section.....	99
6.5 Acknowledgements .....	106
6.6 References and Notes.....	106

## **CHAPTER 7**

### **Application of tetrakisphosphate cavitands in OECT sensors**

7.1 Introduction .....	109
7.2 Results and Discussion .....	112
7.2.1 Simple approach.....	112
7.2.2 Formation of covalently bound 4PO-PEDOT .....	114
7.3 Conclusions .....	118
7.4 Experimental Section.....	119
7.5 Acknowledgements.....	121
7.6 References and Notes .....	121

## **APPENDIX A**

<b>Additional Information for Ch.3 .....</b>	<b>125</b>
<b>Curriculum Vitae .....</b>	<b>133</b>
<b>Acknowledgements .....</b>	<b>135</b>







# ***Chapter 1***

## ***A General Introduction to Supramolecular Chemistry***

### **1.1 The “chemistry beyond the molecule”.**

According to Noble Prize winner in Chemistry, Jean-Marie Lehn, which was awarded together with Donald J. Cram and Charles J. Pedersen in 1987, supramolecular chemistry is the “*chemistry beyond the molecule*”,<sup>1</sup> and it aims at developing highly complex chemical systems starting from molecular components held together by noncovalent forces.<sup>2</sup>

Based on self-assembly<sup>3</sup> and self-organization processes,<sup>4</sup> supramolecular chemistry is intrinsically dynamic, which allows the spontaneous but information-directed generation of organized structures under equilibrium conditions. Suitable manipulation of structural subunits and interaction codes gives rise to a wide and new variety of systems. Thanks to a constant and continuous development, supramolecular chemistry widens the playground for scientists. Simple systems are replaced by ever more complex ones. Building-blocks become more elaborated, with respect to both structure and function. Dynamic chemical bonding ranges from the weak van der Waals forces to the thermodynamically reversible covalent interactions, called dynamic combinatorial chemistry. The attention, previously focused exclusively on the solid and solution states, is now pointing through surfaces and interfaces, tackling more complex systems, featuring multivalency, cooperativity and orthogonality.

With its challenges, ever more function-oriented and application driven, supramolecular science constitutes a multidisciplinary and interdisciplinary domain that provides a highly fertile ground for the creativity of scientists from all origins.

The present thesis takes its place in this context, and it shows, by harnessing noncovalent interactions within different building-blocks, how it is possible to generate functional materials and to realize hierarchical self-assembly on surfaces.

## 1.2 Secondary Interactions: a “glue” to assemble supramolecular architectures.

G. R. Desiraju wrote “*in supramolecular chemistry, one makes higher level aggregates (supermolecules) from lower level entities (molecules) using weak intermolecular interactions as a glue*”.<sup>5</sup>

The term *supramolecular* refers in fact to ordered molecular aggregates, held together by noncovalent interactions, such as metal-ligand bonds, hydrogen bonds, or van der Waals' forces. Because of the weakness of such binding interactions, the formation of supramolecular assemblies is often thermodynamically dictated, and it commonly results from spontaneous self-assembly processes, rather than from sequential bond-forming strategies. In particular, if self-assembly could be simply defined as the reversible collection and aggregation of components into a confined entity, self-organization is the real driving force that leads to complex supramolecular systems. After a first step, involving the complementary molecular recognition among the structural subunits, thanks to selective binding motifs, the growth of a supramolecular structure progresses through sequential and eventually hierarchical interaction of multiple components, according to cooperative or linear behavior.

Therefore the choice of the interactional motifs is crucial in supramolecular chemistry, because it determines their specific physical and chemical properties, like the robustness of the final products, plasticity and structure.

Next paragraphs will present most common weak interactions in supramolecular chemistry.

- **Hydrogen-Bonding.**

Hydrogen bonding is a type of attractive intermolecular force that exists between two partial electric charges of opposite polarity. As the name “hydrogen bond” implies, one part of the bond involves a hydrogen atom, which is attached to a relatively electronegative heteroatom, such as oxygen, nitrogen or fluorine, and it is called the *hydrogen-bond donor (D-H)*. The electronegative

element attracts the electron cloud from around the hydrogen nucleus and, by decentralizing the cloud, leaves the atom with a positive partial charge. The hydrogen bond results when this positive charge density attracts a lone pair of electrons on another heteroatom, which becomes the *hydrogen-bond acceptor* (A). Depending on the reciprocal location of H-donors and H-acceptors, H-bonding can be intramolecular or intermolecular, respectively if donor and acceptor are located on the same molecule or on different ones.

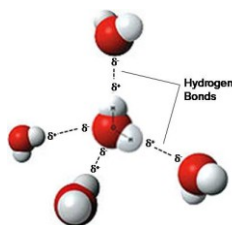


Figure 1: 3D model of hydrogen-bonds in water.

Hydrogen bonding is generally considered with a geometry D-H...A. Some of the functions commonly used to evaluate its strength involve a modified Lennard-Jones potential, with a D-H...A angle dependent term like:

$$E_{H-Bond}(R) = \epsilon A \frac{R_0}{R}^{12} - B \frac{R_0}{R}^{10} \cos\theta_{D-H...A}^4$$

where R is the distance between the D and A,  $R_0$  is the equilibrium distance,  $\epsilon$  is the depth of the potential and A and B are adjustable parameters.<sup>6</sup> From the above reported equation it appears that, for single donor acceptor systems, such as D-H...A, the strongest hydrogen bonds are collinear.<sup>7</sup> Electrostatic calculations suggest that deviation of 20° from linearity leads to a decrease in binding energy of approximately 10%.<sup>8</sup> In double acceptor systems, bifurcated hydrogen bonds with nonlinear angles are preferred. For example, in protein structures, the 90% of N-H...O bonds lie between 140° and 180°, and they are centered around 158°. For C=O...H, the range is more broadly distributed between 90° and 160° and centered around 129°.<sup>9</sup>

Although stronger than most other intermolecular forces, the hydrogen bond is much weaker than both the ionic bond and the covalent bond. Namely it can vary in strength from very weak (1-2 kJ mol<sup>-1</sup>) to extremely strong (higher than 155 kJ mol<sup>-1</sup>), as in the ion [HF<sub>2</sub>]<sup>-</sup>.<sup>10</sup> Typical values include:

F-H...F (155 kJ/mol)

O-H...N (29 kJ/mol)

O-H...O (21 kJ/mol)

N-H...N (13 kJ/mol)

N-H...O (8 kJ/mol)

In contrast to covalent bonds, hydrogen bonds are reversible and their strength depends on the chemical environment. Therefore, a suitable tuning of the external parameters allows the direct control of the physical properties of supramolecular assemblies based on this kind of interaction. For example, the well known solvent dependence of H-bonded complex stability in solution, can be exploited to obtain robust systems in apolar, aprotic solvents, or to reduce the association, by moving to polar solvents, which can act as competitive H-bond acceptor or donor. Improvement in the stability can be obtained by a combination of multiple hydrogen bonds. The stability of final complexes can be finely tuned by the proper choice of primary H-bonds, but also of secondary electrostatic interactions, which can be repulsive or attractive.<sup>11</sup> These effects have been quantified by Sartorius and Schneider<sup>12</sup> for the prediction of multiple H-bonded complex stability in chloroform (Figure 2).

The length of hydrogen bonds depends on the interaction strength, as well as on temperature and pressure. It can range from 1.2 Å, when the interaction features a strong covalent character, to values higher than 2.2 Å, when the binding features a more dispersive nature.<sup>10</sup> As a consequence of their specificity, directionality, and versatility<sup>13</sup> hydrogen bonds have been widely exploited in supramolecular chemistry, giving rise to dynamic and tunable materials, such as polymers, dendrimers and molecular containers.

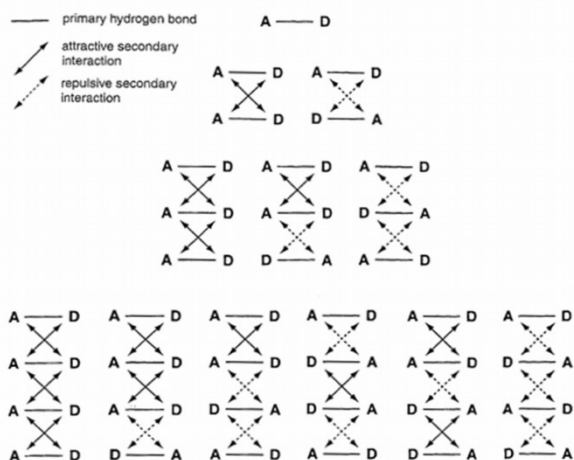


**Figure 2:** Schematic representation of complexes containing one to four H-bond together with the secondary attractive or repulsive electrostatic interactions.<sup>11</sup>

- **Metal-Ligand Coordination.**

Coordinative metal-bonds feature a great versatility, thanks to the large number of structural motifs and bond energies that are available through coordination chemistry. Moreover, the high directionality displayed by coordinative bonds is particularly appealing for supramolecular chemists, allowing the rational design of the structural subunits to bind together, as well as the structural control of the entities formed by self-assembly.

The energy bond related to metal-ligand interactions ranges from the strong value of covalent binding, in carbon-based molecules, to the weak one, characterizing biological systems.

When the energy required to induce a geometrical distortion around the metal center is relatively low, dynamic coordination complexes can be obtained, able to give ligand exchange or pseudorotation around the bond axes, resulting in the tuning of the final shape of the self-assembled entities. Also, the availability of a wide variety of metals, having different coordination numbers and geometries, as well as the chance to act on the orientation of the ligand binding sites, provide powerful means to model the structure of supramolecular architectures.

The most common potential building-blocks embrace nitrogen-containing molecules, cyano-substituted ligands and phosphorous-containing ligands.

The most used metals are zinc and palladium, which form labile reversible complexes, or ruthenium, rhenium and platinum, whose adducts are very stable or become reversible only by addition of competitive adducts.

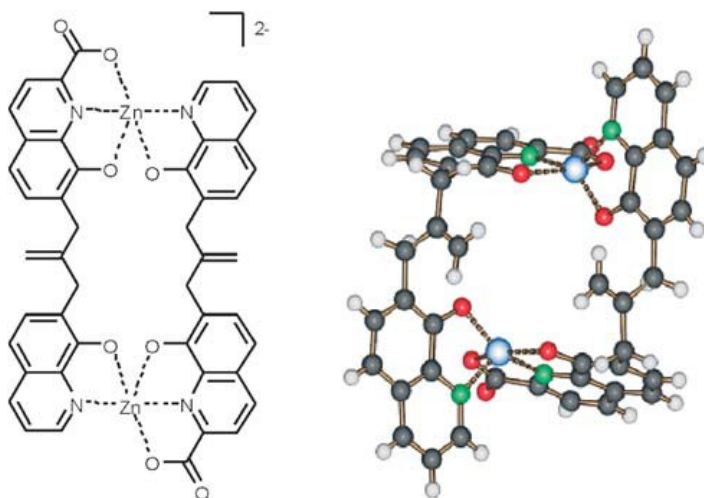


**Figure 3:** An example of binuclear pentacoordinate zinc complex with two bis-8-hydroxyquinoline ligands. [M. Albrecht, O. Osetska, R. Fröhlich, Synlett, 2006, 924.]

Metal-ligand motifs have been frequently used to extend covalent oligomers or polymers, and to improve their initial structural and mechanical properties. Also the cross-link of polymers bearing multiple metal-coordination sites is quite common in supramolecular chemistry, as well as the induction of such redox or thermo-reversibility by exploiting metals properties.

- ***Ion–Dipole Interactions.***

Numerous supramolecular complexes are based on electrostatic forces between a permanent charge and neutral species featuring a dipole. Ion-dipole interactions occur with a strength ranging between 50 and 200  $\text{kJmol}^{-1}$ , and they became stronger with increase of charge or dipole moments. The interaction energy depends also upon the distance from the center of the ion to the midpoint of the dipole. Therefore temperature changes can be used to enhance or to decrease the binding strength.

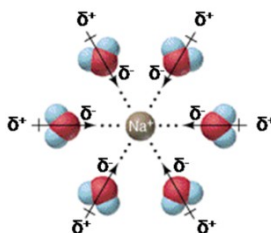


**Figure 4:** Ion-dipole interaction between  $\text{Na}^+$  and  $\text{H}_2\text{O}$  molecules.

Host-guest chemistry displays a huge number of complexes based on ion-dipole interactions. For example, the binding of protonated amines in cucurbituril macrocycle<sup>14</sup> is largely attributable to ion-dipole forces, as well as the inclusion of alkali-metal and alkaline-earth cations by crown ethers<sup>15</sup> and related compounds.

- **CH- $\pi$  Interactions.**

Even if weaker than the ordinary hydrogen-bonds, the CH- $\pi$  interactions ( $2 \sim 8 \text{ kJ mol}^{-1}$ ), were shown to play a substantial role in a variety of chemical and biological phenomena. They can be described as the interactions occurring between soft acids (CHs in an alkyl group) and soft bases ( $\pi$ -systems). Suggestion for the presence of attractive interactions between C-H groups and  $\pi$ -electron systems came from studies on conformational problems of a series of compounds bearing an aliphatic group on one side of the molecule and a phenyl group at the other end.<sup>16</sup> Stabilization of this bond comes essentially from the dispersion forces and charge-transfer interactions, while contribution from the electrostatic energy is relatively unimportant. Orientation dependent and additive in enthalpy, CH- $\pi$  bonds can act in a cooperative fashion when multiple CH groups participate simultaneously in interactions with  $\pi$ -groups.

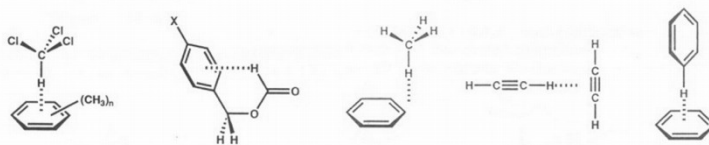


**Figure 5:** Examples of CH- $\pi$  interactions.

A relevant feature of this kind of interaction is its effectiveness in water and in nonpolar media, with significant consequences on molecular recognition in biological environments. CH- $\pi$  interacting species were found to become

more favored as the  $\pi$ -electron density of the involved aromatic system increases, and, of course like in the case of H-bonding, if the hydrogen atoms of the partner molecule become more acidic. CH- $\pi$  interaction plays a crucial role in determining the selectivity of organic reactions, the properties of solid materials, such as graphite and fullerene, as well as the specificity of substrate and biologically important macromolecules.

- **$\pi$ - $\pi$  Interactions.**

Weak electrostatic  $\pi$ - $\pi$  interactions occur between aromatic moieties, because of the intermolecular overlapping of p-orbital in  $\pi$ -conjugated systems,<sup>17</sup> thus more  $\pi$ -electrons are involved in the interaction, the stronger is the bonding. The stabilizing energy of  $\pi$ - $\pi$  interactions also includes induced dipole and dispersion contributions. Aromatic interactions are intriguing in molecular recognition processes, since they are expected to be strong in water (due to the hydrophobic component of the interaction), and at the same time, selective, if the electrostatic component is significant. Consequently they provide the best features of both hydrophobic effects and hydrogen bonding.

Two general types of aromatic  $\pi$ - $\pi$  interactions are face-to-face and edge-to-face. The latter is actually a C-H $\cdots\pi$  interaction (the C-H bond generally having a small dipole moment). The attraction in these two orientations comes from the interaction between positively charged hydrogen atoms and negatively charged  $\pi$ -face of aromatic system. The perfect facial alignment of face-to-face orientation is unlikely because of the electrostatic repulsion between the two negatively charged  $\pi$ -systems of the aromatic rings. The distance between the aromatic  $\pi$ - $\pi$  faces is about 3.3–3.8 Å.



**Figure 6:** The limiting types of aromatic  $\pi$ - $\pi$  interactions: face-to-face and edge-to-face orientations.

$\pi$ - $\pi$  interactions are one of the principal noncovalent forces governing supramolecular organization and recognition processes. They are key interactions influencing the tertiary structure of proteins<sup>18</sup> and the vertical base stacking in DNA.<sup>19</sup> Moreover they also play a major role in stabilizing host-guest complexes<sup>20</sup> and in self-assembly based on synthetic molecules.<sup>21</sup>



- **Halogen Bonding.**

Halogen bonding is the noncovalent interaction occurring between the region of positive electrostatic potential of a covalently bonded halogen atom and an electron-rich atom (or group of atoms) that acts as a Lewis base. In nature halogens are electron withdrawing resulting in a partial negative charge being accumulated on their surface in halocarbons. However, it was demonstrated that, in C–X moieties, the partial negative charge is not evenly distributed around the halogen atom; rather, it forms an equatorial belt around it, coaxial with the C–X bond, that leaves a region of positive electrostatic potential localized at the tip of the C–X bond extension, called “ $\sigma$ -hole”.<sup>22</sup>

It is a relatively new class of interactions in Supramolecular Chemistry, and its definition has been announced only recently in *Pure and Applied Chemistry* by Desiraju *et al.*: “A halogen bond occurs when there is evidence of a net attractive interaction between an electrophilic region associated with a halogen atom in a molecular entity and a nucleophilic region in another, or the same, molecular entity.”<sup>23</sup> A typical halogen bond is denoted by the three dots in R–X•••Y. R–X is the halogen bond donor, X is any halogen atom with an electrophilic (electron-poor) region, and R is a group covalently bound to X. Y is the halogen bond acceptor and is typically a molecule possessing at least one nucleophilic (electron rich) region. Among most common R–X are: dihalogen molecule (e.g., I<sub>2</sub>, Br<sub>2</sub>, ICl, ClF), haloalkanes (e.g., CBr<sub>4</sub>, CHI<sub>3</sub>), haloarenes or haloheteroarenes (e.g., iodobenzene, halopyridinium), halonium ions (e.g., diphenyliodonium) and haloimides (e.g., *N*-bromo- or *N*-iodosuccinimide). Meanwhile most common XB acceptors are lone pair possessing atoms (e.g., N atom of a pyridine or an amine, O atom of a carbonyl group),  $\pi$  systems (e.g., double or triple bonds, arene moiety), anions (e.g., halide anion, oxyanion).

In a typical halogen bond (XB) distance between X and Y is smaller than sum of their van der Waals radii, while R–X is bigger than in pristine complex. Halogen bond is much more directional than H-bonding, and the angle between R–X•••Y is close to 180°, what also implies that Y is approaching X along the extension of R–X axis. The halogen bond strength decreases as the electronegativity of X increases, and the electron withdrawing ability of R decreases. The primary forces involved in the formation of bond are electrostatic, but effect of polarization, charge transfer and dispersion cannot be neglected. Presence of XBs usually can be observed in UV-Vis, Raman, XPS and NMR experiments, as in all this measurements signals of atoms are shifted.<sup>23</sup>

Recently halogen bonding become of great interest<sup>24-27</sup> in chemistry and number of articles reporting “halogen bonding” among keywords is growing,

with maximum of 103 papers reported in 2012 (SCOPUS database). The majority of papers reported in the literature cover 3 topics: crystal engineering,<sup>24</sup> material science<sup>25,26</sup> and biological applications.<sup>27</sup> Strong bonding and well defined angle between XB donor and acceptor is used for building well organized 1D, 2D and 3D architectures in solid state. Recently, the group of Resnati and Metrangolo, reported an example of 3D organic framework self-assembled by orthogonal interactions, HB and XB, exhibiting open 2D channels.<sup>28</sup> Framework, supported only by HBs and XBs, can withstand single-crystal-to-single-crystal guest exchanges from liquid and gas phases without collapsing. In material science, XBs are exploited for enhancing liquid crystal states properties and its self-assembly ability, in the synthesis of MOFs as linkers and specific binding sites for guests<sup>29</sup> and as binding motif for anions in anion recognition systems. Important are also biological applications, where often presence of XBs is responsible for specific binding of pharmaceuticals in enzymes binding sites.<sup>27</sup>

- **Hydrophobic effects.**

Hydrophobic effects are sum of multiple interactions between non-polar molecules and water, resulting in immiscibility between them, e.g. mineral oil and water.<sup>30</sup> The water molecules are attracted strongly to one another resulting in a natural agglomeration of other species (such as non-polar organic molecules) as they are squeezed out of the way of the strong inter-solvent interactions. In addition, between organic molecules are usually present van der Waals and  $\pi$ - $\pi$  stacking attractions.

The hydrophobic effect is very important in biological systems in the creation and maintenance of protein and polynucleotide structure and in the maintenance of phospholipid bilayer cell walls. Hydrophobic effects are of crucial importance in the binding of organic guests, see Gibb's capsules,<sup>31</sup> in water and may be divided into two energetic components: enthalpic and entropic. The enthalpic hydrophobic effect involves the stabilisation of water molecules that are driven from a host cavity upon guest binding. Because host cavities are often hydrophobic, intracavity water does not interact strongly with the host walls and is therefore of high energy. Upon release into the bulk solvent, it is stabilised by interactions with other water molecules. The entropic hydrophobic effect arises from the fact that the presence of two (often organic) molecules in solution (host and guest) creates two 'holes' in the structure of bulk water. Combining host and guest to form a complex results in less disruption to the solvent structure and hence an entropic gain (resulting in a lowering of overall free energy). The process is represented schematically in Figure 7.

Moreover moving water molecules from a hydrophobic environment to the bulk leads to a great energy gain.

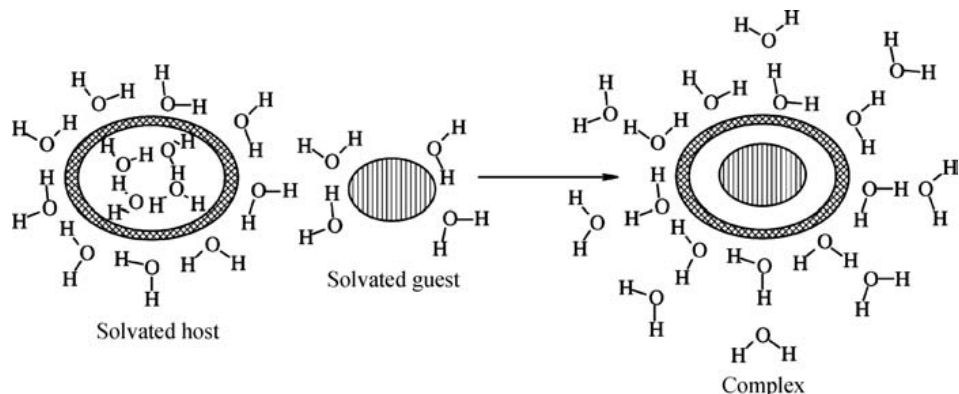


Figure 7. Hydrophobic binding of organic guests in aqueous solution. From ref. 32.

- **Host-Guest Complexation.**

Host-guest complexation involves receptor molecules containing hollow and enforced spaces, and smaller species that can be located inside them. In a kind of designer-chemistry, different functional groups are incorporated into the host molecules, so that their orientation facilitates strong binding to corresponding fragments in the guest.

A variety of forces, such as electrostatic interaction, hydrophobic effects, halogen and hydrogen bonding, are utilized to achieve higher affinity and selectivity in the binding processes.

Equally important are both, the structure of the interacting units and the thermodynamics that control the inclusion phenomena. Namely, host and guest are devised in order to maximize favorable enthalpic and, when possible, entropic contributions during the complexation processes.

Based on structurally well-defined pattern of intermolecular interactions, host-guest chemistry leads to a huge variety of supramolecular architectures, embracing polymers and sensors, molecular machines and functional surfaces.

### 1.3 Structural Subunits for Supramolecular Frameworks.

The following paragraph will describe briefly the structural properties and the most important association features of the macromolecules exploited in this thesis as building-blocks.

- **Cavitands.**

Cram defined cavitands<sup>33</sup> as “*synthetic organic compounds with enforced cavities large enough to complex complementary organic molecules or ions.*” They are versatile molecular receptors and these compounds are extremely interesting in host-guest chemistry and have been extensively studied in the solid state,<sup>34</sup> in solution<sup>35</sup> and in the gas phase.<sup>36</sup>

Suitable scaffolds for the construction of cavitands are resorcin[4]arenes, synthesized in straightforward condensation reaction from resorcinols and aldehydes in acidic or basic conditions.<sup>37</sup>

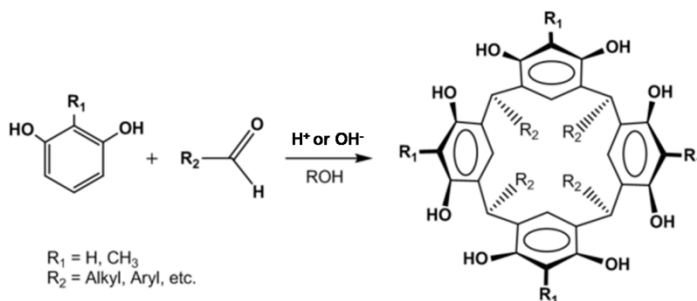


**Figure 7:** Synthesis of resorcin[4]arenes.

A further functionalization of the resulting macrocycles can be achieved by means of bridging reactions on the four couples of adjacent phenolic oxygens. The choice of the bridging groups is pivotal to determine shape, dimensions and complexation properties of the final cavitand.

### ***Tetraphosphonate-bridged Cavitands.***

Bridging of resorcinarene with four P(V) moieties results in formation of tetraphosphonate cavitands.<sup>38</sup> The introduction of phosphonate groups introduce special complexing properties toward positively charged species, such as alkali-metal and alkaline-earth cations,<sup>39</sup> or ammonium and N-methylpyridinium salts.<sup>40</sup> The presence of four stereogenic centers in the tetraphosphonate cavitands gives rise to six possible diastereomeric isomers,

differing from each other for the orientation of the P=O moieties, either inward (i) or outward (o) the cavity.<sup>41</sup>

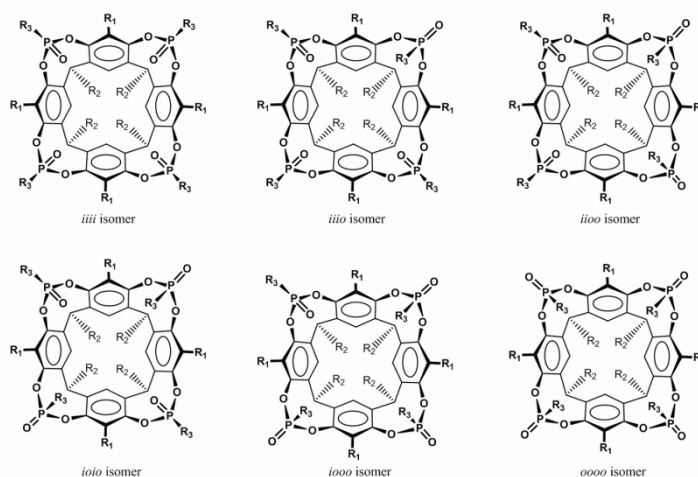


**Figure 8:** Tetraphosphonate cavitand isomers.

Stereochemistry is pivotal to determine the cavitand complexing capability. The higher binding has been observed for the isomer featuring four P=O groups converging toward the center of the cavity.

The main specific interactions responsible for recognition processes are H-bonding, CH- $\pi$ , and cation-dipole forces.<sup>42</sup> A multiple ion-dipole interaction occurs between the inward facing P=O groups and the positively charged guest moieties; directional H-bonding involve two adjacent P=O groups in presence of H-donor species; CH- $\pi$  interaction acts between guest acidic protons (e.g. CH<sub>3</sub> group in N-methylpyridinium salts) and the  $\pi$ -basic cavity. All these forces operate in a synergistic fashion, assuring high association constant<sup>40</sup> for the complex formation (in order of  $10^5 \text{ M}^{-1}$  for methyl ammonium species).

When the P=O moieties are replaced by the P=S ones, by oxidation with sulfur on P(III) precursor,<sup>40b</sup> the structurally related tetrathiophosphonate cavitands are obtained. These compounds feature ionophoric properties toward soft metals,<sup>43</sup> such as Ag<sup>+</sup>, Hg<sup>2+</sup>, Tl<sup>+</sup>, but result inefficient in pyridinium or ammonium binding, because of the weaker H-bonding and ion-dipole interactions that they can form with these guests.<sup>40b</sup>

In this thesis, host-guest properties of tetraphosphonate cavitands have been exploited to form supramolecular hierarchical self-assembly protocols on the surface (Chapter 3), synthesise dyes for Guest-Host Liquid Crystal Dyes

cells (Chapter 4) and for sensing in Organic Electrochemical Transistors (Chapter 7).

### *Tetramethylene-bridged Cavitands.*

Conformationally mobile resorcinar[4]arenes can be converted to bowl-shaped cavitands by fourfold ring closures, which introduce methylene bridges anchored by the four sets of proximate oxygens.<sup>34</sup>

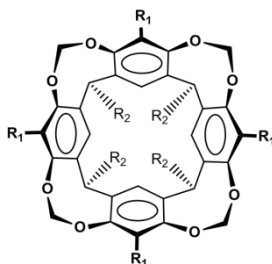


**Figure 11:** Tetramethylene-bridged cavitands.

Cavitand depth and shape vary with the character of the  $R_1$  substituents (H,  $\text{CH}_3$ , Br, I, etc.). These compounds possess enforced concave surfaces of molecular dimensions and form solvates with simple guest molecules, most of which are complementary to their cavities, such as  $\text{CH}_2\text{Cl}_2$ ,  $\text{CHCl}_3$ ,  $\text{CH}_3\text{CN}$ ,  $\text{C}_6\text{H}_5\text{CH}_3$ , and  $\text{C}_6\text{H}_6$ .<sup>44</sup> Methylene-bridged cavitands stand at the lower end of complexation ability, as they bind the guest only through  $\text{CH}_3$ - $\pi$  interaction. Recently, Schalley et al. demonstrated that these cavitands are able to complex anionic species in gas phase,<sup>45</sup> however, in solution, where the solvent effect are important, no evidences have ever been shown of such affinity neither for anions nor for cations.

In this thesis we exploited methylene-bridged cavitand as preorganized rigid scaffold for building secondary building units (SBUs) in metal organic framework (MOFs), which mimic tetraphosphonate cavitands geometry (Chapter 2).

- **Phthalocyanines**

Phthalocyanines (Pcs) <sup>46</sup> were serendipitously discovered in 1928, and since then, these synthetic analogues of the naturally occurring porphyrins have been the subject of extensive research in many different fields.<sup>47</sup> Pcs are planar, symmetrical aromatic macrocycles composed of four isoindole units having 18  $\pi$ -electrons delocalized over alternating macrocycle consisting of carbon and nitrogen atoms. As a consequence they have very strong absorption in visible region and are thermally and chemically stable. They are also very versatile – the central cavity has sufficient size to accommodate over 70 metal ions (e.g.  $\text{Cu}^{2+}$ ,  $\text{Fe}^{2+}$ ,  $\text{Ni}^{2+}$ ,  $\text{Co}^{2+}$ ,  $\text{Zn}^{2+}$ ,  $\text{Mn}^{2+}$ ,  $\text{Al}^{3+}$ ,  $\text{Fe}^{3+}$ ,  $\text{Si}^{4+}$ ,  $\text{Ti}^{4+}$ ), and a variety of substituents can be incorporated (Fig.12) at peripheries ( $\text{R}_1$ - $\text{R}_{16}$ ) and at the axial position ( $\text{R}_{17}$ - $\text{R}_{18}$ ).

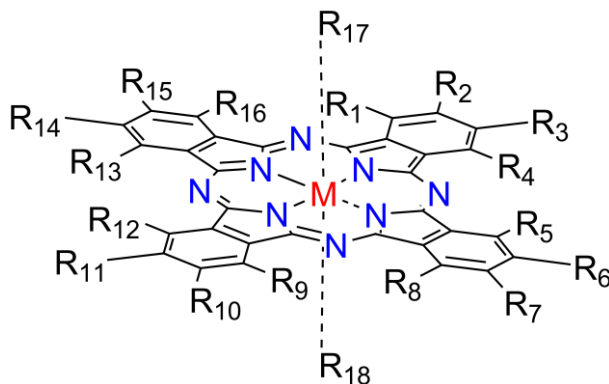
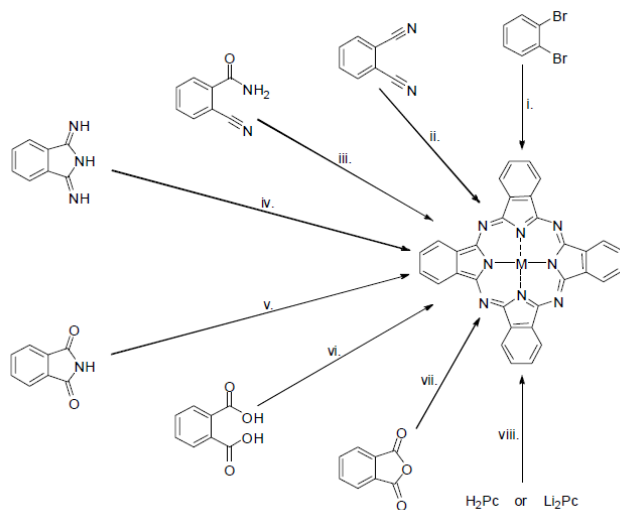


Figure 12. Scheme of phthalocyanine with possible substitution positions.

The most common synthetic pathway towards phthalocyanines used on laboratory scale start from phthalonitrile (*orto*-dicyanobenzene) and its derivatives. On Scheme 13 are presented also other routes towards MPc. Synthesis of metal free Pcs is usually accomplished by use of phthalonitrile in high-boiling alcohol in presence of metallic lithium, followed by protonation with acetic acid.



Scheme 1. Synthetic routes to MPc. Reagent and conditions: i.) Large excess of CuCN in refluxing DMF;<sup>48</sup> ii.) Refluxing DMF with metal salt;<sup>49</sup> iii.) Highboiling-point solvent (e.g. quinoline) with metal salt at 205 °C;<sup>50</sup> iv.) In 2-ethoxyethanol with metal salt at 50 °C;<sup>51</sup> v.) Solvent free, in fused urea with metal salt at 160 °C;<sup>52</sup> vi.) High-boiling-solvent (e.g. nitrobenzene) with urea, metal salt NH<sub>4</sub>Cl and ammonium molybdate at 180 °C;<sup>53</sup> vii.) In nitrobenzene with urea, metal salt and ammonium molybdate at 190 °C;<sup>54</sup> or in HMDS and DMF with metal salt and *p*-TsOH at 130 °C;<sup>55</sup> viii.) In refluxed quinoline with metal salt.<sup>56</sup>

Due to their remarkable absorption properties, since their discovery they found applications in dye industry and are still present there. Later on, their unique properties allow them to be studied for applications in optics (UV-vis, fluorescence,<sup>57</sup> nonlinear optics – NLO<sup>58</sup>), electronic conductivity (sensors,<sup>59</sup> charge-transfer complexes<sup>60</sup>), optoelectronics (photoconductivity,<sup>61</sup> light harvesting/photovoltaic,<sup>62</sup> OLEDs<sup>63</sup>), catalysis,<sup>64</sup> adsorption,<sup>65</sup> magnetics,<sup>66</sup> and recently also in the medicine.<sup>67</sup>

In this thesis, good optical absorption and electronic properties have been exploited in the synthesis of donor-acceptor systems for organic photovoltaic solar cells and strong complexing properties towards lanthanides and unique magnetic properties of such complexes have been utilized for the synthesis of building blocks, which can be deposited on the silicon surface and operate as single molecule magnets.



## 1.4 References and Notes.

1. J.-M. Lehn, *Angew. Chem. Int. Ed.* **1988**, 27, 89-112.
2. J.-M. Lehn, *Proc. Natl. Acad. Sci. U.S.A.* **2002**, 99, 4763-4768.
3. G. M. Whitesides, B. Grzybowski, *Science* **2002**, 295, 2418-2421.
4. J.-M. Lehn, *Science* **2002**, 295, 2400-2403.
5. G. R. Desiraju, *Curr. Sci.* **2005**, 88, 374-380.
6. F. Jensen, in *Introduction to Computational Chemistry*, Wiley, Chichester, **1999**.
7. T. Steiner, *Angew. Chem. Int. Ed.* **2002**, 41, 48-76.
8. M. Akke, S. Forsen, *Proteins: Struct. Funct. Genet.* **1990**, 8, 23-29.
9. E. Baker, R. Hubbard, *Prog. Biophys. Mol. Biol.* **1984**, 44, 97-179.
10. G.A. Jeffrey, in *An Introduction to Hydrogen Bonding*, Oxford University Press, Oxford, **1997**.
11. a) W. L. Jorgensen, J. Pranata, *J. Am. Chem. Soc.* **1990**, 112, 2008-2010; b) J. Pranata, S. G. Wierschke, W. L. Jorgensen, *J. Am. Chem. Soc.* **1991**, 113, 2810-2819.
12. J. Sartorius, H.-J. Schneider, *Chem. Eur. J.* **1996**, 2, 1446-1452.
13. L. J. Prins, D. N. Reinhoudt, P. Timmerman, *Angew. Chem. Int. Ed.* **2001**, 40, 2382-2426.
14. a) J. Lagona, P. Mukhopadhyay, S. Chakrabarti, L. Isaacs, *Angew. Chem. Int. Ed.* **2005**, 44, 4844-4870; b) J. W. Lee, S. Samal, N. Selvapalam, H. J. Kim, K. Kim, *Acc. Chem. Res.* **2003**, 36, 621-630.
15. K. A. Nielsen, W. S. Cho, J. O. Jeppesen, V. M. Lynch, J. Becher, J. L. Sessler, *J. Am. Chem. Soc.* **2004**, 126, 16296-16297.

16. M. Nishio, M. Hirota, Y. Umezawa, *The CH- $\pi$  Interactions*, Wiley-VCH, New York, 1998; M. Nishio, Y. Umezawa, M. Hirota, Y. Takeuchi, *Tetrahedron* **1995**, *51*, 8665-8700.
17. C. A. Hunter, K. R. Lawson, J. Perkins, C. J. Urch, *J. Chem. Soc., Perkin Trans. 2* **2001**, 651-669.
18. S. K. Burley, G. A. Petsko, *Science* **1985**, *229*, 23-28.
19. W. Seanger, *Principles of Nucleic Acid Structure*, Springer-Verlag, New York, **1984**.
20. a) C. A. Hunter, *Chem. Soc. Rev.* **1994**, *23*, 101-109; b) E. A. Meyer, R. K. Castellano, F. Diederich, *Angew. Chem. Int. Ed.* **2003**, *42*, 1211-1250.
21. C. G. Claessens, J. F. Stoddart, *J. Phys. Org. Chem.* **1997**, *10*, 254-272.
22. E. Parisini, P. Metrangolo, T. Pilati, G. Resnati, G. Terraneo, *Chem. Soc. Rev.* **2011**, *40*, 2267-2278.
23. G. R. Desiraju, P. S. Ho, L. Kloo, A. C. Legon, R. Marquardt, P. Metrangolo, P. Politzer, G. Resnati, K. Rissanen, *Pure Appl. Chem.* **2013**, *85*, 1711-1713.
24. R. Bertani, P. Sgarbossa, A. Venzo, F. Leij, M. Amati, G. Resnati, T. Pilati, P. Metrangolo, G. Terraneo, *Coord. Chem. Rev.*, **2010**, *254*, 677-695.
25. P. Metrangolo, F. Meyer, T. Pilati, G. Resnati, G. Terraneo, *Angew. Chem. Int. Ed.* **2008**, *47*, 6114 - 6127.
26. G. Cavallo, P. Metrangolo, T. Pilati, G. Resnati, M. Sansotera, G. Terraneo, *Chem. Soc. Rev.* **2010**, *39*, 3772-3783.
27. E. Parisini, P. Metrangolo, T. Pilati, G. Resnati, G. Terraneo, *Chem. Soc. Rev.* **2011**, *40*, 2267-2278.
28. J. Martí-Rujas, L. Colombo, J. Lu, A. Dey, G. Terraneo, P. Metrangolo, T. Pilati, G. Resnati, *Chem. Commun.* **2012**, *48*, 8207-8209.
29. F. Pigge, V. Vangala, P. Kapadia, D. Swenson, N. Rath, *Chem. Commun.* **2008**, *38*, 4726-2728.
30. N. T. Southall, K. A. Dill, A. D. J. Haymet, *J. Phys. Chem. B* **2002**, *106*, 521-533.

31. C. L. D. Gibb, B. C. Gibb, *J. Am. Chem. Soc.* **2004**, *126*, 11408–11409.
32. J. W. Steed, J. L. Atwood in *Supramolecular Chemistry: Second Edition*, Wiley, Chichester, **2009**.
33. D. J. Cram, J. M. Cram, in *Container Molecules and Their Guests* (Ed.: J. F. Stoddart), **1994**, The Royal Society of Chemistry, Cambridge, Chap. 5.
34. D. J. Cram, S. Karbach, H.-E. Kim, C. B. Knobler, E. F. Maverick, J. L. Ericson, R. C. Helgeson, *J. Am. Chem. Soc.* **1988**, *110*, 2229–2237.
35. a) J. A. Tucker, C. B. Knobler, K. N. Trueblood, D. J. Cram, *J. Am. Chem. Soc.* **1989**, *111*, 3688–3699 ; b) P. Soncini, S. Bonsignore, E. Dalcanale, F. Ugozzoli, *J. Org. Chem.* **1992**, *57*, 4608–4612; c) T. Haino, D. M. Rudkevich, A. Shivanyuk, K. Rissanen, J. Rebek, Jr., *Chem. Eur. J.* **2000**, *6*, 3797–3805; (d) K. Paek, J. Cho, *Tetrahedron Lett.* **2001**, *42*, 1927–1929.
36. a) M. Vincenti, E. Dalcanale, P. Soncini, G. Guglielmetti, *J. Am. Chem. Soc.* **1990**, *112*, 445–447; b) M. Vincenti, E. Pelizzetti, E. Dalcanale, P. Soncini, *Pure Appl. Chem.* **1993**, *65*, 1507–1512.
37. L. M. Tunstad, J. A. Tucker, E. Dalcanale, J. Weiser, J. A. Bryant, J. C. Sherman, R. C. Helgeson, C. B. Knobler, D. J. Cram, *J. Org. Chem.* **1989**, *54*, 1305–1312.
38. R. Pinalli, M. Suman, E. Dalcanale, *Eur. J. Org. Chem.* **2004**, *3*, 451–462.
39. a) P. Delangle, J.-C. Mulatier, B. Tinant, J.-P. Declercq, J.-P. Dutasta, *Eur. J. Org. Chem.* **2001**, 3695–3704; b) J.-P. Dutasta, *Top. Curr. Chem.* **2004**, *232*, 55–91.
40. a) E. Biavardi, G. Battistini, M. Montalti, R. M. Yebeutchou, L. Prodi, E. Dalcanale, *Chem. Commun.* **2008**, 1638–1640; b) R. M. Yebeutchou, F. Tancini, N. Demitri, S. Geremia, R. Mendichi, E. Dalcanale, *Angew. Chem., Int. Ed.* **2008**, *47*, 4504–4508; M. Dionisio, G. Oliviero, D. Menozzi, S. Federici, R. M. Yebeutchou, F. P. Schmidtchen, E. Dalcanale, P. Bergese, *J. Am. Chem. Soc.* **2012**, *134*, 2392–2398.
41. a) T. Lippmann, E. Dalcanale, G. Mann, *Tetrahedron Lett.* **1994**, *35*, 1685–1688; b) T. Lippmann, H. Wilde, E. Dalcanale, L. Mavilla, G. Mann, U. Heyer, S.

Spera, *J. Org. Chem.* **1995**, *60*, 235-242; c) P. Delangle, J.-P. Dutasta, *Tetrahedron Lett.* **1995**, *36*, 9325-9328.

42. R. M. Yebeutchou, E. Dalcanale, *J. Am. Chem. Soc.* **2009**, *131*, 2452-2453.

43. B. Bibal, J.-P. Declercq, J.-P. Dutasta, B. Tinant, A. Valade, *Tetrahedron* **2003**, *59*, 5849-5854.

44. *CRC Handbook of Chemistry and Physics* (Ed. D. R. Lide), **2005**, Taylor & Francis, Boca Raton, FL, USA.

45. S. S. Zhu, H. Staats, K. Brandhorst, J. Grunenberg, F. Gruppi, E. Dalcanale, A. Lützen, K. Rissanen, C. A. Schalley, *Angew. Chem. Int. Ed.* **2008**, *47*, 788-792.

46. G. De la Torre, M. Nicolau, T. Torres, *Supramolecular photosensitive and electroactive materials* (Ed. H. Nalwa), Academic, New York, **2001**.

47. G. De La Torre, G. Bottari, U. Hahn, T. Torres, *Struct. Bond* **2010**, *135*, 1-44.

48. G. Pawlowski, M. Hanack, *Synthesis* **1980**, 287-289.

49. S. Z. Yildiz, Y. Gök, *New. J. Chem.* **1998**, *22*, 1365-1369.

50. M. K. Lowery, A. J. Starshak, J. N. Esposito, P. C. Krueger, M. E. Kenny, *Inorg. Chem.* **1965**, *4*, 128.

51. B. Cabezón, E. Quesada, S. Esperanza, T. Torres, *Eur. J. Org. Chem.* **2000**, 2767-2775.

52. F.-D. Cong, B. Ning, X.-G. Du, C.-Y. Ma, H.-F. Yu, B. Chen, *Dyes and Pigments* **2005**, *66*, 149-154.

53. K. R. Venugopala Reddy, J. Keshavayya, *Dyes and Pigments* **2002**, *53*, 187-194.

54. J. Metz, O. Schneider, M. Hanack, *Inorg. Chem.* **1984**, *23*, 1065-1071.

55. H. Uchida, H. Yoshiyama, P. Y. Reddy, S. Nakamura, T. Toru, *Synlett* **2003**, *13*, 2083-2085.

56. R. D. Joyner, M. E. Kenney, *J. Am. Chem. Soc.* **1960**, *82*, 5790-5791.
57. J.-D. Huang, S. Wang, P.-C. Lo, W.-P. Fong, W.-H. Kod, D. K. P. Ng, *New. J. Chem.* **2004**, *28*, 348-354.
58. G. De la Torre, P. Vázquez, F. Agulló-López, T. Torres, *J. Mater. Chem.* **1998**, *8*, 1671-1683.
59. A. Cole, R. J. McIlroy, S. C. Thorpe, M. J. Cook, J. McMurdo, A. K. Ray, *Sensors and Actuators, B* **1993**, *13*, 416-419.
60. R. O. Loutfy, J. H. Sharp, *J. Phys. Chem.* **1978**, *82*, 2787-2789.
61. T. Iwase, Y. Haga, *J. Mater. Sci.: Materials in Electronics* **2004**, *15*, 617-621.
62. Y. Chen, X. Zhuang, W. Zhang, Y. Liu, Y. Lin, A. Yan, Y. Araki, O. Ito, *Chem. Mater.* **2007**, *19*, 5256-5261.
63. W. Riess, T. A. Beierlein, H. Riel, *Phys. Status Solidi A* **2004**, *201*, 1360-1371.
64. K. Ohkubo, K. Takano, *J. Coord. Chem.* **1985**, *14*, 169-173.
65. G. Baffou, A. J. Mayne, G. Comtet, G. Dujardin, Ph. Sonnet, L. Stauffer, *Appl. Phys. Lett.* **2007**, *91*, 73101.
66. V. Kolotovska, M. Friedrich, D. R. T. Zahn, G. Salvan, *J. Cryst. Growth* **2006**, *291*, 166-174.
67. T. Gośliński, J. Piskorz, *J. Photoch. Photobio. C* **2011**, *12*, 304-321.



# Chapter 2

## Design and synthesis of a cavitand pillar for MOFs\*

### 2.1. Introduction

In 2009 Yaghi, Stoddart and co-workers<sup>1</sup> published the first example of a MOF architecture incorporating polyether ring components as specific molecular recognition units in the construction of cubic frameworks. In this way the complexation of the incoming guest into the MOF structure is not only shape- and size-selective, but it is based on a specific molecular recognition event. In general, to be incorporated into the MOF architecture, an organic molecule needs to be equipped with a stiff backbone, e.g. polyynes, phenyl rings, etc., and two metal binding sites, e.g.  $-\text{COO}^-$ ,  $-\text{CN}$ ,  $-\text{SCN}$ , pyridine derivatives, conveniently oriented to match the MOF geometry.<sup>2</sup> The most important and widely used bridging ligands for constructing MOFs are carboxylate linkers, due to the high thermal and chemical stabilities of the carboxylate–metal framework.<sup>3</sup>

Cavitands are particularly appealing as molecular receptors, due to their tuneable and outstanding host-guest properties. In the design of these macrocycles, shape, dimension, nature of the host-guest interactions involved in the recognition processes can be tuned by the choice of the bridging groups connecting the phenolic hydroxyls of the resorcinarene scaffold.<sup>4</sup> The versatile molecular recognition properties of cavitand receptors can be harnessed in sensing when they are arranged in a solid material suited to be used in specific devices.<sup>5</sup> For example, cavitands presenting four quinoxaline groups at the upper rim, have a deep cavity capable to interact selectively with aromatic guests via  $\pi$ - $\pi$  and CH- $\pi$  interactions;<sup>6,7</sup> cavitands functionalized with phosphonate groups pointing inside the cavity, present really high affinity

---

\* The work described in this Chapter has been published online: K. Misztal, A. Sartori, R. Pinalli, C. Massera, E. Dalcanale, "Design and synthesis of a cavitand pillar for MOFs" *Supramolecular Chemistry*, **2013**, DOI:10.1080/10610278.2013.835051.

towards alcohols, thanks to the synergistic presence of H-bonds and CH- $\pi$  interactions.<sup>8</sup> Simple tetramethylene bridged cavitands are reported to be suitable hosts for molecules like acetonitrile and nitromethane.<sup>9</sup>

If opportunely functionalized at the lower rim, cavitands could be suitable host molecules to be incorporated into MOF structures to act as specific binding sites. In its simpler form, a cavitand pillar for MOF must fulfil the structural requirement of having the two distally positioned carboxylic groups at the lower rim in equatorial configuration. In this way the carboxylates will be rigidly held at 180° angularity, pivotal for MOF assembly.

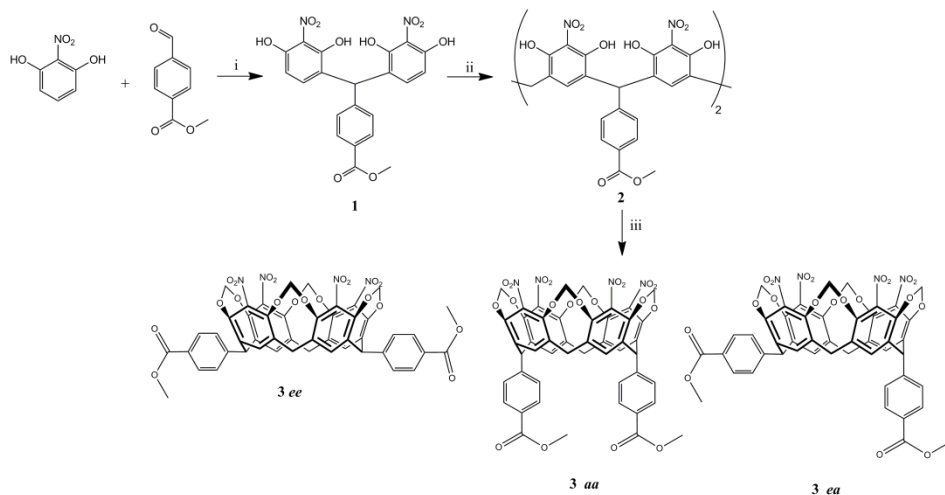
In this work we introduce a general synthetic strategy to insert two distal benzoic acid derivatives at the lower rim of cavitands, in the desired equatorial configuration (compound **3ee**, Scheme 1). The introduction of the benzoic acid derivatives is planned at the resorcinarene scaffold level, in order to make this synthetic strategy of general value for the synthesis of a wide variety of cavitands.

## 2.2. Results and Discussion

In 1989 Cram et al.<sup>10</sup> reported a study in which they showed that the acid-catalyzed condensation reaction of aldehydes with 2-nitroresorcinol stopped to the formation of the dimer, like **1** reported in Scheme 1, without proceeding further to the corresponding cyclic tetramer. The presence of the electron-withdrawing group NO<sub>2</sub> on the resorcinol deactivates the phenyl ring toward multiple electrophilic aromatic substitutions. In 2005 Bourgeois and Stoeckli-Evans<sup>11</sup> published an interesting study in which they showed that, under alkaline conditions, paraformaldehyde and 2-nitroresorcinol do form a cyclic tetramer in high yield. More recently, Beyeh and Rissanen<sup>12</sup> reported the first example of a direct synthesis of a tetranitroresorcinarene starting from 2-nitroresorcinol and acetaldehyde under alkaline conditions. The X-ray structure of the obtained compound confirmed that the macrocycle assumes the usual *rcct-flattened cone* stereoisomer.<sup>10</sup>

These three papers were instrumental in providing the synthetic background for the design of a di-substituted resorcinarene having the desired R substituents on the lower rim in equatorial conformation. The reduction of the R substituents at the lower rim from 4 to 2, calls for a stepwise synthesis of the tetramer, following the procedure reported in Scheme 1.





Scheme 1. Synthesis of the methylene bridged cavitands **3**. All three different isomers are obtained: **3aa**, **3ee** and **3ea**. Reagents and conditions: i) HCl, MeOH, 75°C, 5 days; ii) formaldehyde, NaOH, MeOH, 50°C, 24h; iii) bromochloromethane, K<sub>2</sub>CO<sub>3</sub>, dry DMA, 80°C, 3 days.

The acid-catalysed condensation reaction between 2-nitroresorcinol and methyl 4-formylbenzoate resulted in the formation of dimer **1**. The subsequent reaction of **1** with formaldehyde in basic medium brought to the formation of resorcinarene **2**. The preference for the axial (a) conformation of R substituents in resorcinarenes is well documented.<sup>10</sup> The ring inversion of the resorcinarene macrocycle allows the R groups to exchange between the equatorial (e) and the axial positions.<sup>13</sup> In this case, the ring inversion is eased by the removal of two of the four substituents, allowing the interconversion between the three possible conformers in solution. The introduction of the four methylene bridges at the upper rim blocks the benzoate substituents in either axial or equatorial configuration. Therefore **2** was reacted directly with bromochloromethane in presence of K<sub>2</sub>CO<sub>3</sub>, to yield cavitand **3** in all three possible configurations. The three isomers were separated via column chromatography, giving **3aa**, **3ee** and **3ea**, in a 5:3:1 ratio. The configuration of each of the three isomers was determined via <sup>1</sup>H NMR, as reported in Figure 1. The isomers **3ee** and **3aa**, having a C<sub>2v</sub> symmetry, presented one singlet for the methine proton, as highlighted in the figure (empty circle for cavitand **3ee**, empty square for cavitand **3aa**). The upfield shift of the methine proton is indicative of the equatorial position of the R substituents.<sup>13</sup> The **3ea** isomer presented two different singlets for the methine proton, one shifted upfield,

diagnostic of the equatorial position of the leg (black square), and the other one shifted downfield, diagnostic of the axial position of the substituent (black circle). The asymmetry of the molecule is also confirmed by the multiplicity of all the other signals.

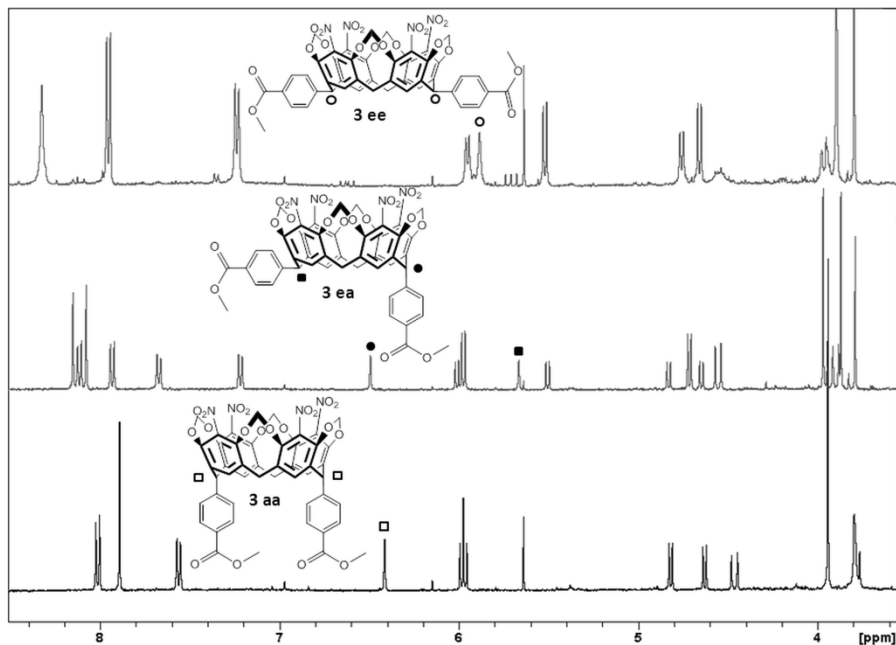
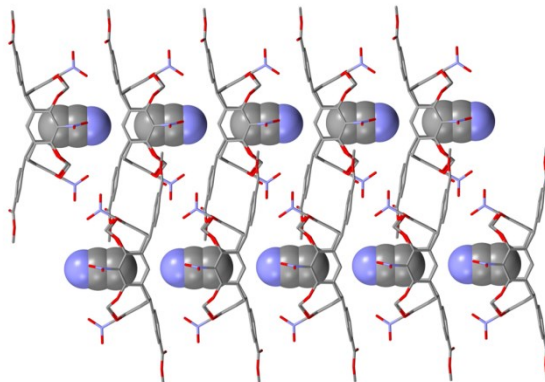


Figure 1.  $^1\text{H}$  NMR spectra of the three different isomers of cavitanol **3**. Diagnostics methine peaks for the configuration attribution are highlighted with different symbols.

The stereochemistry of the **3ee** isomer has been univocally confirmed also via single crystal X-ray diffraction analysis (Figure 2). Suitable crystals were obtained by slow evaporation of a solution of **3ee** in acetonitrile. The solvent is included inside the cavitanol, stabilized by CH- $\pi$  interactions between the methyl group of the guest and the nitrobenzene rings of the host.





**Figure 3.** Crystal structure of compound **3ee** showing the channels formed in the lattice along the crystallographic axis *b*. Hydrogen atoms have been omitted for clarity.

### 2.3. Conclusions

The introduction of distal benzoate substituents in equatorial configuration at the lower rim of a methylene-bridged cavitand has been achieved via a stepwise synthesis. All three possible stereoisomers are accessible via this approach (**3aa**, **3ae**, **3ee**). Crystal structure analysis proved that the elusive **3ee** isomer was indeed formed. This approach shows that, by carefully choosing the conditions of the different reaction steps (acid or alkaline environment), it is possible to introduce different substituents at the lower rim of cavitands in the desired position and configuration. Moreover, the formation of the resorcinarene intermediate **2** makes this synthetic protocol amenable to be extended to the preparation of a wide variety of cavitands, featuring different bridges at the upper rim. The particular configuration of cavitand **3ee** isomer and the nature of the benzoate legs open the way to use this molecule as molecular recognition unit in MOF architecture.

### 2.4. Experimental Section

Unless specified, all the reagents and solvents needed were used as purchased without further purification. Reactions were carried out under argon using dry solvent, unless otherwise noted.  $^1\text{H}$  NMR spectra were collected on a Bruker Avance 400 MHz; ESI-MS spectra were collected on a API 100 SCIEX electrospray ionization mass spectrometer, single quadrupole. HR-MS spectra were collected on a Thermo Scientific LTQ Orbitrap XL electrospray

ionization mass spectrometer.

### **Methyl 4-(bis(2,4-dihydroxy-3-nitrophenyl)methyl)benzoate (dimer) 1**

2-nitrobenzene-1,3-diol (200 mg, 1.29mmol) and methyl-4-formylbenzoate (105 mg, 0.64mmol) were dissolved in 10 mL of methanol. To the red-orange clear solution obtained, hydrochloric acid (37% water solution) was added dropwise over a period of 10 min. After 5 days at 75°C, a red-orange precipitate appeared. The reaction was cooled down to room temperature, filtrated and the solid was washed with cold methanol. No further purification was necessary and the crude product was used as is in the next step. (235 mg; yield = 80%).

$^1\text{H}$  NMR (400 MHz, acetone- $d_6$ )  $\delta$ : 10.90 (s, 2H, Ar-OH), 10.47 (s, 2H, Ar-OH), 7.97 (d, 2H, (O)C-Ar-H,  $J$  = 6.56 Hz), 7.27 (d, 2H, HO-Ar-H,  $J$  = 8.20 Hz), 7.10 (d, 2H, CH-Ar-H,  $J$  = 8.72 Hz), 6.62 (d, 2H, CH-Ar-H,  $J$  = 8.76 Hz), 6.19 (s, 1H, CH), 3.88 (s, 3H,  $\text{CH}_3$ ). ESI-MS (neg mode): calculated for  $\text{C}_{21}\text{H}_{16}\text{N}_2\text{O}_{10}(\text{M})$  456.37; found  $[\text{M} - \text{H}]^-$  = 455.34.

### **Tetranitroresorcin[4]arene, 2 (mixture of ee, ae and aa isomers):**

To a solution of **1** (150 mg, 0.33mmol, 1 eq.) and sodium hydroxide (26.3 mg, 0.66mmol, 2eq.) in methanol cooled at 0°C, paraformaldehyde (10 mg, 0.33mmol, 1 eq.) was added in one portion. The mixture was stirred for 2 hours at 0°C and then heated at 60°C for 20 h. The resulting dark red mixture was cooled to room temperature and quenched by one pot addition of acetic acid (38  $\mu\text{L}$ , 0.66mmol, 2 eq.). The solvent was removed under reduced pressure, and the solid was dissolved in acetone and filtrated on silica gel. Flash chromatography of the crude ( $\text{SiO}_2$ ; eluent  $\text{CH}_2\text{Cl}_2/\text{Hexane}/\text{Aceton}$ , 4:9:1) yielded tetramer **2** (20 mg, yield 12%) as mixture of three isomers. No other attempts to separate the isomers were performed at this stage.

ESI-MS (neg mode): calculated for  $\text{C}_{44}\text{H}_{32}\text{N}_4\text{O}_{20}(\text{M})$  936.75; found  $[\text{M} - \text{H}]^-$  = 935.68.

### **Methylene-bridged tetranitrocavitand, 3:**

A solution of **2** (80 mg, 0.085mmol) in dry DMA (10 mL) in a schlenktube was

degassed with bubbling Ar. After 30 minutes a large excess of anhydrous  $K_2CO_3$  (600 mg) was added, followed by bromochloromethane (56  $\mu$ L, 0.85 mmol, 10 eq.). The reaction mixture was stirred at 80°C under Argon atmosphere for three days. During this period, two portions of  $K_2CO_3$  (300 mg each portion) and three of  $BrCH_2Cl$  (4 eq. every portion) were added. The complete disappearance of reagent **2** was monitored via TLC. At the end the solvent was evaporated under reduced pressure. The crude was dissolved in water and extracted three times with dichloromethane; the organic phase was collected and evaporated. The obtained precipitate was purified by flash chromatography ( $SiO_2$ ; eluent  $CH_2Cl_2$ /Hexane/Acetone, 5:5:0.3). Three different isomers were recovered: **3aa** (7 mg, yield 8%); **3ae** (3 mg, yield 4%); **3ee** (4 mg, yield 5%). The reaction was repeated on a larger scale with similar yields.

**3aa**:  $^1H$  NMR (400 MHz, acetone- $d_6$ )  $\delta$ : 8.01 (d, 4H, (O)C-Ar-H,  $J = 8.44$  Hz), 7.89 (s, 4H, Ar-H), 7.56 (d, 4H, CH-Ar-H,  $J = 7.48$  Hz), 6.41 (s, 2H, CH), 5.97 (dd, 4H, O- $CH_2$ -O,  $J_1 = 7.52$  Hz,  $J_2 = 7.84$  Hz), 4.81 (d, 2H, O- $CH_2$ -O,  $J = 7.44$  Hz), 4.62 (d, 2H, O- $CH_2$ -O,  $J = 7.72$  Hz), 4.46 (d, 2H, Ar- $CH_2$ -Ar,  $J = 12.84$  Hz), 3.94 (s, 6H,  $CH_3$ ), 3.78 (d, 2H, Ar- $CH_2$ -Ar,  $J = 12.72$  Hz). HR-MS: calculated for  $C_{48}H_{33}N_4O_{20}[M+H]^+$  985.168815; found  $[M + H]^+ = 985.16874$ .

**3ae**:  $^1H$  NMR (400 MHz, acetone- $d_6$ )  $\delta$ : 8.15 (s, 2H, Ar-H), 8.11 (d, 2H, (O)C-Ar-H,  $J = 8.44$  Hz), 8.08 (s, 2H, Ar-H), 7.93 (d, 2H, (O)C-Ar-H,  $J = 8.48$  Hz), 7.67 (d, 2H, CH-Ar-H,  $J = 7.52$  Hz), 7.21 (d, 2H, CH-Ar-H,  $J = 7.76$  Hz), 6.49 (s, 1H, CH), 6.01 (d, 1H, O- $CH_2$ -O,  $J = 7.56$  Hz), 5.97 (d, 1H, O- $CH_2$ -O,  $J = 7.68$  Hz), 5.66 (s, 1H, CH), 5.50 (d, 1H, O- $CH_2$ -O,  $J = 7.60$  Hz), 4.82 (d, 1H, O- $CH_2$ -O,  $J = 7.56$  Hz), 4.71 (d, 2H, O- $CH_2$ -O,  $J = 7.72$  Hz), 4.64 (d, 1H, O- $CH_2$ -O,  $J = 7.60$  Hz), 4.55 (d, 2H, Ar- $CH_2$ -Ar,  $J = 12.76$  Hz), 3.97 (s, 3H,  $CH_3$ ), 3.89 (d, 2H, Ar- $CH_2$ -Ar,  $J = 12.84$  Hz), 3.86 (s, 3H,  $CH_3$ ). HR-MS: calculated for  $C_{48}H_{33}N_4O_{20}[M+H]^+$  985.168815; found  $[M + H]^+ = 985.16875$ .

**3ee**:  $^1H$  NMR (400 MHz, acetone- $d_6$ )  $\delta$ : 8.32 (s, 4H, Ar-H), 7.95 (d, 4H, (O)C-Ar-H,  $J = 8.40$  Hz), 7.23 (d, 4H, CH-Ar-H,  $J = 7.12$  Hz), 5.95 (d, 2H, O- $CH_2$ -O,  $J = 7.72$  Hz), 5.88 (s, 2H, CH), 5.51 (d, 2H, O- $CH_2$ -O,  $J = 7.68$  Hz), 4.75 (d, 2H, O- $CH_2$ -O,  $J = 7.60$  Hz), 4.65 (d, 2H, O- $CH_2$ -O,  $J = 7.64$  Hz), 3.98 (s, 2H, Ar- $CH_2$ -Ar), 3.95 (s, 2H, Ar- $CH_2$ -Ar), 3.89 (s, 6H,  $CH_3$ ). HR-MS: calculated for  $C_{48}H_{33}N_4O_{20}[M+H]^+$  985.168815; found  $[M + H]^+ = 985.16875$ .

#### Crystal structure determination of isomer 3ee

The molecular structure of compound **3ee** was determined by single-crystal X-ray diffraction methods. Crystallographic and experimental details are summarized in Table 1.

Table 1. Crystallographic data and refinement details for compound **3ee**.

Compound <b>3ee</b>	
Formula	C <sub>50</sub> H <sub>35</sub> N <sub>5</sub> O <sub>20</sub>
Formula weight	1025.83
Crystal system	Monoclinic
Space group	<i>P2/c</i>
<i>a</i> /Å	13.351(2)
<i>b</i> /Å	7.5160(10)
<i>c</i> /Å	22.798(3)
$\beta$ /°	98.135(2)
<i>V</i> /Å <sup>3</sup>	2264.7(5)
<i>Z</i>	2
<i>D<sub>c</sub></i> /g cm <sup>-3</sup>	1.504
<i>F</i> (000)	1060
$\mu$ /mm <sup>-1</sup>	0.119
$\theta_{\min, \max}$ /°	1.54, 24.77
Reflections collected	23238
Independent reflections	3885 ( <i>R</i> <sub>int</sub> = 0.1078)
Obs. refl. [ <i>I</i> > 2 $\sigma$ ( <i>I</i> )]	1925
Data / restraints / parameters	3885/ 0 / 343
R indices [ <i>I</i> > 2 $\sigma$ ( <i>I</i> )] <sup>a</sup>	R1 = 0.0520, wR2 = 0.1156
R indices (all data)	R1 = 0.1262, wR2 = 0.1463
$\Delta\rho_{\min, \max}$ /e Å <sup>-3</sup>	-0.184, 0.196
<i>S</i> <sup>b</sup>	0.997

<sup>a</sup> $R_1 = \sum ||F_o| - |F_c|| / \sum |F_o|$ ,  $wR_2 = [\sum w(F_o^2 - F_c^2)^2 / \sum wF_o^4]^{1/2}$ .

<sup>b</sup>Goodness-of-fit  $S = [\sum w(F_o^2 - F_c^2)^2 / (n-p)]^{1/2}$ , where *n* is the number of reflections and *p* the number of parameters.

Intensity data and cell parameters were recorded at 293 K on a Bruker Apex II single-crystal diffractometer (employing a Mo K $\alpha$  radiation and a CCD area detector). The raw frame data were processed using SAINT and SADABS to yield the reflection data file.<sup>14</sup> The structure was solved by Direct Methods using the SIR97 program<sup>15</sup> and refined on  $F_o^2$  by full-matrix least-squares procedures, using the SHELXL-97 program<sup>16</sup> in the WinGX suite.<sup>17</sup> All non-hydrogen atoms were refined with anisotropic atomic displacements. The hydrogen atoms were included in the refinement at idealized geometry (C-H 0.95 Å) and refined “riding” on the corresponding parent atoms. The weighting schemes used in the last cycle of refinement was  $w = 1 / [\sigma^2 F_o^2 + (0.0604P)^2]$ , where  $P = (F_o^2 + 2F_c^2)/3$ . Drawings were obtained using the programs Mercury<sup>18</sup> and Chimera.<sup>19</sup>

Crystallographic data (excluding structure factors) for the structure reported have been deposited with the Cambridge Crystallographic Data Center as supplementary publication no. CCDC-947610 and can be obtained free of charge on application to the CCDC, 12 Union Road, Cambridge CB2 1EZ, U.K. [Fax: (internat.) + 44-1223/336-033; E-mail: [deposit@ccdc.cam.ac.uk](mailto:deposit@ccdc.cam.ac.uk)]

## 2.5. Acknowledgements

The work described here was supported by the EC through the FP7 project “FINELUMEN” (FP7-PEOPLE-2007-1-1-ITN 215399). Centro Interdipartimentale Misura “G. Casnati” of the University of Parma is acknowledged for the use of NMR and HR ESI-MS facilities.

## 2.6. References

1. Q. Li, W. Zhang, O. Š. Miljanić, C.-H. Sue, Y.-L. Zhao, L. Liu, C. B. Knobler, J. F. Stoddart, O. M. Yaghi, *Science* **2009**, *325*, 855-859.
2. T. R Cook, Y.-R. Zheng, P. J. Stang, *Chem. Rev.* **2013**, *113*, 734-777.
3. W. Xuan, C. Zhu, Y. Liu, Y. Cui, *Chem. Soc. Rev.* **2012**, *41*, 1677-1695.
4. D. J. Cram, J. M. Cram, *Container Molecules and Their Guests*, The Royal Society of Chemistry, Cambridge, **1994**.
5. R. Pinalli, E. Dalcanale, *Acc. Chem. Res.* **2013**, *46*, 399-411.
6. F. Bianchi, R. Pinalli, F. Ugozzoli, S. Spera, M. Careri, E. Dalcanale, *New J. Chem.* **2003**, *27*, 502-509.
7. S. Zampolli, P. Betti, I. Elmi, E. Dalcanale, *Chem. Commun.* **2007**, 2790-2792.



8. F. Maffei, P. Betti, D. Genovese, M. Montalti, L. Prodi, R. De Zorzi, S. Geremia, E. Dalcanale, *Angew. Chem. Int. Ed.* **2011**, *50*, 4654–4657.
9. D. J. Cram, S. Karback, H.-E. Kim, C. B. Knobler, E. F. Maverick, J. L. Ericson, R. C. Helgeson, *J. Am. Chem. Soc.* **1988**, *110*, 2229-2237.
10. L. M. Tunstad, J. A. Tucker, E. Dalcanale, J. Weiser, J. A. Bryant, J. C. Sherman, R. C. Helgeson, C. B. Knobler, D. J. Cram, *J. Org. Chem.* **1989**, *54*, 1305-1312.
11. J.-M. Bourgeois, H. Stoeckli-Evans, *Helv. Chim. Acta* **2005**, *88*, 2722-2730.
12. N. K. Beyeh, K. Rissanen, *Tetrahedron Lett.* **2009**, *50*, 7369-7373.
13. L. Abis, E. Dalcanale, A. Du vosel, S. Spera, *J. Chem. Soc. Perkin Trans. 2* **1990**, 2075-2080.
14. SADABS Bruker AXS; Madison, Wisconsin, USA, 2004; SAINT, Software Users Guide, Version 6.0; Bruker Analytical X-ray Systems. In Software Users Guide, Version 6.0; Bruker Analytical X-ray Systems, Madison, WI, 1999. G. M. Sheldrick, SADABS v2.03: Area-Detector Absorption Correction. University of Göttingen, Germany, 1999.
15. A. Altomare, M. C. Burla, M. Camalli, G. L. Cascarano, C. Giacovazzo, A. Guagliardi, A. G. G. Moliterni, G. Polidori, R. Spagna, *J. Appl. Crystallogr.* **1999**, *32*, 115-119.
16. G. M. Sheldrick, SHELXL97. Program for Crystal Structure Refinement, University of Göttingen: Göttingen, Germany, 1997;. G. M. Sheldrick *Acta Cryst.* **2008**, *A64*, 112-122.
17. WinGX 1.80.05, L. J. Farrugia, *J. Appl. Crystallogr.* **1999**, *32*, 837-838.
18. Mercury CSD 3.1 Development, I. J. Bruno, J. C. Cole, P. R. Edgington, M. K. Kessler, C. F. Macrae, P. McCabe, J. Pearson, R. Taylor, *Acta Crystallogr.* **2002**, *B58*, 389-397.
19. UCSF Chimera, version 1.4.1, E. F. Pettersen, T. D. Goddard, C. C. Huang, G. S. Couch, D. M. Greenblatt, E. C. Meng, T. E. Ferrin, *J. Comput. Chem.* **2004**, *25*(13), 1605-1612.



# Chapter 3

## ***Hierarchical Self-Assembly of Luminescent Eu(III) Complexes on Silicon\****

### 3.1 Introduction

Formation of hierarchical monolayers and multilayers on different surfaces by exploiting supramolecular interactions represents a theme of great interest in contemporary chemistry.<sup>1,2</sup> The idea behind this approach is to use the thermodynamic control and reversibility of non-covalent interactions for the error-free generation of specific architectures directly on surfaces.<sup>3</sup> A substantial contribution to the self-assembly protocols for 2D and 3D structures was given by the development of molecular recognition schemes on surfaces,<sup>4</sup> tapping into the large body of available synthetic receptors that have been designed, prepared and tested in the last three decades. Among them cavitands<sup>5</sup> are particularly versatile systems whose complexation ability was exploited not only for recognition of target molecules<sup>6</sup> but also for the fabrication of well-defined 2D and 3D molecular assemblies.<sup>7</sup> Some examples of cavitand-decorated surfaces of gold<sup>8</sup> and silicon<sup>9</sup> in which the molecular recognition properties of cavitands have been exploited for the precise fabrication of specific molecular structure have been reported. Recently  $\beta$ -cyclodextrins were employed as molecular receptors for the self-assembly of Eu(III) luminescent complexes on glass.<sup>10</sup> The antenna sensitizer and the Eu complex were independently anchored on the glass surface via hydrophobic adamantyl-cyclodextrin complexation using the multivalency approach. The two components interact on the surface leading to localized sensitized emission.

In the present work we describe an alternative, sequential self-assembly protocol aimed at building Eu(III) luminescent coordination structures on silicon. Our approach is based on the combination of the molecular recognition

---

\* Content of this chapter has been submitted for publication.

properties of a tetraphosphonate cavitand with the metal-coordination ability of specific guests.

Eu(III) and Tb(III) complexes display exceptional photophysical properties<sup>11</sup> such as high photoluminescence quantum yield (PLQY) in the visible spectral region, long excited state lifetimes, large Stokes shifts, and sharp emission profiles related to f–f electronic transitions. The characteristic red and green photoluminescence of trivalent Eu and Tb ions,<sup>12</sup> upon ultraviolet light irradiation, has been exploited from the fundamental and applicative point of view. Accordingly, materials based on Eu(III) and Tb(III) are extensively utilized in light-conversion molecular devices, as phosphors in lighting technologies, as well as for sensing purposes and memory devices.<sup>13,14</sup> However, although in literature some examples of Eu(III) complexes covalently attached on surfaces have been reported,<sup>15,16</sup> to the best of our knowledge no examples of non-covalent self-assembly of lanthanide luminescent probes on silicon surfaces have been described in the literature.

The main goal of the present work is the development of a strategy for the precise and reversible hierarchical assembly on silicon of a luminescent Eu(III) complex, which is bound to a surface-anchored cavitand by means of a sarcosine bearing a phenanthroline ligand. The design of the connecting ligand was determined by the following experimental observations: i) the high association constant of sarcosine with tetraphosphonate cavitands,<sup>17</sup> ii) the well-known ability of phenanthroline<sup>18,19</sup> to serve as a strong bidentate ligand and efficient sensitizer for Eu(III)  $\beta$ -diketonates.

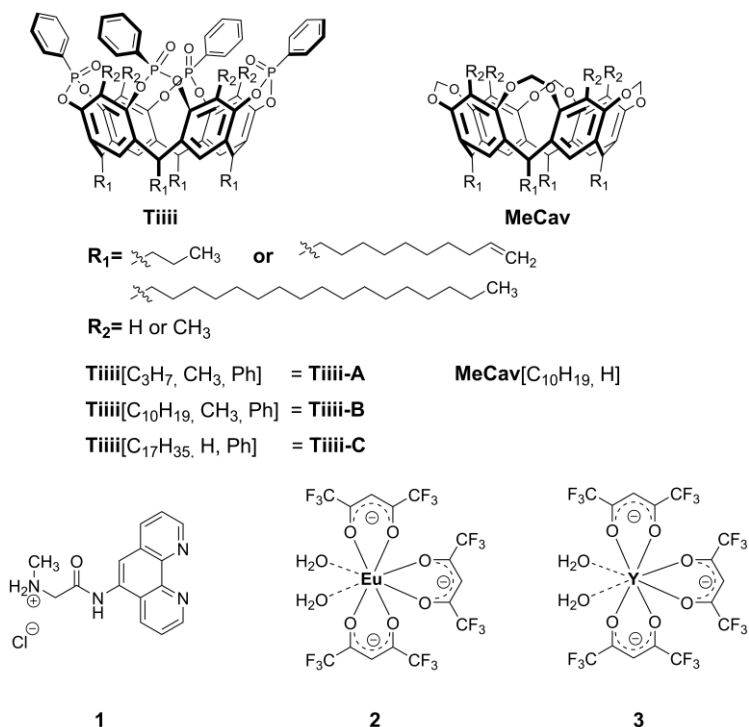


Chart 1. Molecular structure of the compounds used in the present work.

## 3.2 Results and Discussion

### 3.2.1 Design and strategy

The compounds used in the present work are shown in Chart 1. The precise and reversible hierarchical assembly on silicon was obtained by using host-guest interactions and metal-ligand coordination in sequence. This multi-step approach involves the recognition process of tetraphosphonate cavitands (**TiIII**)<sup>20</sup> anchored on the silicon surfaces towards a sarcosine unit<sup>[17]</sup> connected to a phenanthroline ligand (**1**), followed by the coordination of the phenanthroline with the europium  $\beta$ -diketonate complex **2** used as luminescent probe. The related non-luminescent and diamagnetic yttrium  $\beta$ -diketonate **3** was chosen as reference compound for the NMR characterization in solution and for photophysical control experiments on the surface. Cavitand decorated silicon surfaces were prepared by photochemical grafting.<sup>[21]</sup> The entire process was fully tested in solution, and then successfully transferred to the solid state, where it was monitored via XPS and luminescence spectroscopy.

### 3.2.2 Self-assembly in solution

The formation of ternary complexes was first carried out in solution to prove feasibility (Figure 1). The first step is the complexation of the methylammonium guest **1** inside the **TiIII**[**C**<sub>3</sub>**H**<sub>7</sub>, **CH**<sub>3</sub>, **Ph**] (from now onward **TiIII-A**) cavity in methanol, monitored by <sup>31</sup>P and <sup>1</sup>H NMR measurements. Figure S1 shows the <sup>1</sup>H NMR spectrum of the host-guest complex formed by **1** and **TiIII-A** (**TiIII-A•1**). Diagnostic upfield shifts of the guest signals were observed, as expected for hosted species that experience the shielding effect of the cavity.<sup>[17]</sup> In particular, the signals of *N*-CH<sub>3</sub> moiety moved over 3 ppm upfield to -0.53 ppm; other resonances attributed to the sarcosine moiety as well as to the phenanthroline unit were also shifted. The <sup>31</sup>P resonance of the four P=O groups moved downfield of almost 5 ppm (from 5.9 to 10.8 ppm, Figure S2). The upfield shift of the methyl residue is diagnostic of the *N*-CH<sub>3</sub> inclusion into the cavity whereas the downfield shift of P=O signals is a clear indication of the participation of phosphonates in the complexation of the guest.

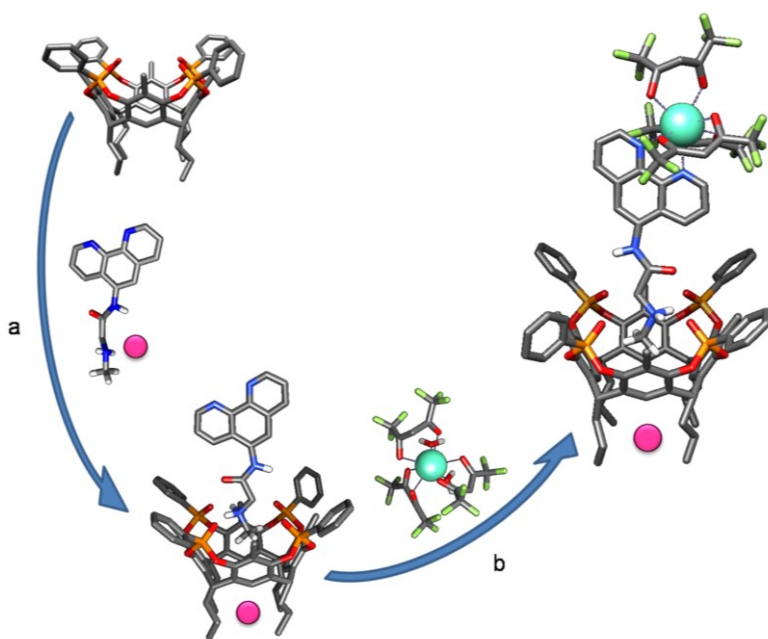


Figure 1. Ternary complex formation in solution: a) Host-guest **TiIII-A•1** complex formation in methanol; b) coordination between **TiIII-A•1** and **2** (or **3**) in dichloromethane. The pink ball represents the chloride anion of the ammonium-based ligand **1**.

The ternary complexes between **Tiiii-A•1** and the metal precursors **2** or **3** were formed quantitatively by simply mixing the components in dichloromethane. The formation of **Tiiii-A•1•3** was monitored via  $^1\text{H}$  and  $^{31}\text{P}$  NMR. In the proton spectrum of **Tiiii-A•1•3** the downfield shift of the peaks belonging to the phenanthroline was observed, diagnostic of the metal complexation (Figure S1). The phosphorous peak remained almost unchanged, indicating that metal ion does not compete with sarcosine for the cavity. Because of the paramagnetic properties of Eu(III),  $^1\text{H}$  NMR was not used for monitoring the formation of the **Tiiii-A•1•2** complex, while the phosphorus spectrum is similar to that of the diamagnetic yttrium derivative **Tiiii-A•1•3** (figure S3), so it is safe to assume that the **Tiiii-A•1•2** complex was formed. The presence of both complexed species was also confirmed by high resolution mass spectrometry (HR-MS). The HR-MS spectrum in acetonitrile of the analogous complex **Tiiii-C•1•2**, in which the cavitand has longer alkyl chain at the lower rim exhibited a peak at  $m/z$  corresponding to the complex without the chloride anion (Figure S4).

### 3.2.3 Absorption and luminescence spectra in solution

The formation of the hierarchical complexes **Tiiii-A•1•2** and **Tiiii-A•1•3** is further supported by photophysical investigations. The UV-Vis absorption spectrum of **2** in dichloromethane spans across the range 260-350 nm with the maximum centred at 290 nm (Figure S5). The phenanthroline ligand **1** absorbs in the same spectral range but its maximum is located at higher energies (275 nm, Figure S5). In line with these findings, the absorption spectrum of the compound obtained from the phenanthroline system **1** and the Eu  $\beta$ -diketonate complex **2** (**1•2**) is the sum of the spectral features of its building blocks and shows a maximum at 285 nm (Figure S5). The absorption spectrum of the analogous yttrium- $\beta$ -diketonate complex **1•3** is virtually identical to that of **1•2**, indicating the same electronic transitions in both compounds, as expected (Figure S6). The **Tiiii-A** cavitand does not absorb the light beyond 290 nm, and the formation of **Tiiii-A•1•2** leads only to a broadening of the absorption band (Figure S5). Absorption spectra of **1•2**, **1•3**, **Tiiii-A**, **Tiiii-A•1** are presented in Figure S7.

All the investigated europium compounds, **2**, **1•2** and **Tiiii-A•1•2** exhibit characteristic Eu(III) emission bands due to the f-f transitions. The emission spectra consist of  $^5\text{D}_0 \rightarrow ^7\text{F}_J$  transitions ( $J = 0-4$ ) mainly dominated by the  $^5\text{D}_0 \rightarrow ^7\text{F}_1$  and  $^5\text{D}_0 \rightarrow ^7\text{F}_2$  sharp emissions bands centred at 590 and 613 nm, respectively. The perfect overlapping of the emission spectra between **2**, **1•2** and **Tiiii-A•1•2** complexes shows that the coordination sphere of the europium cation remains virtually unchanged after the encapsulation in the cavity. Notably,

the PLQY of **2** is 15.5%, and increases to 25.9% for **1•2**. In the latter, the phenanthroline ligand fills the coordination sphere around the europium cation and eliminates vibrational quenching from water molecules and, on the other hand, it serves as light harvesting antenna. PLQY of the ternary complex **Ti(III)-A•1•2** in solution is 20.0% that is intermediate between those of **2** and **1•2**. The trend of lifetimes values is in perfect agreement with that observed for the quantum yields (Table 1).

Y(III) complexes (**1•3** and **Ti(III)-A•1•3**), which do not exhibit metal-centred emission due to the closed-shell configuration of the ion. Therefore they were investigated as reference compounds. The only luminescence band observed was that of the sarcosine-phenanthroline ligand **1** at  $\lambda_{\max} = 440$  nm. The emission profiles of **1** in **Ti(III)-A•1•3** matches well the emission of the ligand in **Ti(III)-A•1** and is shifted towards longer wavelengths compared to the free **1** ( $\lambda_{\max} = 290$  nm) due to the confinement effect of the cavitand. PLQY of the free ligand **1** was 5.7%. This value decreases to 2.7% in **Ti(III)-A**, suggesting the presence of some electronic interaction between the phenanthroline moiety and the cavitand. In the case of the metal complex **1•3**, PLQY is decreased to 1.9%. The difference with free **1** suggests some electronic perturbation induced by the yttrium cation.



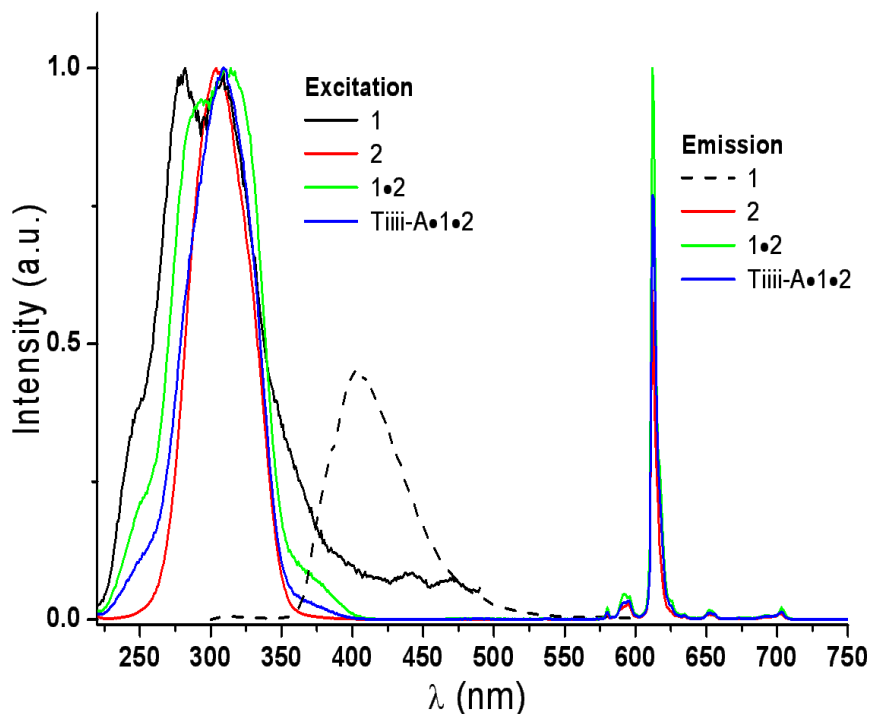


Figure 2. Emission and excitation spectra in dichloromethane at 298 K. Excitation spectra:  $\lambda_{em}$  = 612 nm in all cases but **1** for which  $\lambda_{em}$  = 410 nm. Emission spectra:  $\lambda_{ex}$  = 280 nm.

### 3.2.4 Self-assembly on the Tiiii functionalized Si surface

The non-covalent anchoring on the silicon surface is schematically illustrated in Figure 3. The preliminary step was the preparation of **Tiiii-B** functionalized Si surface (**Si-Tiiii-B**) by covalent grafting of a mixed **Tiiii-B**/1-octene (*Oct*) monolayer, via photochemical hydrosilylation. According to previous studies,<sup>[9b,21]</sup> the use of *Oct* as spectator spacer in the mixed monolayers improves the passivation of the Si surface, thus minimizing substrate oxidation due to aging. X-ray photoelectron spectroscopy (XPS) measurements of the grafted surfaces showed the typical P 2p band of the silicon-anchored Tiiii cavitant. The detailed characterization of the **Si-Tiiii-B** surface is reported elsewhere.<sup>[9b]</sup>

Table 1. Photophysical data in dichloromethane solution at 298 K.

Compound	PLQY (%)	Excited state lifetime
<b>1</b>	5.7	<b>4.9 ns</b> <sup>[b]</sup>
<b>2</b>	15.5	<b>0.75 ms</b> <sup>[a]</sup>
<b>1•2</b>	25.9	<b>0.85 ms</b> <sup>[a]</sup>
<b>Tiiii-A•1•2</b>	20.0	<b>0.80 ms</b> <sup>[a]</sup>
<b>Tiiii-A•1</b>	2.7	<b>3.70 ns</b> <sup>[b]</sup>
<b>1•3</b>	1.9	<b>3.10 ns</b> <sup>[b]</sup>
<b>Tiiii-A•1•3</b>	<b>1.7</b>	<b>3.50 ns</b> <sup>[b]</sup>

[a] Eu(III) centred luminescence. [b] Phenanthroline centred fluorescence.

The self-assembly protocol implemented in solution was then transferred to the silicon surface, as illustrated in Figure 3. The first step was the binding of **1** on the Si-grafted cavitant through the complexation of the methyl ammonium moiety. This was accomplished by dipping **Si-Tiiii-B** in a 1 mM methanol solution of **1**. The surface functionalized with the host-guest adduct (**Si-Tiiii-B•1**) was then dipped in a 1 mM THF solution of **2** (or **3**) in order to bind the metal complex through the coordination with the phenanthroline moiety, yielding **Si-Tiiii-B•1•2** (or **Si-Tiiii-B•1•3**, respectively).

### 3.2.5 Step-by-step monitoring of the self-assembly process via XPS

Each self-assembly step was monitored by XPS. The atomic compositions of **Si-Tiiii-B**, **Si-Tiiii-B•1**, **Si-Tiiii-B•1•2** and **Si-Tiiii-B•1•3** are reported in Table 2.

Table 2. Elemental composition data from XPS measurements for selected surfaces.

	Atomic fractions [%]							
	P	Si	O	C	N	F	Eu	Y
<b>Si-Tiiii-B</b>	1.1	16.3	31.9	50.4	0.3	-	-	-
<b>Si-Tiiii-B•1</b>	1.0	12.9	30.5	53.9	1.7	-	-	-
<b>Si-Tiiii-B•1•2</b>	0.9	12.2	28.8	49.3	1.2	6.9	0.38	-
<b>Si-Tiiii-B•1•3</b>	0.9	11.1	21.3	59.9	1.1	5.4	-	0.32
<b>Si-MeCav•1•2</b>	-	19.9	26.9	52.4	0.3	0.5	<0.03	-

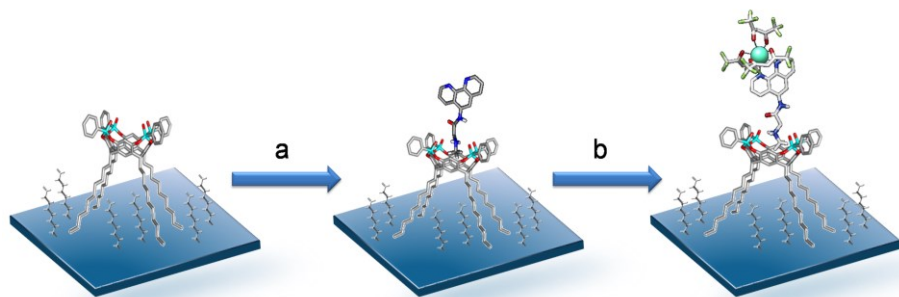


Figure 3. **Si-TiIII-B** hierarchical self-assembly protocol with a) guest **1** and subsequently b) with metal complexes **2** or **3**.

Although a low N 1s signal is already present in the **Si-TiIII-B** sample due to adventitious N-containing species. However, after treatment with guest **1**, a significant increase of the N 1s signal was observed. In addition, the shape of the XPS N 1s band (Figure 4) is consistent with the molecular formula of **1**. In fact, the band consists of two components: i) a main feature at 400.0 eV assigned to the two phenanthroline nitrogens and the nitrogens of the amidic bond ( $N_{\text{lig}}$ ), and ii) a less intense component at 402.0 eV assigned to the protonated nitrogen of sarcosine ( $N_{\text{sar}}$ ). The observed intensity ratio  $N_{\text{lig}}/N_{\text{sar}}$  is about 3:1 as expected from the molecular structure. The successful coordination affording **Si-TiIII-B•1•2** and **Si-TiIII-B•1•3** respectively were corroborated by the presence of Eu (or Y) XPS bands together with the F 1s signal due to the coordinated  $\beta$ -diketonate ligands (Table 2).

The Eu 3d XPS region of **Si-TiIII-B•1•2** sample shows the characteristic doublet of Eu 3d<sub>5/2</sub>- and Eu 3d<sub>3/2</sub> that are centred respectively at 1164.8 eV and 1135.1 eV; this is consistent with the presence of Eu(III) (Figure 5a).<sup>[16]</sup> It is worth noticing that a low intensity doublet is observed at 1155.1 eV and 1125.1 eV, which could indicate the presence of reduced Eu(II).<sup>22</sup> The relative intensity of these bands (with respect to the main doublet) increases with X-rays irradiation times and the amount of Eu(II) is negligible for very short XPS acquisition times (Figure S8). This suggests that europium is present only as Eu(III) in the monolayer and that reduction is produced during the XPS analysis. In the **Si-TiIII-B•1•3** sample, Y 3d<sub>5/2</sub> and Y 3d<sub>3/2</sub> peaks (Figure 5b) appear respectively at 158.8 eV and 160.6 eV, consistent with the presence of a Y(III) compound.

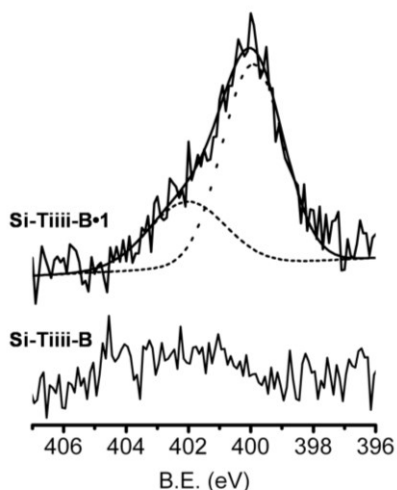


Figure 4. High resolution N 1s XPS region of **Si-Tiiii-B** and **Si-Tiiii-B•1**.

In order to demonstrate that the self-assembly on the surface is driven by the molecular recognition properties of the **Tiiii-B** cavity and to rule out any physisorption phenomena of the metal complexes on the surface, a specific control experiment has been designed and executed.

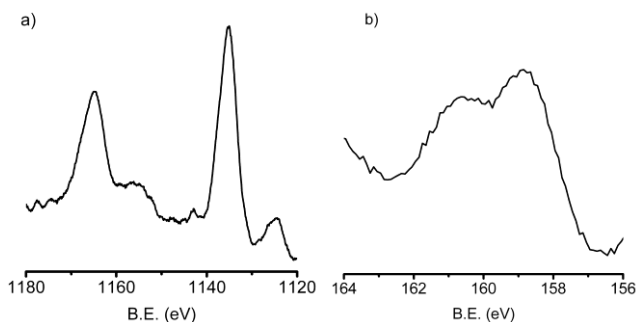


Figure 5. High resolution XPS regions of a) Eu 3d of **Si-Tiiii-B•1•2** and b) Y 3d of **Si-Tiiii-B•1•3**.

A blank sample made of a complexation inactive methylene-bridged cavitant grafted on silicon (**Si-MeCav**) was prepared. The resulting **Si-MeCav** surface was treated with guest **1** and **2** (**Si-MeCav•1•2**) similarly to **Si-Tiiii-B•1•2**. XPS analysis of **Si-MeCav•1•2** (Table 2) did not show significant amounts of nitrogen, europium or fluorine, showing that physisorption on the surface is negligible, and the complexation capability of the **Tiiii-B** cavity is a key requirement for the self-assembly process.

The atomic ratios Eu/N/F and Y/N/F of **Si-Ti<sub>iii</sub>-B•1•2** and **Si-Ti<sub>iii</sub>-B•1•3** are 1/3.2/18.2 and 1/3.4/16.9, respectively. They are close to the theoretical expected ratio 1/4/18, although a slightly lower amount of N is observed in both cases. This behaviour can be due to a direct coordination of the metal complexes in the **Ti<sub>iii</sub>-B** cavity, to a very limited extent. To investigate this possible side reaction pathway, **Si-Ti<sub>iii</sub>-B** surfaces without guest **1** were treated with **2** and **3**. XPS analyses of the samples thus obtained (**Si-Ti<sub>iii</sub>-B•2** and **Si-Ti<sub>iii</sub>-B•3**) showed the presence of the metals and fluorine in amounts comparable to **Si-Ti<sub>iii</sub>-B•1•2** and **Si-Ti<sub>iii</sub>-B•1•3**, indicating that the **Ti<sub>iii</sub>-B** cavity can interact directly with complex **2** or **3**.

### 3.2.6 Photophysical measurements on the surface

To evaluate the presence of free or uncomplexed phenanthroline ligand in the self-assembled systems, the luminescence properties of **Si-Ti<sub>iii</sub>-B•1**, **Si-Ti<sub>iii</sub>-B•1•2**, **Si-Ti<sub>iii</sub>-B•1•3** and **Si-Ti<sub>iii</sub>-B•2** surfaces have been examined in the spectral window of the phenanthroline fluorescence band ( $\lambda_{\text{ex}}=270$  nm, Figure 6) for the various surfaces. Only **Si-Ti<sub>iii</sub>-B•1** sample showed the band of the phenanthroline ligand ( $\lambda_{\text{max}} = 440$  nm), whereas in all the other samples no luminescence was detected (Figure 6). For **Si-Ti<sub>iii</sub>-B•2** this result is obvious, since phenanthroline is not present on the surface. However, in the case of **Si-Ti<sub>iii</sub>-B•1•2** the absence of phenanthroline emission corroborates the occurrence of energy transfer properties to the Eu(III) ion.

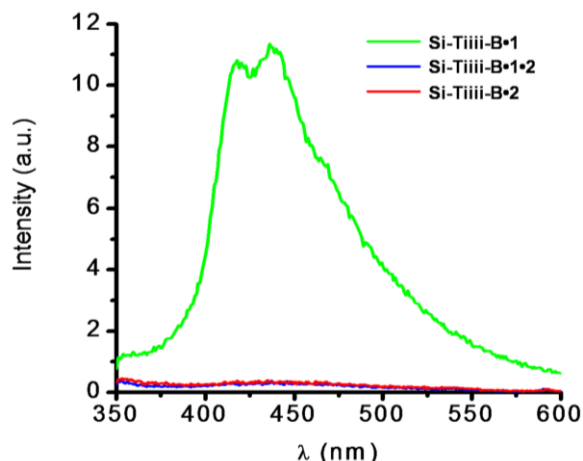


Figure 6. Emission spectra of different surfaces in the spectral window of the phenanthroline fluorescence.

Eu(III) emission was evaluated in the 480-750 nm range ( $\lambda_{\text{ex}} = 320$  nm) for both **Si-Tiiii-B•1•2** and **Si-Tiiii-B•2** surfaces. **Si-Tiiii-B•1•2** exhibits emission bands related to  $^5\text{D}_0 \rightarrow ^7\text{F}_1$ ,  $^5\text{D}_0 \rightarrow ^7\text{F}_2$ ,  $^5\text{D}_0 \rightarrow ^7\text{F}_3$  and  $^5\text{D}_0 \rightarrow ^7\text{F}_4$  transitions, at 592, 610, 648 and 690 nm respectively, shifted a few nanometers towards higher energies in comparison to the compound in solution. For **Si-Tiiii-B•2** only the strong signals of  $^5\text{D}_0 \rightarrow ^7\text{F}_1$ ,  $^5\text{D}_0 \rightarrow ^7\text{F}_2$  were observed (Figure 7). The emission intensity recorded for the **Si-Tiiii-B•1•2** surfaces is significantly higher compared to **Si-Tiiii-B•2**, thanks to the sensitizing properties of the phenanthroline towards Eu(III), which ultimately improves light absorption and, accordingly, emission output. Moreover, the relative intensities of the  $^5\text{D}_0 \rightarrow ^7\text{F}_1$  and  $^5\text{D}_0 \rightarrow ^7\text{F}_2$  transitions are different for the two surfaces. In particular, for **Si-Tiiii-B•1•2** the intensity ratio between the  $^5\text{D}_0 \rightarrow ^7\text{F}_1$  and  $^5\text{D}_0 \rightarrow ^7\text{F}_2$  transitions (1:4) is similar to that in solution (1:5), whilst for **Si-Tiiii-B•2** it is remarkably different (1:2). These results suggest that the self-assembly process in the presence of **1** occurs without significant changes of the Eu coordination environment compared to the solution process. By contrast, the direct complexation of **2** in the Tiiii cavity leads to a significant modification of the original Eu environment.

Finally, no emission was observed for **Si-MeCav•1•2**. This result matches with XPS findings, indicating no Eu(III) complex anchored on the surface in the absence of specific Tiiii receptors.

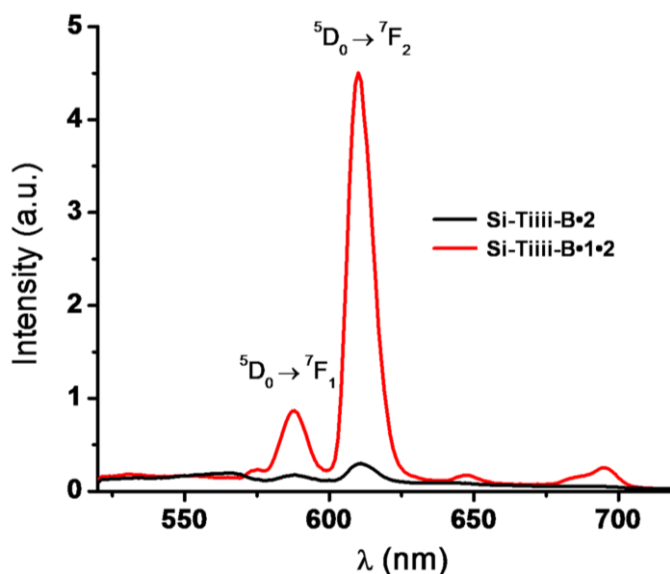


Figure 7. Fluorescence spectra of **Si-Tiiii-B•1•2** (red trace) and **Si-Tiiii-B•2** surfaces (black trace) probed at 5 different points of the samples.  $\lambda_{\text{ex}} = 320$  nm.

### 3.3 Conclusions

In the present study we have reported the first example of hierarchical self-assembly of luminescent lanthanide complexes on silicon. Formation of these supramolecular structures on Si surface has been confirmed by two independent analytical techniques (XPS and fluorescence) and validated by control experiments with surfaces decorated with a complexation inactive methylene-bridged cavitand. Self-assembly on the cavitand functionalized surface with sarcosine-phenanthroline ligand followed by  $\text{Eu}(\text{hfac})_3$  coordination afforded a more strongly emitting surface than direct coordination of  $\text{Eu}(\text{hfac})_3$  in the cavity, due to the sensitization of the  $\text{Eu}(\text{III})$  ion by the phenanthroline ligand. The present approach can be implemented for applications in sensing, bio-imaging and optoelectronic devices. The use of the universal bidentate ligand **1** allows the complexation of other lanthanide ions, as well as of metals in general. Moreover, the self-assembly of these ternary complexes on silicon will widen the spectrum of possible applications, since silicon is a technologically important inorganic platform.

### 3.4 Experimental Section

**General:** All commercial reagents were ACS reagent grade and used as received. Solvents were dried and distilled using standard procedures.  $^1\text{H}$  NMR spectra were recorded on Bruker Avance 400 (400MHz) and Bruker Avance 300 (300 MHz) NMR spectrometers. All chemical shifts ( $\delta$ ) were reported in parts per million (ppm) relative to proton resonances resulting from incomplete deuteration of NMR solvents. ESI-MS experiments were performed on a Waters ZMD spectrometer equipped with an electrospray interface. Exact mass was determined using a LTQ ORBITRAP XL Thermo spectrometer equipped with an electrospray interface. This section only includes the synthesis and characterization of the ligand **1** from commercially available 5-amino-[1,10]-phenanthroline **5**, through modified literature procedure<sup>[14]</sup> and self-assembly in solution and on silicon surface; syntheses of tetraphosphonate cavitands with  $\text{C}_3\text{H}_7$  (**Tiiii-A**)<sup>23</sup> and  $\text{C}_{10}\text{H}_{19}$  (**Tiiii-B**)<sup>24</sup> on lower rim were reported previously. In Supporting Information are also NMR and MS spectra of formation of complexes.

**Bromo-N-[1,10]-phenanthroline-5-yl-acetamide, 4:** 5-Amino-[1,10]-phenanthroline (0.20 g, 1.03 mmol) was placed in a round bottomed flask under argon. ACN (dry, 40 mL) and triethylamine (0.11 g, 1.04 mmol, 0.15 mL) were added and the suspension was stirred for 30 min at room temperature. The mixture was cooled to 0°C before bromoacetylchloride (0.19 g, 1.23 mmol, 0.10

mL, 1.2 equivalents) in ACN (5 mL) was added drop-wise. The mixture was left stirring for 16 h at RT and TLC (CH<sub>2</sub>Cl<sub>2</sub>:MeOH(saturated with NH<sub>3</sub>) 9:1) showed no further progress of reaction. Solvent was removed under reduced pressure and residue was solubilised in 10 mL of 5% K<sub>2</sub>CO<sub>3</sub> aqueous solution. Triple extraction with dichloromethane was conducted and organic layers were collected and evaporated, yielding a brown residue (0.25 g) which was next purified by silica column chromatography using 95:5 CH<sub>2</sub>Cl<sub>2</sub> : MeOH(NH<sub>3</sub>) as eluent, giving pale brown solid (0.166 g, 51%). <sup>1</sup>H NMR (400 MHz, CDCl<sub>3</sub>, 298 K) δ=9.26 (d, 1H, J = 4.2 Hz), 9.18 (d, 1H, J = 5.6 Hz), 8.81 (bs, 1H, NH), 8.39 (s, 1H), 8.36 (d, 1H, J = 8.5 Hz), 8.27 (d, 1H, J = 8.0 Hz), 7.74 (dd, 1H, J = 4.0 Hz, J = 5.4 Hz), 7.67 (dd, 1H, J = 5.8 Hz, J = 5.9 Hz), 4.21 (s, 2H, CH<sub>2</sub>).

**Ligand 1:** To 0.166 g (0.63 mmol) of **4** dissolved in 20 ml of dry ACN (pale-yellow solution) 1.2 equivalents of sodium iodide (0.94 g; 0.63 mmol) were added. Solution was stirred for 10 min at RT until a white precipitate appears (NaBr). Next 5 mL of 30% methylamine solution in ethanol were added by portion during 6h stirring at RT until TLC indicated no starting compound. Reaction mixture was evaporated at reduced pressure and was further purified by silica column chromatography using 95:5 CH<sub>2</sub>Cl<sub>2</sub> : MeOH(NH<sub>3</sub>) as eluent, giving yellow-brown solid (0.126 g, 90%). <sup>1</sup>H NMR (400 MHz, CDCl<sub>3</sub>, 298 K) δ=10.23 (s broad, 1H, NH), 9.26 (d, 1H, J = 4.0 Hz), 9.14 (d, 1H, J = 4.0 Hz), 8.65 (s, 1H), 8.34 (d, 1H, J = 8.4 Hz), 8.26 (d, 1H, J = 8.0 Hz), 7.73 (dd, 1H, J = 4.3 Hz, J = 4.3 Hz), 7.67 (dd, 1H, J = 4.3 Hz, J = 4.3 Hz), 3.58 (s, 2H, CH<sub>2</sub>), 2.68 (s, 3H, CH<sub>3</sub>). <sup>13</sup>C NMR (100 MHz, CDCl<sub>3</sub>, 298 K) δ=170.2, 150.2, 149.6, 135.9, 130.2, 128.7, 123.5, 123.2, 122.8, 116.6, 55.4, 37.2. Calculated for C<sub>15</sub>H<sub>15</sub>N<sub>4</sub>O ([M+H]): *m/z*=267.12. Found:*m/z*=267.2.

**Tiii-C:** To a solution of heptadecyl-footed resorcinarene (130 mg, 0.090 mmol) in fresh distilled pyridine (10 mL), dichlorophenylphosphine (0.081 mL, 0.582 mmol) was added slowly, at room temperature. After 3 hours of stirring at 70 °C, the solution was allowed to cool at room temperature and 2 mL of aqueous 35% H<sub>2</sub>O<sub>2</sub> was added. The resulting mixture was stirred for 30 minutes at room temperature and H<sub>2</sub>O (100 mL) was added and solution was filtrated. Solid was suspended in water (100 mL), sonicated for 30 min and filtrated again resulting as white powder (140 mg, 80%). <sup>31</sup>P NMR (160 MHz, CDCl<sub>3</sub>): 7,6 (s, 4P). <sup>1</sup>H NMR (400 MHz, CDCl<sub>3</sub>): 8.10-8.04 (m, 8H, PO-Ar-H<sub>o</sub>), 7.64 (m, 4H, POArH<sub>p</sub>), 7.55-7.51 (m, 8H, POArH<sub>m</sub>), 7.31 (s, 4H, Ar-H<sub>up</sub>), 7.02 (s, 4H, Ar-H<sub>down</sub>), 4.82 (bt, 4H, Ar-CH-Ar), 2.36 (bd, 8H, -CH-CH<sub>2</sub>-CH<sub>2</sub>-), 1.47 (m, 8H, -CH<sub>2</sub>-CH<sub>2</sub>-CH<sub>3</sub>), 1.28 (m, 112H, -CH<sub>2</sub>-(CH<sub>2</sub>)<sub>14</sub>-CH<sub>3</sub>), 0.90 (m, 12H, -CH<sub>2</sub>-CH<sub>3</sub>).

**Cavitaand-guest-ligand complex Tiii-A•1:** To a methanol solution containing **1** (20 mg, 0.0752 mmol) a CH<sub>3</sub>COCl solution in methanol (0.752 M, 0.1 ml used)



was added dropwise. To this transparent solution cavitand **Tiiii-A** (89 mg, 0.0752 mmol) was added. Mixture was stirred until everything becomes solubilized (5 min, rt). Next, solvent was removed under reduced pressure and orangish residue **Tiiii-A•1** was dried under vacuum.  $^1\text{H}$  NMR (400 MHz,  $\text{CDCl}_3$ , 298 K): **1**: 9.34 (bs, 1H), 9.26 (bs, 1H), 9.02 (bs, 1H), 8.43 (bs, 1H), 7.80 (s, 1H), 7.71 (s, 1H), 7.30 (bs, 1H), 6.83 (bs, 2H,  $\text{NH}_2$ ) 3.76 (s, 2H,  $\text{CH}_2$ ), -0.50 (s, 3H,  $\text{CH}_3$ ); **Tiiii-A**: 8.15 (q, 8H, Ar-H,  $J = 7.2$  Hz), 7.82 (bs, 4H, Ar-H), 7.73 (t, 4H, Ar-H, 7.6 Hz), 7.60 (m, 8H, Ar-H), 4.83 (t, 4H, Ar-CH-Ar,  $J = 7.6$  Hz), 2.63 (m, 8H,  $\text{CH-CH}_2\text{-CH}_2$ ), 2.20 (s, 12H, Ar- $\text{CH}_3$ ), 1.46 (m, 8H,  $\text{CH}_2\text{-CH}_2\text{-CH}_3$ ), 1.10 (m, 12H,  $\text{CH}_2\text{-CH}_3$ ).  $^{31}\text{P}$  NMR (160 MHz,  $\text{CDCl}_3$ , 298 K): 10.8 (s, 4P).

**Tiiii-C•1**: To methanol solution containing **1** (11 mg, 0.040 mmol) a  $\text{CH}_3\text{COCl}$  solution in methanol (0.403 M, 0.1 ml used) was added by drops. To this transparent solution cavitand **Tiiii-C** (78 mg, 0.040 mmol) was added. Mixture was stirred for 5 min at room temperature. Resulting orangish residue was dried under vacuum.  $^{31}\text{P}$  NMR (160 MHz,  $\text{CDCl}_3$ , 298 K): 12.1 (s, 4P).  $^1\text{H}$  NMR (400 MHz,  $\text{CDCl}_3$ , 298 K): **1**: 9.30 (bs, 2H), 9.02 (bs, 1H), 8.49 (m, 4H), 3.80 (s, 2H,  $\text{CH}_2$ ), -0.64 (s, 3H,  $\text{CH}_3$ ); **Tiiii-C**: 8.10 (m, 8H, PO-Ar-H), 7.69 (m, 4H, PO-Ar-H), 7.58 (m, 8H, PO-Ar-H), 7.25 (bs, 4H, Ar-H), 6.97 (bs, 4H, Ar-H), 4.78 (t, 4H, Ar-CH-Ar,  $J = 6.6$  Hz), 2.85 (bs, 8H,  $\text{CH-CH}_2\text{-CH}_2$ ), 1.51 (bs, 8H,  $\text{CH-CH}_2\text{-CH}_2$ ), 1.42 (m, 112H,  $\text{CH}_2\text{-(CH}_2\text{)}_{14}\text{-CH}_3$ ), 0.89 (m, 12H,  $\text{CH}_2\text{-CH}_2\text{-CH}_3$ ).

**Ternary complex Tiiii-A•1•2**: To dichloromethane solution containing **Tiiii-A•1** (25 mg, 0.017 mmol) **2** (14 mg, 0.017 mmol) was added at once and mixture was stirred for 1 h at RT. Solvent was removed under reduced pressure and orange residue **Tiiii-A•1•2** was dried under vacuum.  $^{31}\text{P}$  NMR (160 MHz,  $\text{CDCl}_3$ , 298 K): 11.3 (s, 4P).

**Ternary complex Tiiii-A•1•3**: To dichloromethane solution containing **Tiiii-A•1** (30 mg, 0.02 mmol) **3** (14.2 mg, 0.02 mmol) was added at once and mixture was stirred for 1 h at RT. Solvent was removed under reduced pressure and orange residue **Tiiii-A•1•3** was dried under vacuum.  $^1\text{H}$  NMR (400 MHz,  $\text{CDCl}_3$ ): **1**: 9.25 (bs, 1H), 9.18 (bs, 1H), 8.70 (bs, 1H), 8.46 (s, 1H), 8.23 (bs, 1H), 7.70 (bs, 1H), 7.09 (bs, 1H), 6.83 (bs, 2H,  $\text{NH}_2$ ) 3.58 (bs, 2H,  $\text{CH}_2$ ), -0.58 (s, 3H,  $\text{CH}_3$ ); **2**: 6.07 (bs, 2H), 6.00 (bs, 1H); **Tiiii-A**: 8.10 (q, 8H, Ar-H,  $J = 7.2$  Hz), 7.82 (bs, 4H, Ar-H), 7.75 (t, 4H, Ar-H, 7.04 Hz), 7.59 (m, 8H, Ar-H), 4.83 (t, 4H, Ar-CH-Ar,  $J = 7.2$  Hz), 2.61 (m, 8H,  $\text{CH-CH}_2\text{-CH}_2$ ), 2.18 (s, 12H, Ar- $\text{CH}_3$ ), 1.47 (m, 8H,  $\text{CH}_2\text{-CH}_2\text{-CH}_3$ ), 1.10 (m, 12H,  $\text{CH}_2\text{-CH}_3$ ).  $^{31}\text{P}$  NMR (160 MHz,  $\text{CDCl}_3$ , 298 K): 11.0 (s, 4P).

**Ternary complex Tiiii-C•1•2**: **Tiiii-C•1** (29 mg, 0.013 mmol) and  $\text{Eu}(\text{hfac})_3$  (10.5 mg, 0.013 mmol) were solubilized in dichloromethane (10 mL) and solution was

stirred for 1 hour at RT until everything was solubilized. Solvent was removed under reduced pressure and residue was dried under vacuum.  $^{31}\text{P}$  NMR (160 MHz,  $\text{CDCl}_3$ , 298 K): 12.6 (s, 4P). HR-MS: calculated for  $[\text{M-Cl}]^+$   $\text{C}_{150}\text{H}_{190}\text{EuF}_{18}\text{N}_4\text{O}_{19}\text{P}_4^+$   $m/z=2971.19277$ , found  $m/z=2971.18155$ .

**Synthesis of Si-TiIII-B:** TiIII-B/1-octene mixture ( $\chi_{\text{cav}} = 0.05$ ) was dissolved in mesitylene (solution concentration = 50mM) and 2.0 mL of this solution were placed in a quartz cell and deoxygenated by stirring in a dry box for at least 1 h. A Si(100) substrate was dipped in  $\text{H}_2\text{SO}_4/\text{H}_2\text{O}_2$  (3:1) solution for 12 min to remove organic contaminants, then it was etched in a hydrofluoric acid solution (1% v/v) for 90 s and quickly rinsed with water. The resulting hydrogenated silicon substrate was immediately placed in the above mentioned mesitylene solution. The cell remained under UV irradiation (254 nm) for 2 h. The sample was then removed from the solution and sonicated twice in dichloromethane for 10 min to remove residual physisorbed material.

**Host-guest system on silicon, Si-TiIII-B•1:** Si-TiIII-B wafer was dipped in a  $1 \times 10^{-3}$  M solution of guest **1** in  $\text{CH}_3\text{OH}$  for 60 min, sonicated in  $\text{CH}_3\text{OH}$  for 5 minutes and dried in nitrogen flux.

**Ternary complex on silicon with 2 and 3, Si-TiIII-B•1•2 and Si-TiIII-B•1•3:** Si-TiIII-B•1 was dipped in THF solutions of complexes **2** and **3** ( $1 \times 10^{-3}$  M) for 30 min, sonicated in THF for 5 minutes and dried in nitrogen flux.

**Photophysical measurements:** Absorption spectra were recorded in Hellma quartz cells (1 cm) with a Perkin-Elmer Lambda 950 UV/Vis/NIR spectrophotometer. Steady-state photoluminescence spectra and excitation spectra were recorded with an Edinburgh FLS920 spectrometer (continuous 450 W Xe lamp), equipped with a Peltier-cooled Hamamatsu R928 photomultiplier tube (185–850 nm). Emission quantum yields of Eu(III)-based samples were determined according to the approach described by Demas and Crosby,<sup>25</sup> using  $[\text{Ru}(\text{bipy})_3\text{Cl}_2]$  ( $\Phi_{\text{em}} = 0.028$  in air-equilibrated water solution)<sup>26</sup> as standard.

Excited state lifetimes in the ns time scale were measured with IBH 5000F time-correlated single-photon counting spectrometer, by using pulsed NanoLED excitation sources at 278 nm; analysis of the luminescence decay profiles was done with Decay Analysis Software DAS6 provided by the manufacturer. Emission decays in the ms time scale were measured with a Perkin-Elmer LS-50B spectrofluorimeter equipped with a pulsed Xe lamp and in gated detection mode. The phosphorescence decay analysis was performed with the PHOS Decay software provided by the manufacturer. Experimental uncertainties are

estimated to be  $\pm 2$  and  $\pm 5$  nm for absorption and emission peaks,  $\pm 20\%$  for emission quantum yields, and  $\pm 8\%$  for lifetimes.

**XPS measurements:** XPS spectra were run with a PHI 5600 multi-technique ESCA-Auger spectrometer adopting a standard Al  $K\alpha$  X-ray source. Analyses were carried out with a photoelectron angle of  $10^\circ$  (relative to the sample surface) with an acceptance angle of  $\pm 7^\circ$ . The XPS binding energy (B.E) scale was calibrated by centering the C 1s peak due to hydrocarbon moieties and “adventitious” carbon at 285.0 eV.<sup>27</sup>

### 3.5 Acknowledgements

This work was supported by EC (contract PITN-GA-2008-215399 - FINELUMEN). We thank Dr. Nicola Armaroli of Molecular Photoscience Group, Istituto per la Sintesi Organica e la Fotoreattività del CNR (ISOF-CNR) for support with the photophysical measurements and for fruitful discussion of the results. Centro Interdipartimentale Misure “G. Casnati” of the University of Parma is acknowledged for the use of NMR and HR ESI-MS facilities. Eu(hfac)<sub>3</sub> was kindly provided by Prof. Marek Pietraszkiewicz of the Institute of Physical Chemistry of the Polish Academy of Science, Warsaw.

### 3.6 References and Notes

1. W. A. Lopes, H. M. Jaeger *Nature* **2001**, *414*, 735-738.
2. J. Paczesny, A. Kamińska, W. Adamkiewicz, K. Winkler, K. Sozanski, M. Wadowska, I. Dziecielewski, R. Holyst *Chem. Mater.* **2012**, *24*, 3667-3673.
3. M. J. W. Ludden, D. N. Reinhoudt, J. Huskens *Chem. Soc. Rev.* **2006**, *35*, 1122-1134.
4. A. B. Descalzo, R. Martínez-Máñez, F. Sancenón, K. Hoffmann, K. Rurack *Angew. Chem. Int. Ed.* **2006**, *45*, 5924-5948.
5. D. J. Cram, J. M. Cram, *Container Molecules and Their Guests* (Ed.: J. F. Stoddart), The Royal Society of Chemistry, Cambridge, **1994**.
6. a) D. M. Rudkevich, J. Rebek, Jr. *Eur. J. Org. Chem.* **1999**, *9*, 1991-2005; b) H.-J. Choi, Y.-S. Park, J. Song, S.J. Youn, H.-S. Kim, S.-H. Kim, K. Koh, K. Paek *J. Org. Chem.*, **2005**, *70*, 5974-5981; c) T. Gottschalk, B. Jaun, F. Diederich *Angew. Chem. Int. Ed.* **2007**, *46*, 260-264; d) S. M. Biroš, J. Rebek, Jr. *Chem. Soc. Rev.*, **2007**, *36*, 93-104; e) M. Nikan, J. C. Sherman

- J. Org. Chem.* **2009**, *74*, 5211–5218; f) D. Ajami, J. Rebek, Jr. *Nat. Chem.* **2009**, *1*, 87–90; g) S. M. Grayson, B. C. Gibb *Soft Matter*, **2010**, *6*, 1377–1382; h) S. Liu, H. Gan, A. T. Hermann, S. W. Rick, B. C. Gibb *Nat. Chem.* **2010**, *2*, 847–852; i) F. Maffei, P. Betti, D. Genovese, M. Montalti, L. Prodi, R. De Zorzi, S. Geremia, E. Dalcanale *Angew. Chem. Int. Ed.*, **2011**, *50*, 4654–4657; j) J. Hornung, D. Fankhauser, L. D. Shirtcliff, A. Praetorius, W. B. Schweizer, F. Diederich *Chem. Eur. J.* **2011**, *17*, 12362–12371; k) J. Vachon, S. Harthong, E. Jeanneau, C. Aronica, N. Vanthuynne, C. Roussel, J.-P. Dutasta *Org. Biomol. Chem.* **2011**, *9*, 5086–5091.
7. F. Tancini, D. Genovese, M. Montalti, L. Cristofolini, L. Nasi, L. Prodi, E. Dalcanale *J. Am. Chem. Soc.* **2010**, *132*, 4781–4789.
8. E. Menozzi, R. Pinalli, E. A. Speets, B. J. Ravoo, E. Dalcanale, D. N. Reinhoudt *Chem. Eur. J.*, **2004**, *10*, 2199–2206; M. Dionisio, F. Maffei, E. Rampazzo L. Prodi, A. Pucci, G. Ruggeri, E. Dalcanale *Chem. Commun.* **2011**, *47*, 6596–6598.
9. a) M. Busi, M. Laurenti, G. G. Condorelli, A. Motta, M. Favazza, I. L. Fragala, M. Montalti, L. Prodi, E. Dalcanale *Chem. Eur. J.* **2007**, *13*, 6891–6898; b) E. Biavardi, M. Favazza, A. Motta, I. L. Fragalà, C. Massera, L. Prodi, M. Montalti, M. Melegari, G. G. Condorelli, E. Dalcanale *J. Am. Chem. Soc.*, **2009**, *131*, 7447–7455; c) C. Tudisco, P. Betti, A. Motta, R. Pinalli, L. Bombaci, E. Dalcanale, G.G. Condorelli *Langmuir* **2012**, *28*, 1782–1789.
10. a) S. H. Hsu, M. D. Yilmaz, C. Blum, V. Subramaniam, D. N. Reinhoudt, A. H. Velders, J. Huskens *J. Am. Chem. Soc.* **2009**, *131*, 12567–12569; b) M. D. Yilmaz, S. H. Hsu, D. N. Reinhoudt, A. H. Velders, J. Huskens *Angew. Chem. Int. Ed.* **2010**, *49*, 5938–5941; c) S. H. Hsu, M. D. Yilmaz, D. N. Reinhoudt, A. H. Velders, J. Huskens *Angew. Chem. Int. Ed.* **2013**, *52*, 714–719.
11. a) S. V. Eliseeva, J. C. G. Bünzli *Chem. Soc. Rev.* **2010**, *39*, 189–227; b) K. Binnemans *Chem. Rev.* **2009**, *109*, 4283–4374.
12. J.-C. G. Bünzli, A.-S. Chauvin, H. K. Kim, E. Deiters, S. V. Eliseeva *Coord. Chem. Rev.* **2010**, *254*, 2623–2633.
13. a) J.-C. G. Bünzli *Chem. Rev.* **2010**, *110*, 2729; b) S. V. Eliseeva, J.-C. G. Bünzli *New J. Chem.* **2011**, *35*, 1165–1176.

14. A. M. Nonat, A. J. Harte, K. Sénéchal-David, J. P. Leonard, T. Gunnlaugsson *Dalton Trans.* **2009**, 4703–4711.
15. G. G. Condorelli, C. Tudisco, A. Di Mauro, F. Lupo, A. Gulino, A. Motta, I. L. Fragalà *Eur. J. Inorg. Chem.* **2010**, 4121-4129.
16. A. Gulino, F. Lupo, G. G. Condorelli, A. Motta, I. Fragalà *J. Mater. Chem.*, **2009**, *19*, 3507-3511.
17. E. Biavardi, C. Tudisco, F. Maffei, A. Motta, C. Massera, G. G. Condorelli, E. Dalcanale *Proc. Natl. Acad. Sci. U.S.A.* **2012**, *109*, 2263–2268.
18. G. Accorsi, A. Listorti, K. Yoosaf, N. Armaroli *Chem. Soc. Rev.*, **2009**, *38*, 1690-1700.
19. A. Bencini, V. Lippolis *Coord. Chem. Rev.* **2010**, *254*, 2096–2180.
20. For the nomenclature adopted for phosphonate cavitands, see: R. Pinalli; M. Suman; E. Dalcanale *Eur. J. Org. Chem.*, **2004**, 451–462.
21. G. G. Condorelli, A. Motta, M. Favazza, I. L. Fragalà, M. Busi, E. Menozzi, E. Dalcanale *Langmuir*, **2006**, *22*, 11126-11133.
22. J. Qi, T. Matsumoto, M. Tanaka, Y. Masumoto *J. Phys. D*, **2000**, *22*, 2074-2078.
23. E. Biavardi, G. Battistini, M. Montalti, R. M. Yebeutchou, L. Prodi, E. Dalcanale, *Chem. Commun.* **2008**, 1638-1640.
24. B. Bibal, B. Tinant, J.-P Declercq, J.-P. Dutasta *Supramol. Chem.* **2003**, *15*, 25–32.
25. J. N. Demas, G. A. Crosby, *J. Phys. Chem.* **1971**, *75*, 991-1024.
26. K. Nakamaru, *Bull. Chem. Soc. Jpn.* **1982**, *55*, 2697 –2705.
27. a) I. L. Swift *Surf. Interface Anal.* **1982**, *4*, 47–51; b) D. Briggs & G. Beamson *Anal. Chem.* **1992**, *64*, 1729–1736.



# **Chapter 4**

## ***Cavitand-based luminescent dopants for liquid crystals cells***

### **4.1. Introduction**

Liquid crystals are materials which exhibit properties of two states of the matter – liquid and solid. They can flow just like ordinary liquids but at the same time be oriented like molecules in crystals, mostly having orientational order. Mesogenes, as are called liquid crystalline molecules, are usually highly anisotropic in shape. Most often they shape resemble cylinders or spindles. The most common liquid crystal phases are: nematic, smectic A, smectic C, smectic C\* (chiral) and cholesteric. Each of them is characterized by different alignment of molecules, as presented in Fig. 1. Nematic LCs have only orientational order and all molecules are pointing in one direction, called director. Smectic LCs have orientational order and some degree of positional order, as molecules are positioned in layers perpendicular to the director. In the smectic A layers are oriented  $90^\circ$  to director, the smectic C phase has a director tilted with respect to the layers. The chiral analogue of the smectic C phase is denoted by a star (\*). In this phase, the tilt direction of the mesogens rotates as one progresses through the layers. If a nematic liquid crystal is inherently chiral, then adjacent mesogens will have a preferential twist with respect to one another, which leads to the larger-scale twisting of the internal order. The chiral nematic phase is also called the cholesteric phase.

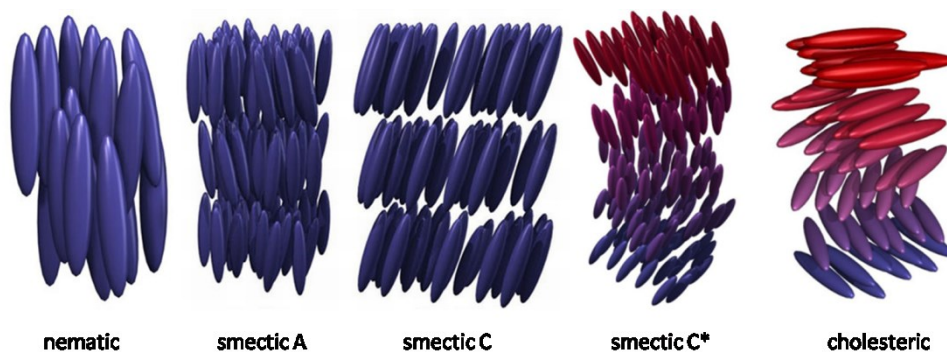


Figure 1. Schematic representations of a nematic LC phase, smectic LC phases oriented along (smectic A) and away (smectic C) from the normal of the layer, and a chiral LC phases – smectic C\* and cholesteric. [picture from [http://barrett-group.mcgill.ca/tutorials/liquid\\_crystal/](http://barrett-group.mcgill.ca/tutorials/liquid_crystal/)]

Luminescent materials emitting polarized light attract a lot of attention for their potential applications in flat panel displays and other optoelectronic devices.<sup>1</sup> Liquid crystalline dyes are of particular interest due to the fact that polarized absorption/emission intensity can be controlled by application of electric field, which changes orientation of molecules in the LC cells.<sup>2</sup> LCDs consume appreciable electric power for back light systems and in portable devices these displays decrease operational time when only battery is used. In addition, use of dye emitting only polarized light would cut down costs, since in device would have to be used only one polarizer instead of two used currently. However, development of fluorescent liquid crystals is challenging, as suitable molecules have to possess characteristics of both LCs and efficient dyes, which are not easy to incorporate in one molecule. It also limits the scope of colors which can be used in devices, as only organic compounds can be expected to form liquid crystal phases and, at the same time organic dyes have many limitations, as purity and range of colors and quantum yields. On this background emerged the idea of guest (dye) – host (LC) liquid crystal displays (GH-LCDs), which merges advantages of both: LCs and efficient organic/inorganic dyes.<sup>3,4</sup> For successful development of this kind of LCDs it is crucial to develop strongly fluorescent dyes with a highly dichroic property and strong emission in the blue-red region.<sup>5</sup>

The dichroism of dyes is a characteristic of the anisotropy of the molecular transition moment in either absorption or emission. When a dichroic dye with a geometric anisotropy is dissolved in a nematic liquid crystal, the dye molecules tend to arrange themselves in a way that their long molecular axis aligns along the LC director and a change of color intensity is obtained by controlling the direction of the LC molecules (Fig. 2). A rod-like, long molecular structure is favorable for a strongly dichroic dye. In principle, the design of



dichroic fluorescent molecules follows the same guidelines needed for the creation of highly dichroic absorption dyes.<sup>6</sup> In addition, it is necessary for the molecules to be strongly fluorescent, and the fluorescence should not be quenched by other molecules or by the LC matrix itself. In general, absorption dyes with a dichroic ratio ( $N$ ) of more than 8.0 are required for practical use of the absorption dyes in LCDs.<sup>7</sup>

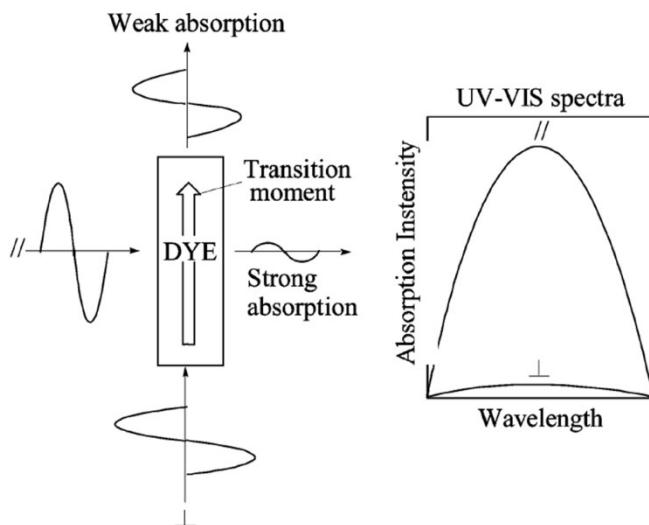


Figure 2. UV-Vis spectra of an idealized dye for GH-LCDs applications. (From Ref. 7)

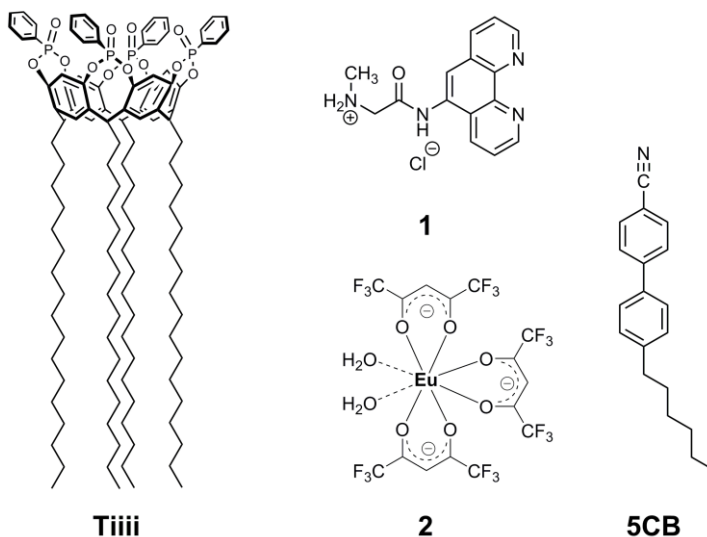
Most common dyes used in GH-LCDs are based on scaffold of strongly emitting organic dyes, like anthraquinone, naphthalimide,<sup>8</sup> acenequinone,<sup>9</sup> oligothiophene,<sup>10</sup> benzothiadiazole,<sup>5</sup> indole, and enzimidazole cyanine.<sup>11</sup> However these dyes are usually emitting in blue-orange range, while strong emitter in longer wavelength, particularly in red, are still rare.<sup>12</sup> One of the ways to overcome it might be use of lanthanide complexes, particularly of europium, which is known to emit strongly in red region.

Ternary complexes studied in solution and described in previous chapter seem to be good candidates as dyes for guest-host liquid crystal displays. The use of universal bidentate ligand – phenanthroline – allows easy exchange of luminescent complex within lanthanide group. Combination of complexes of  $\text{Eu}^{3+}$  (red luminescence),  $\text{Tb}^{3+}$  (green) and  $\text{Tm}^{3+}$  (blue) within one cell allow creation of emissive LC cell with pure RGB colours.<sup>13</sup>

In order to obtain RGB LC cell first we ran trails with europium ternary complex as model. Some modifications in structure of complex had to be introduced in order to increase solubility in liquid crystal matrix and enhance

rodlike shape, namely elongation of the alkyl chain at the lower rim of tetraphosphonate cavitands. These features in combination with already possessed characteristics, like high quantum yield, emission in visible region and stability, make this ternary complex a contender for GH-LCDs.

## 4.2. Results and discussion



Scheme 1. Structure of the molecules used in present work.

On scheme 1 are presented molecules employed as building blocks during this project. Compound **1** was synthesised in 2 steps from commercially available 5-Amino-[1,10]-phenanthroline and was presented in the previous chapter, together with synthesis of **Tiiii**. Dye **2** was chosen as strong red light emitter with high quantum yields and two empty coordination sites, ready for complexation. **5CB** is common compound exhibiting nematic liquid crystal properties in room temperature range and is commercially available. Tetraphosphonate cavitand **Tiiii** bears on lower rim four alkyl chains consisting of 17 carbon atoms, which we consider should be sufficient to provide good mixing with liquid crystals and to give molecule elongated shape triggering orientation of molecule along long axis of liquid crystals.

Formation of ternary complex is sketched on Figure 3. The sarcosine-phenanthroline **1** ligand was exposed, in the form of ammonium salt, to a tetraphosphonate cavitand to test the complexation in organic solution (first step). The formation of the host-guest complex was monitored by  $^1\text{H}$  and  $^{31}\text{P}$  NMR measurements. In particular, the signals of  $N\text{-CH}_3$  moiety moved more

than 3 ppm upfield to -0.64 ppm and other resonances attributed to sarcosine part as well as to phenanthroline unit were also shifted. The  $^{31}\text{P}$  resonance of the four P=O groups moved downfield of 4.5 ppm (from 7.6 to 12.1 ppm). The upfield shift of the methyl residue is diagnostic of *N*-CH<sub>3</sub> inclusion into the cavity, whereas the downfield shift of P=O signals is a clear indication of the participation of phosphonates in the guest complexation. The next step was the complexation of a suitable Europium complex, to this host-guest preformed species to form the desired ternary complex, namely Eu(hfac)<sub>3</sub> (Fig. 3, step B). Although Eu is paramagnetic complexation can be monitored by  $^{31}\text{P}$  NMR and by some means by  $^1\text{H}$  NMR. Formation of complex was also confirmed by High Resolution Mass Spectrometry measurements.

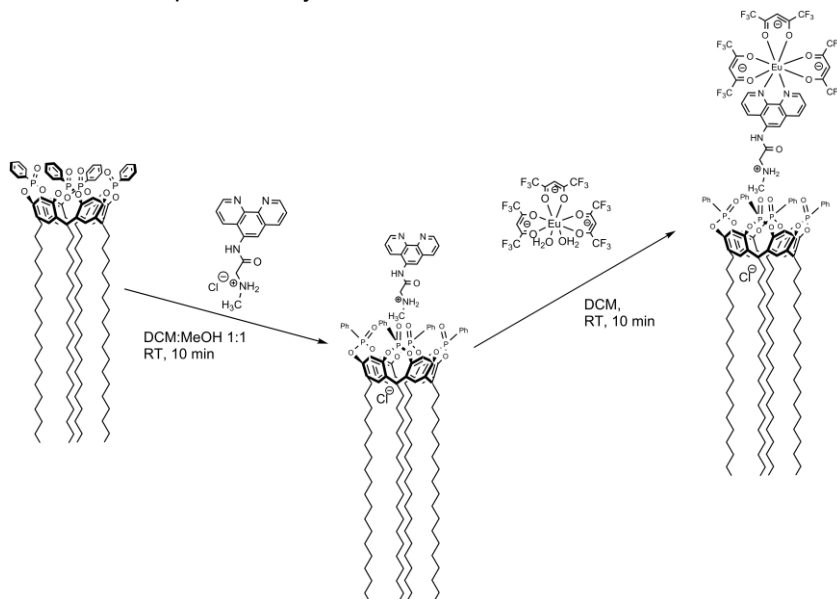


Figure 3. Formation of ternary complex.

The orientation properties of new-synthesized cavitand were investigated by means of measuring polarized absorption and luminescence spectra in aligned media. The experiments were implemented using a standard sandwich glass cell filled with mixture of nematic liquid crystal (4-cyano-4'-pentylbiphenyl - 5CB, clearing point 35°C) and ternary complex as a dopant (weight concentration: 1%). Cavitand structural formula is presented in Fig.3 (final product on the right). The thickness of the cell was approximately 50  $\mu\text{m}$ . The inner surfaces of the glass were covered with a thin nylon film. Surfaces of glasses were rubbed in one direction providing a strong uniaxial anchoring of

nematic LC molecules on the surfaces. Such oriented surfaces impose planar orientation of the nematic director for the whole cell.

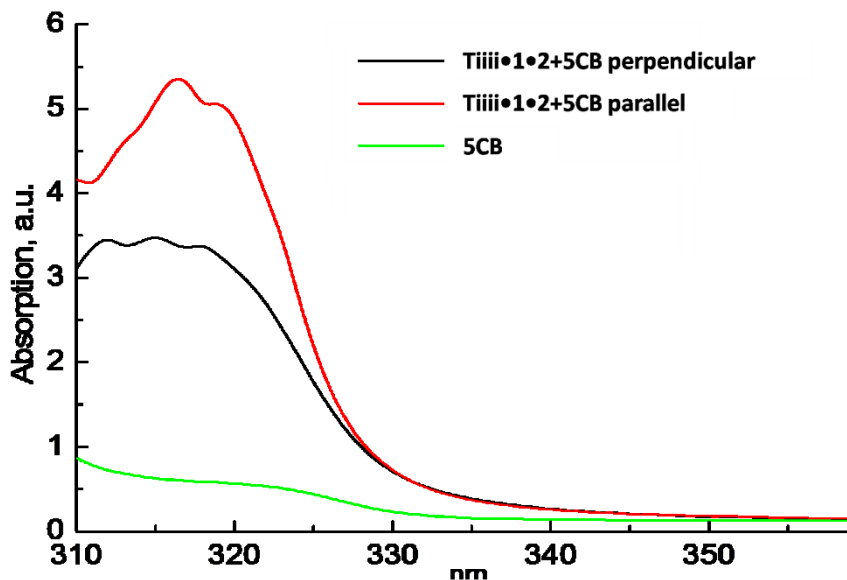


Figure 4. Parallel and perpendicular absorption spectra of **5CB** and **Tiii•1•2** mixture.

Parallel and perpendicular absorption spectra of **5CB** and **Tiii•1•2** mixture (1%) were obtained (Fig.4). The band near 320 nm which appears in absorption spectra arises from presence of **Tiii•1•2**. Its profile is alike to absorption spectra in DCM of similar ternary complexes, with only shorter chains on lower rim, as presented in previous chapter. Therefore the **5CB** matrix does not interfere with Europium complex absorption.

Anisotropy of complex absorption in parallel and perpendicular direction testifies that the transitions of cavitand absorption bands are aligned with the long cavitand axis. Dichroic ratio  $N_A$  is calculated as follows:

$$N_A = \frac{A_{par}}{A_{perp}}$$

and results are shown in Table 1. The obtained value is low in comparison with requirements<sup>7</sup> for  $N_A > 8$  for complex to act as LC dopant and in comparison with highest reported value for triphenodioxazine-based dyes of 22.1<sup>14</sup>, but it is promising for further studies.

Table 1.

	<b>Tiiii•1•2+5CB</b>
Dichroic ratio, $N_A$	1.57
Luminescence anisotropy, $S_{lum}$	0.16

Luminescence spectra of **Tiiii•1•2+5CB** (1%) (under the 340 nm excitation) are studied (Fig. 5). Luminescence band with the maxima nearly 437 nm (not shown) is caused by electron transition in **5CB** molecule, namely, by electron transition in biphenyl group.<sup>15</sup> Highly intensive luminescence band with the maxima nearly 615 nm is caused by  $^5D_0 \rightarrow ^7F_2$  transition in  $Eu^{3+}$  ion.

As it was mentioned before, LC cells were coated by parallel rubbed nylon layer, which provides the orientation of LC molecules as well as cavitand molecules parallel to the cell plane (parallel to the rubbing direction). In this way the Eu-based cavitands give higher emission under excitation with the polarization parallel to long molecular axis.

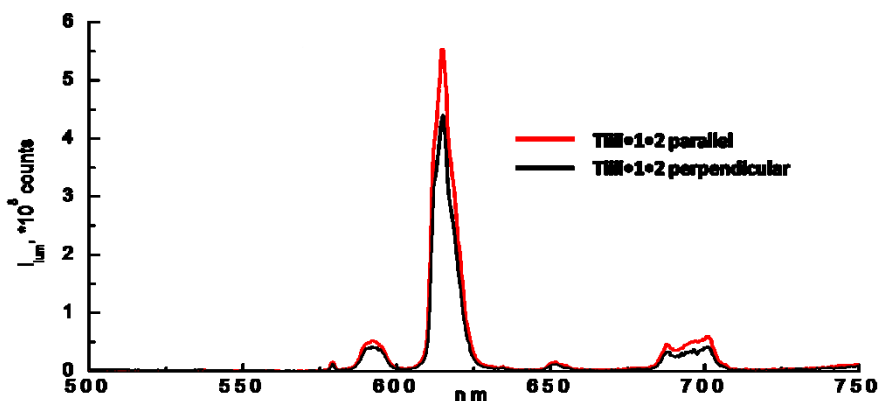


Fig. 5. Luminescence emission of Eu-based cavitand in **5CB**;  $\lambda_{ex}=340$  nm.

Luminescence anisotropy can be calculated as follows:

$$S_{lum} = \frac{I_{par} - I_{perp}}{I_{par} + I_{perp}}$$

and it is shown in Table 1. The obtained value is acceptable for complex as dopant in LC cells.

These results are promising for further activity. In particular orientation of LC molecules as well as cavitands can be changed by applying electrical field. This effect will result in decreasing of absorption and as a consequence lead to the decreasing of luminescence intensity. The polarized luminescence can be rapidly recovered upon voltage removal.

The next step in formation of RGB LC cell was design, synthesis and characterization of Terbium complex (emission in green region) followed by measurements in liquid crystal matrix. Tb(hfac)<sub>3</sub> complex is not commercially available so it has been synthesized by standard synthetic procedure developed by prof. Marek Pietraszkiewicz from IPC from Warsaw, and applied for these studies without further modifications. Terbium carbonate salt has been produced through anion exchange with potassium carbonate starting from Terbium nitrate. Product was then reacted with hexafluoroacetylacetone in diethyl ether. Resulting white solid was next recrystallized from mixture diethyl ether:hexane affording whitish-transparent needle-like crystals exhibiting green luminescence under standard UV lamp irradiation. Product has been characterized by ESI-MS, <sup>19</sup>F NMR and elemental analysis.

Formation of ternary complex is virtually the same as for europium complex, outlined on Figure 1, only with use of Tb(hfac)<sub>3</sub>. Firstly, the sarcosine-phenanthroline ligand was complexed by a tetraphosphonate cavitand. Monitoring of the reaction by <sup>31</sup>P NMR and <sup>1</sup>H NMR confirmed formation of host-guest assembly. Complexation of a terbium complex to this host-guest preformed species has proven to be difficult step. Tb is more paramagnetic than europium and monitoring by <sup>1</sup>H NMR was impossible, meanwhile in <sup>31</sup>P NMR were present 2 signals, suggesting the dimer complexation of Tb<sup>3+</sup> by the four P=O of the cavitand, bypassing the phenanthroline coordination. Unfortunately, the High Resolution Mass Spectrometry, that in the case of Eu ternary complex provided good evidence of its formation, returned no results.

### 4.3. Conclusions

In conclusions Eu-based cavitand+**5CB** mixture possesses highly intensive luminescence with the maxim nearly 615 nm at laser excitation ( $\lambda=340$  nm), which is polarized (luminescence anisotropy  $S_{lum}$  equals to 0.16) and exhibits moderate dichroism ( $N_A=1.57$ ). Therefore it can be assumed that cavitand based dopants for liquid crystal displays are a versatile group of dyes for further applications. The complexation of the other lanthanide ions (Tb<sup>3+</sup> and Tm<sup>3+</sup>) by the **Tiiii•1** complex turned out to be less straightforward than expected.

## 4.4. Experimental section

**General:** All commercial reagents were ACS reagent grade and used as received. Solvents were dried and distilled using standard procedures.  $^1\text{H}$  NMR spectra were recorded on Bruker Avance 400 (400MHz) and Bruker Avance 300 (300 MHz) NMR spectrometers. All chemical shifts ( $\delta$ ) were reported in parts per million (ppm) relative to proton resonances resulting from incomplete deuteration of NMR solvents. ESI-MS experiments were performed on a Waters ZMD spectrometer equipped with an electrospray interface. Exact mass was determined using a LTQ ORBITRAP XL Thermo spectrometer equipped with an electrospray interface. This section includes the synthesis of tetraphosphonate cavitand **Tiiii** and self assembly in the solution; the synthesis and characterization of the ligand **1** was reported in Chapter 3.  $\text{Eu}(\text{hfac})_3$  was kindly provided by Prof. Marek Pietraszkiewicz of the Institute of Physical Chemistry of the Polish Academy of Science, Warsaw. All of the luminescence measurements in liquid crystal cells were conducted at University of Ghent, in group of Prof. Kristiaan Neyts.

**Tiiii:** To a solution of heptadecyl-footed resorcinarene (130 mg, 0.090 mmol) in fresh distilled pyridine (10 mL), dichlorophenylphosphine (0.081 mL, 0.582 mmol) was added slowly, at room temperature. After 3 hours of stirring at 70 °C, the solution was allowed to cool at room temperature and 2 mL of aqueous 35%  $\text{H}_2\text{O}_2$  was added. The resulting mixture was stirred for 30 minutes at room temperature and  $\text{H}_2\text{O}$  (100 mL) was added and solution was filtrated. The solid was suspended in water (100 mL), sonicated for 30 min and filtrated again resulting as white powder (140 mg, 80%).  $^{31}\text{P}$  NMR (160 MHz,  $\text{CDCl}_3$ ): 7.6 (s, 4P).  $^1\text{H}$  NMR (400 MHz,  $\text{CDCl}_3$ ): 8.10-8.04 (m, 8H, PO-Ar- $\text{H}_o$ ), 7.64 (m, 4H, POAr $\text{H}_p$ ), 7.55-7.51 (m, 8H, POAr $\text{H}_m$ ), 7.31 (s, 4H, Ar- $\text{H}_{up}$ ), 7.02 (s, 4H, Ar- $\text{H}_{down}$ ), 4.82 (bt, 4H, Ar-CH-Ar), 2.36 (bd, 8H, -CH- $\text{CH}_2$ - $\text{CH}_2$ -), 1.47 (m, 8H, - $\text{CH}_2$ - $\text{CH}_2$ - $\text{CH}_3$ ), 1.28 (m, 112H, - $\text{CH}_2$ -( $\text{CH}_2$ ) $_{14}$ - $\text{CH}_3$ ), 0.90 (m, 12H, - $\text{CH}_2$ - $\text{CH}_3$ ).

**Tiiii•1:** To methanol solution containing **1** (11 mg, 0.040 mmol)  $\text{CH}_3\text{COCl}$  solution in methanol (0.403 M, 0.1 ml used) was added by drops. To this transparent solution cavitand **Tiiii-C** (78 mg, 0.040 mmol) was added. Mixture was stirred for 5 min at room temperature. Resulting orangish residue was dried under vacuum.  $^{31}\text{P}$  NMR (160 MHz,  $\text{CDCl}_3$ , 298 K): 12.1 (s, 4P).  $^1\text{H}$  NMR (400 MHz,  $\text{CDCl}_3$ , 298 K): **1**: 9.30 (bs, 2H), 9.02 (bs, 1H), 8.49 (m, 4H), 3.80 (s, 2H,  $\text{CH}_2$ ), -0.64 (s, 3H,  $\text{CH}_3$ ); **Tiiii**: 8.10 (m, 8H, PO-Ar-H), 7.69 (m, 4H, PO-Ar-H), 7.58 (m, 8H, PO-Ar-H), 7.25 (bs, 4H, Ar-H), 6.97 (bs, 4H, Ar-H), 4.78 (t, 4H, Ar-CH-Ar,  $J=6.6$  Hz), 2.85 (bs, 8H, CH- $\text{CH}_2$ - $\text{CH}_2$ ), 1.51 (bs, 8H, CH- $\text{CH}_2$ - $\text{CH}_2$ ), 1.42 (m, 112H,  $\text{CH}_2$ -( $\text{CH}_2$ ) $_{14}$ - $\text{CH}_3$ ), 0.89 (m, 12H,  $\text{CH}_2$ - $\text{CH}_2$ - $\text{CH}_3$ ).

**Ternary complex Tiiii•1•2: Tiiii-C•1** (29 mg, 0.013 mmol) and  $\text{Eu}(\text{hfac})_3$  (10.5 mg, 0.013 mmol) were solubilized in dichloromethane (10 mL) and solution was stirred for 1 hour at RT until everything was solubilized. Solvent was removed under reduced pressure and residue was dried under vacuum.  $^{31}\text{P}$  NMR (160 MHz,  $\text{CDCl}_3$ , 298 K): 12.6 (s, 4P). HR-MS: calculated for  $[\text{M-CI}]^+$   $\text{C}_{150}\text{H}_{190}\text{EuF}_{18}\text{N}_4\text{O}_{19}\text{P}_4^+$   $m/z=2971.19277$ , found  $m/z=2971.18155$ .

## 4.5. Acknowledgements

This work was supported by EC (contract PITN-GA-2008-215399 - FINELUMEN). Doping LC with dyes, fabrication of LC cell and all of the measurements of the cells were carried on in group of Prof. Kristian Neyts from University of Ghent, by PhD student Oksana Drobchak. Centro Interdipartimentale Misura "G. Casnati" of the University of Parma is acknowledged for the use of NMR and HR ESI-MS facilities.  $\text{Eu}(\text{hfac})_3$  was kindly provided by Prof. Marek Pietraszkiewicz of the Institute of Physical Chemistry of the Polish Academy of Science, Warsaw.

## 4.6. References and notes

1. D. Ford, S. M. Morris, H. J. Coles *Mater. Today* **2006**, *9*, 36-42.
2. X. Tong, Y. Zhao, B.-K. An, S. Y. Park, *Adv. Funct. Mater.* **2006**, *16*, 1799-1804.
3. G. H. Heilmeier, L. A. Zanoni *Appl. Phys. Lett.* **1968**, *13*, 91.
4. I. K. Grabtchev, V. B. Bojinov, I. T. Moneva, *J. Mol. Struct.* **1998**, *471*, 19-25.
5. X. Zhang, R. Yamaguchi, K. Moriyama, M. Kadowaki, T. Kobayashi, T. Ishii, T. Thiemann, S. Mataka, *J. Mater. Chem.* **2006**, *16*, 736-740.
6. A. V. Ivashchenko, *Dichroic Dyes for Liquid Crystal Displays*, **1994**, CRC Press, London.
7. X. Zhang, H. Gorohmaru, M. Kadowaki, T. Kobayashi, T. Ishii, T. Thiemann, S. Mataka, *J. Mater. Chem.* **2004**, *14*, 1901-1904.



8. I. Grabchev, I. Moneva, V. Bojinov, S. Guittonneau, *J. Mater. Chem.* **2000**, *10*, 1291-1296.
9. Z. Chen, T. Swager, *Org. Lett.* **2007**, *9*, 997-1000.
10. H. Iwanaga, K. Naito, F. Effenberger, *Liq. Cryst.* **2000**, *27*, 115-123.
11. Z.-H. Peng, L. Qun, X.-F. Zhou, S. Carroll, H. J. Geise, B.-X. Peng, R. Dommissie, R. Carleer, *J. Mater. Chem.* **1996**, *6*, 559-565.
12. M. Choi, D. Jin, T. J. Kang, S. C. Jeoung, H. Kim, D. Kim *J. Phys. Chem. B* **1997**, *101*, 8092-8097.
13. J.-C.G. Bünzli, G.R. Choppin, *Lanthanide Probes in Life, Chemical and Earth Sciences. Theory and Practice*, **1989**, Elsevier, Amsterdam.
14. T. Tanaka, T. Ashida, S. Matsumoto, *Chem. Lett.* **2011**, *40*, 573-575.
15. Yu. P. Piryatinskiĭ, O. V. Yaroshchuk, *Opt. Spectrosc.* **2000**, *89*, 942-948.



# CHAPTER 5

## *Phthalocyanines for Applications in Organic Photovoltaic Solar Cells*\*

### 5.1 Introduction

Limited amount of natural resources, growing population followed by increasing energy demand, hazards connected with current energy sources (atomic plant malfunctions), ultimately cost and political issues (energy independence) lead to seek alternative energy sources. Hydroelectric energy, wind energy, biomass, geothermal energy and solar energy contributed to the 19% worldwide energy consumption in 2011 according to *Renewables Energy Policy Network (REN'21)* report.<sup>1</sup> Taken out hydroelectric contribution, wind, solar, biomass and geothermal power accounted for 1.1% worldwide consumed energy. In particular, in the last years, solar power has established itself as the second fastest growing source of energy increasing its power capacity by a 60% in 2007-2012 period.

The first example of converting solar light into electric current was reported by young French scientist Becquerel in 1839.<sup>2</sup> Upon irradiation of Pt and Ag electrodes immersed in different acidic, basic and neutral solutions, he observed generation of small current in the system, phenomenon called Becquerel Effect. The era of modern photoelectrochemistry started for good in 1954 with the development of the first silicon solar cell in Bell Telephone Lab, USA, with an efficiency of 4.5%.<sup>3</sup> This kind of crystalline solar cells, known as the 1<sup>st</sup> generation solar cells, currently dominates the photovoltaic market (over 90% in 2008).<sup>4</sup> The efficiency of the single junction cells has a theoretical limit of about 30% (the Shockley–Queisser limit)<sup>5,6</sup> and currently the common silicon wafer based devices show an average of nearly 20% efficiency, with the highest reported efficiencies reaching 25%.<sup>7</sup> Their main drawback is the high price originating from the use of high purity silicon and from the processing technologies; moreover the devices are rigid and relatively heavy. These

---

\* The work presented in this chapter has been carried out on in the laboratories of Prof. Davide Bonifazi at the University of Namur, Belgium.

reasons were the driving force for the development of the 2<sup>nd</sup> generation solar cells. To overcome the cost issue, scientists decided to decrease the amount of expensive materials by depositing thin films on inexpensive substrates, preferably glass. The materials that proved to be more successful were amorphous silicon, CuIn(Ga)Se<sub>2</sub> (CIGS) and CdTe/CdS deposited on thin substrates by different techniques like solution deposition, vapor deposition, electroplating, etc.. Efficiency is usually lower, in respect to the 1<sup>st</sup> generation solar cells, with a maximum up to 19%, moreover the module efficiencies reach only a 14 % due to the difficulties in producing large scale homogeneous films.<sup>7</sup>

An alternative to these two classes of devices are the 3<sup>rd</sup> generation solar cells, which are using different materials and working principles. As for the 2<sup>nd</sup> generation, the main driving force here was a decrease in the costs together with an increase in efficiencies. The 3<sup>rd</sup> generation solar cells relies on multi junction solar cells, which can significantly increase the device efficiency via improvement in harvesting of photons and even overcome the theoretical limit of 30 %. Currently the highest efficiencies reported for multijunction solar cells are over 33 %.<sup>7</sup> Besides these three approaches there are also different types of solar cells, namely Dye-Sensitized Solar Cells (DSSCs)<sup>8,9</sup> and Organic Solar Cells (OSCs). DSSCs are based on combination of dyes with metal oxides and electrolyte. The efficiencies of DSSC are in the range of 12% for small lab scale devices, while the lifetime of the devices is rather low compared to inorganic solar cells.

The term Organic Solar Cells refers to devices which have layered structure, and the active absorbing layer comprises only organic materials, while for other layers (for example electrodes), metals and other inorganic materials can be used. There are a number of reasons that generated the big interest towards organic solar cells: a) they can be fabricated easily in a cost effective way; b) they are lightweight and flexible and c) their performance can be modulated by molecular designing and synthesis of new molecules. Functionalization is mostly driven by two factors: correction of energy levels (HOMO, LUMO) of semiconductor to optimize the system and peripheral functionalization in order to ease processing. For example phthalocyanines, typical absorbing material eager to lose electron upon irradiation, (electron donor), can be transformed into electron acceptors by changing the character of substituents from electron donating into electron withdrawing.<sup>10</sup>

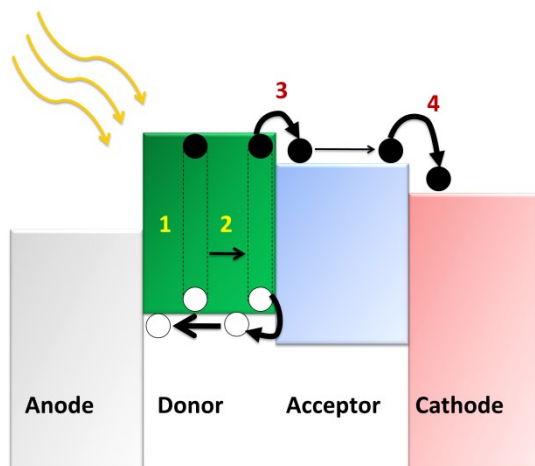


Figure 1. Schematic representation of photoelectric conversion mechanism in organic solar cell.

The mechanism by which the light is converted into electric power in organic photovoltaics (OPVs) consists of 4 basic steps (Figure 1): 1) The photon is absorbed by the active material (electron donor, D), which promotes the electron to the lowest unoccupied molecular orbital (LUMO), while leaving the positive charge carrier or the so called “hole”, in the highest occupied molecular orbital (HOMO). The excited pair electron-hole is still tightly bounded by coulomb attraction forces forming an exciton; 2) the exciton diffuses through the donor-acceptor interface (D-A) heterojunction; 3) if the interface energy level offset exceeds the exciton binding energy, the exciton is dissociated into free carriers at the donor-acceptor interface<sup>11,12</sup> and 4) finally the free carriers are being transported and collected at their respective electrodes.<sup>13</sup> The part of photogenerated excitons that reaches the D–A interface is called the exciton diffusion efficiency. Similarly, the charge collection efficiency is defined as the fraction of dissociated charge carriers that reaches the electrodes. In a planar heterojunction OPV, the device performance is limited by a low-absorption efficiency since the active layer thickness is comparable to the exciton diffusion length ( $L_D$ ), which is much smaller than the optical absorption length.<sup>11</sup>

The competition between the requirements for efficient optical absorption and exciton diffusion is known as the “exciton bottleneck”. Multiple approaches have been developed to overcome the exciton bottleneck and to realize efficient photoconversion in OPVs. One approach was to use long-lived phosphorescent materials, for example  $C_{60}$ ,<sup>14</sup> which permit larger  $L_D$  than with the use of fluorescent organic materials.<sup>14-18</sup> To date, the most significant improvements in device performance have come from advances in the control

of film composition and morphology. Architectures including mixed,<sup>19-21</sup> hybrid planar-mixed,<sup>22,23</sup> nanocrystalline,<sup>24,25</sup> and bulk,<sup>15, 26-28</sup> heterojunctions have attempted to overcome the short  $L_D$  by increasing the D–A interface area thereby improving the exciton diffusion efficiency. The use of a uniformly mixed D–A heterojunction is attractive as it permits efficient exciton diffusion by extending the dissociating interface throughout the film.<sup>19-21</sup> Unfortunately, the charge carrier mobility is typically reduced in these structures, especially in mixtures of small molecules, potentially leading to lower charge collection efficiency.<sup>29, 30</sup> A promising alternative to the use of uniform mixtures aggregates D–A heterojunctions (GHJs).<sup>19,31,32</sup> Careful fabrication of graded growth OPV cell with use of  $C_{60}$  and CuPc allow increase in power conversion of a 60% in comparison with planar heterojunction OPV and of a 20% with uniformly mixed heterojunction OPV consisting of the same materials. The GHJ has a larger D–A interface area than a planar heterojunction, and for an optimized composition profile, maintains a high-charge collection efficiency relative to a uniform mixture.

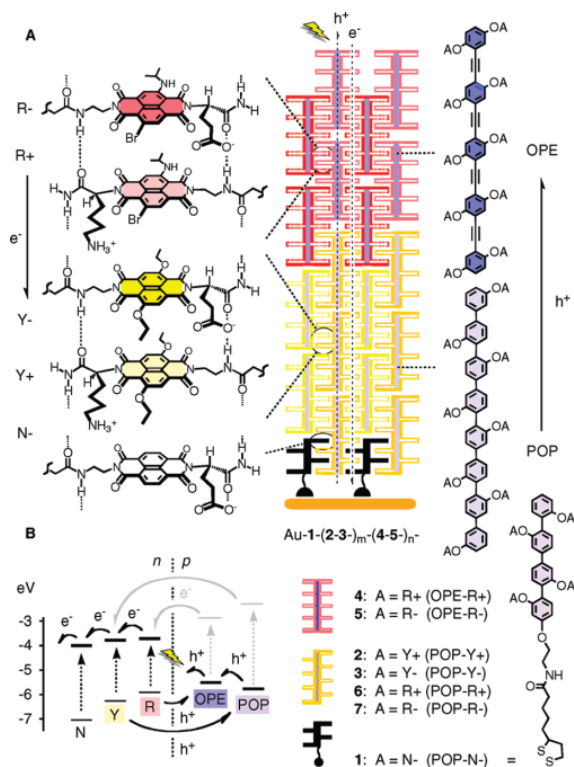


Figure 2. A) Molecular structures and hypothetical OMARG-SHJ architecture Au-1-(2-3)<sub>m</sub>(4-5)<sub>n</sub> of POP-N initiator (1) and POP-Y (2, 3) and OPE-R (4, 5) propagators on gold. B) HOMO and LUMO levels show photoinduced (dashed arrows) e<sup>-</sup> (gray) and h<sup>+</sup> (black) injection into e<sup>-</sup> (n)- and h<sup>+</sup> (p)-transporting pathways (bold) (from Ref.33).

Graded growth heterojunction OPVs realized by means of high vacuum thermal sublimation can be optimized by varying mixture composition, conditions, support, etc., as physicist in this process do not have direct means to control organization of molecules on the surface and during deposition. Chemists, on the other hand, can use weak interactions for assembly of molecules between themselves in a strictly controlled and predictable way. This approach was pioneered in the group of Stefan Matile from University of Geneva and is presented on Figure 2.<sup>33</sup> Scientists were able to organize complicated supramolecular system on gold surface by a combination of different supramolecular forces, like H-bonding and  $\pi$ - $\pi$  stacking. The system presented on Figure 2 is called OMARG-SHJ, which stays for Oriented Multicolored Antiparallel Redox Gradients Supramolecular Heterojunction. Gradient in charge channels is needed for transport on long distances and molecules having different absorption region, joined together, can contribute to capture whole solar light spectrum (panchromatism), increasing efficiency. Both  $e^-$  (or  $n^-$ ) and  $h^+$  (or  $p^-$ )-transporting channels are situated very close to each other, forming very large heterojunction, and, at the same, time minimizing possibility of recombination or trapping of charges.

The idea presented in this chapter is to organize different types of phthalocyanines, electron donor and acceptor, on surfaces in a planned and controlled manner. Phthalocyanines are known to form long columnar aggregates, which size depends on functionalization and conditions, both in solution and on the surfaces, due to their planarity and particular polarity. However, different types of phthalocyanines cannot be expected to aggregate together but might be “glued” using supramolecular forces, like hydrogen bonding, hydrophobic/hydrophilic interactions, and thermodynamic forces (Figure 3).

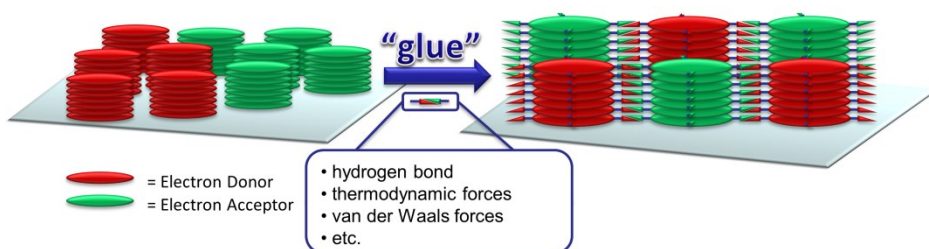


Figure 3. Idea of organization phthalocyanine columnar aggregates on surface.

Herein we present the synthesis of three different types of phthalocyanines (Pcs) designed to exploit their hydrophobic-hydrophilic characters as driving forces for assembly: 1) hydrophobic Pc functionalized with

long alkyl chains; 2) hydrophilic Pc bearing ethylene glycol derivatives; and 3) amphiphilic Pc bearing both functionalization.

## Columnar architectures on surfaces controlled by hydrophilic–hydrophobic interactions

### 5.1.1 General Design

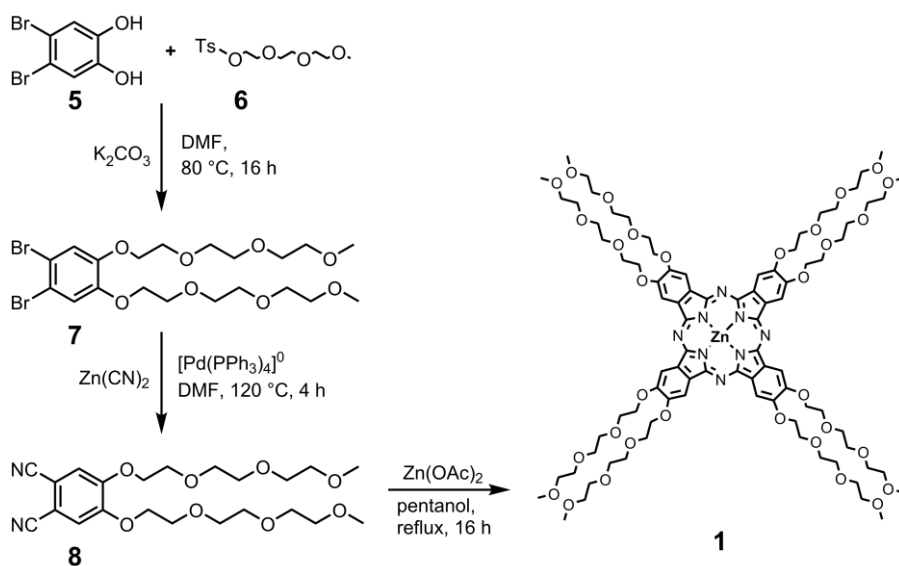
We designed electron donor and electron acceptor phthalocyanines with major differences on energy levels caused mostly by the central metal ion. Therefore functionalization on peripheries should not affect them, leaving us freedom in functionalization of Pcs peripheries.

We chose to obtain good mixing of these two types of Pcs, electron donor and acceptor, on surfaces by proper functionalization with hydrophobic/hydrophilic units. In our system we want to employ three types of molecules: hydrophobic Pc functionalized with dodecyloxy chains; hydrophilic Pc functionalized with triethylene glycol chains; and amphiphilic molecules bearing both functionalizations. At first we would like to test our hypothesis that two different types of Pcs, the hydrophobic and the hydrophilic, do not mix forming domains instead of a homogenous mixture.

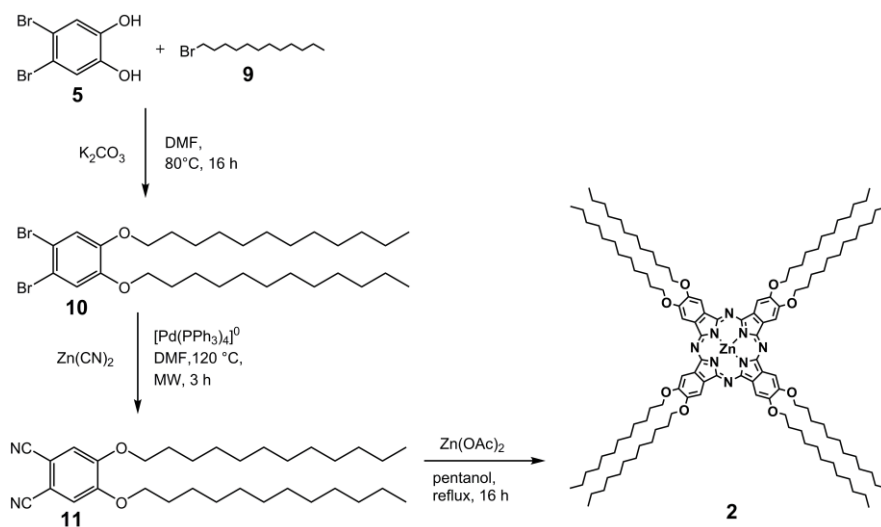
## 5.2 Results and discussion

Synthesis of molecules **1** and **2** (Schemes 1 and 2, respectively) was accomplished by condensations of suitable functionalized phthalonitriles in presence of metal salts. For both compounds, the same three steps synthesis protocol was followed.



Scheme 1. Synthesis of hydrophilic ZnPc **1**.

The synthesis of hydrophilic phthalocyanine **1** is presented in Scheme 1. Dibromocatechol **5** is reacted with triethylene glycol tosylate **6** giving **7** in good yield. Subsequent Pd-catalyzed cyanation gave **8** after purification in good yield. Phthalocyanine is then obtained in 8% total yield by reacting **8** with  $\text{Zn(OAc)}_2$  in refluxing pentanol. **1** is well soluble in polar solvents, including water.



Scheme 2. Synthesis of hydrophobic zinc ZnPc **2**.

The synthesis of hydrophobic ZnPc **2** is presented in Scheme 2. The starting material is dibromocatechol **5**, which is functionalized with long alkyl chains (**10**) by Williamson reaction with 1-bromododecane **9**. The subsequent Palladium catalyzed cyanation reaction with  $\text{Zn}(\text{CN})_2$  in DMF was carried out in the microwave, since the reaction under standard conditions gave poor yields. The final macrocyclization was conducted in refluxing pentanol in presence of zinc acetate obtaining **2** in 12% total yield.

Then, the optical properties and the formation of assemblies on surfaces of compounds **1** and **2** were evaluated. First, we observed the formation of aggregates in solution by means of UV-Vis absorption spectrometry. To a  $5 \times 10^{-5}$  M solution of **1** or **2** in  $\text{CHCl}_3$  (300  $\mu\text{L}$ ) 300  $\mu\text{L}$  of MeOH were added (Figure 4). In the case of solution of **1** the absorption peaks are stronger upon addition of methanol due to the aggregates breakage. The opposite behaviour is observed for molecule **2**: addition of polar solvent causes formation of aggregates, as absorption peaks becomes weaker and smudgy.

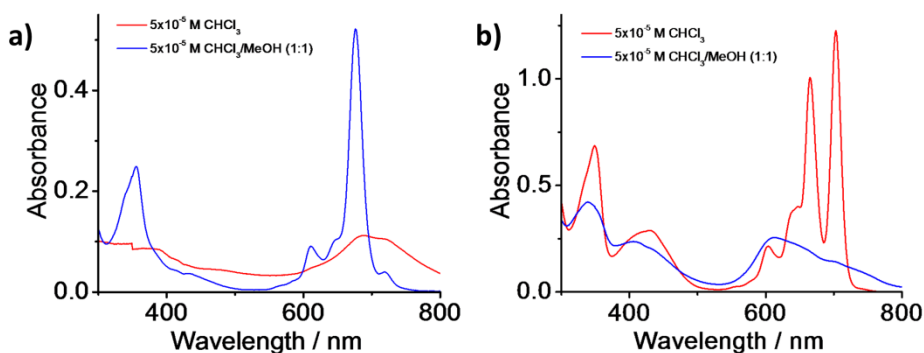


Figure 4. UV-Vis absorption spectra of **1** (a) and **2** (b) in  $\text{CHCl}_3$  (300  $\mu\text{L}$ ), red line, and upon addition of 300  $\mu\text{L}$  of MeOH, blue line.

Since we observed the formation of aggregates for **2** when methanol was added, we decided to verify this in the solid state. 300  $\mu\text{L}$  of  $5 \times 10^{-5}$  M solution of **2** in  $\text{CHCl}_3$  were rapidly added to 3 mL of MeOH. The solution was kept at room temperature for 15 hours and then drop casted onto silicon wafer surface. The surface was covered with nanoparticles, which homogeneity was then controlled with SEM technique. Formation of aggregates is homogeneous over vast areas (Figure 5 a-d). These species are very small (Figure 5d). From these images it is impossible to conclude that we have the formation of columnar aggregates or of some other type of aggregates. We tried also to form

aggregates from a solution containing both **1** and **2**, but in this case addition of MeOH to the chloroform solution caused the aggregation of **2** and the dissolution of the aggregates of **1**. In the solid state, nanoparticles formed on silicon surface from this solution treated in the same way as **2**, were very similar to the results shown in Figure 5 and the size of nanoparticles was in the same range. Therefore we can assume that **1** and **2** did not mix in solid state, otherwise the size of nanoparticles should differ.

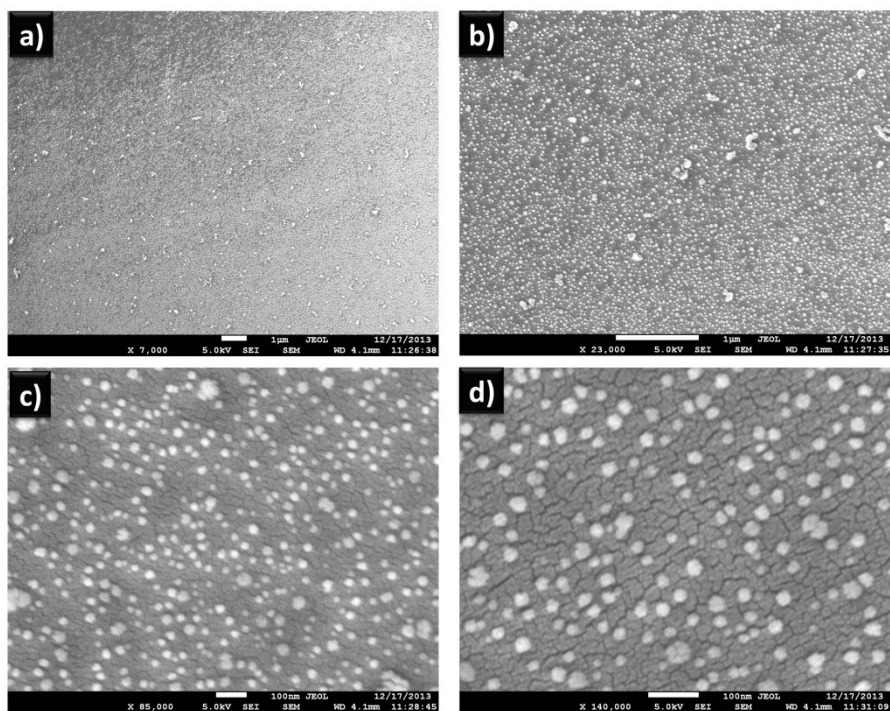


Figure 5. SEM images of aggregates of **2** on silicon. Zooming in from a) to d).

In order to facilitate the mixing of the two compounds **1** and **2**, we decided to use the amphiphilic molecule as a connector, as mentioned before in paragraph 5.1. Two target molecules for the amphiphilic Pc are shown in Scheme 3, namely **3** and **4**. They both have 4 alkyl chains and 4 PEG chains, but **3** is ABAB type while **4** is AABB type. We expect compound **3** to be less effective in mixing than molecule **4** since the different polarity substituents are adjacent (Figure 6). Four adjacent units of the same character should be more efficient in formation of self-assembly with other molecule bearing the same motifs, than only 2 like in case of **3**.

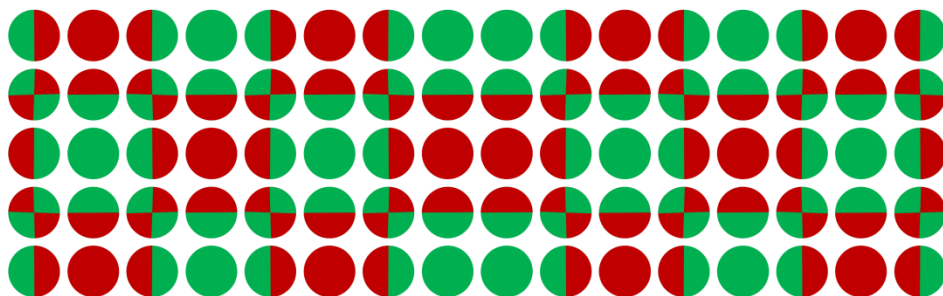
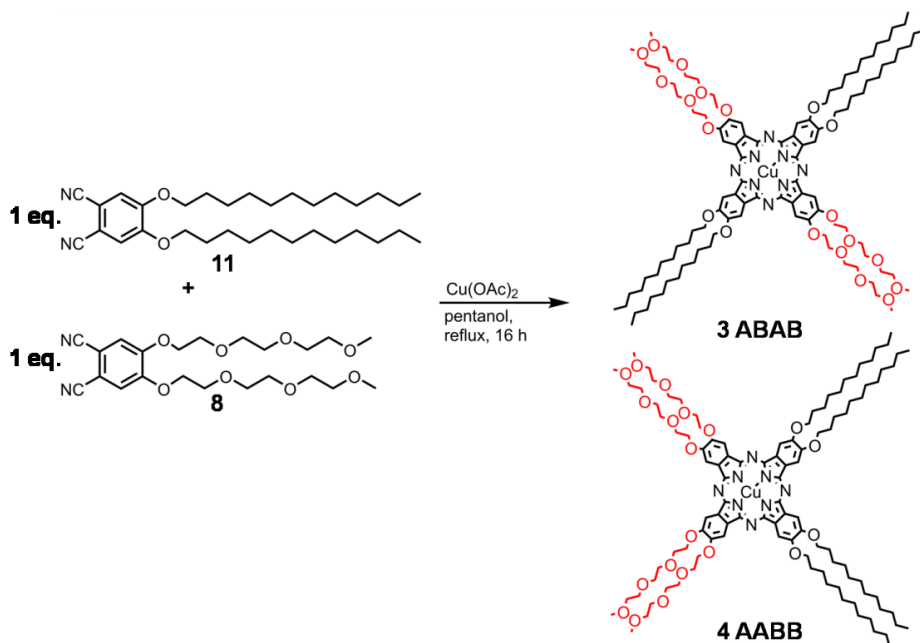


Figure 6. 2D view of hypothetical mixing of molecules **1** (red circle), **2** (green circle), **3** (quarter red, quarter green circle) and **4** (half red, half green circle) on surface.

The synthesis of molecules **3** and **4** is depicted in Scheme 3. Monomers **8** and **11** in equal molar quantities were mixed in presence of copper salt in refluxing pentanol for 16 hours. Copper was chosen to better differentiate the two phthalocyanines **3** and **4** from **1** and **2**. The reaction mixture, containing all the possible isomers, was subjected to several chromatographic columns in order to isolate **3** and **4** in pure form; however, it was impossible to isolate the individual isomers, or even the enriched mixture. Problems connected with the purification arise from equal solubility and polarity of **3** and **4**, since both molecules have the same functional groups in equal amounts.



Scheme 3. Synthesis of mixed AABB and ABAB zinc phthalocyanines.

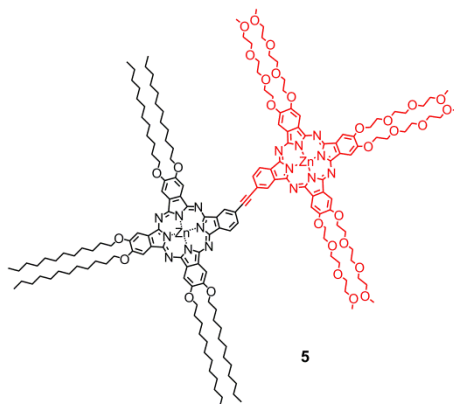


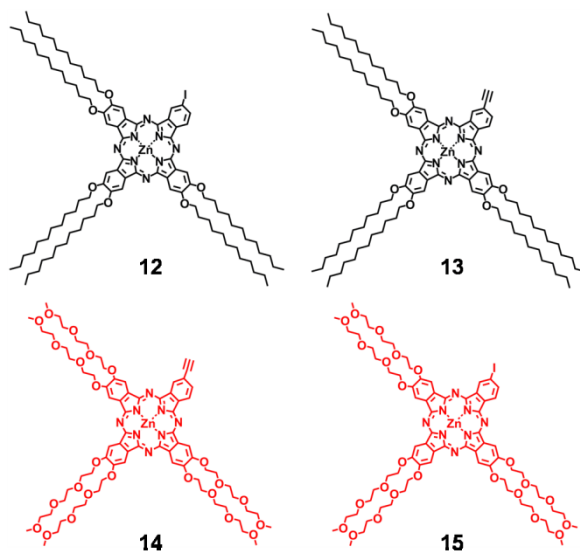
Figure 7. Molecular structure of target molecule **5** – hydrophobic-hydrophilic dyad.

Due to these purification problems we decided to change strategy and synthesize the dyad shown in Figure 7, which consists of two asymmetric phthalocyanines joined by a triple bond. The requirements for this Janus-type molecule **5** were the follows: i) it should retain character of both hydrophobic and hydrophilic Pcs; ii) the bond between Pcs should be conjugated and should allow formation of columnar aggregates; iii) ease of synthesis. In the literature similar dyads are reported, joined by triple bonds, which can be introduced by Sonogashira cross-coupling reaction. The starting molecules should possess either terminal triple bonds or iodides.

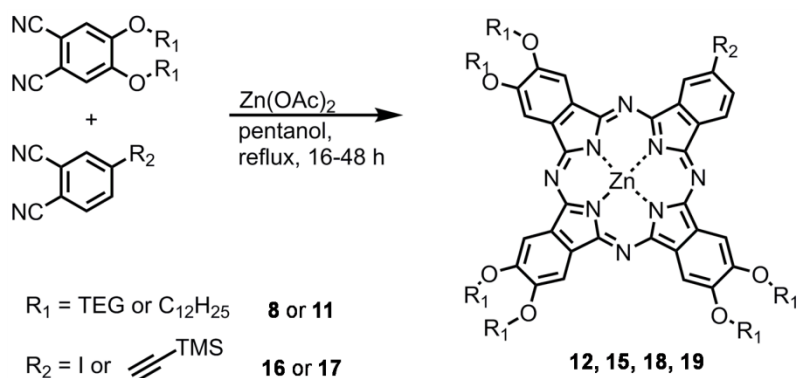
Dyad **5** precursors are therefore Pcs bearing terminal alkyne or iodide functional groups, e.g. **12** and **14**. However, since there is a large difference in solubility between hydrophilic and hydrophobic Pc **1** and **2**, we decided to test Sonogashira reaction first between monomers of different functionality, iodide or alkyne, but of the same character, e.g. **12** and **13** and **14** with **15**. In addition, having hydrophilic or hydrophobic dyad we could test formation of aggregates in the solution and on the solid state and evaluate effect of junction between them on aggregation properties.

Therefore we decided to synthesise a series of asymmetric phthalocyanines presented on Scheme 4, all following reaction depicted on Scheme 5. Pcs **13** and **14** could not be synthesised directly, since the presence of the triple bond during Pc formation could lead to byproducts. Therefore we decided to prepare TMS protected derivatives, **18** and **19** (Scheme 5). Phthalonitrile with TMS-protected triple bond **17** was synthesised by Sonogashira reaction of 4-iodophthalonitrile **16** and TMS-acetylene in presence of palladium. All ZnPcs **12**, **15**, **18**, **19**, were synthesised as in the previous

cases by cyclization of stoichiometric mixtures of starting phthalonitriles in ratio 2:1, where **16** and **17** were the less abundant. The purification of all 4 compounds was very demanding, as the reaction mixture contained other products of cyclization, namely isomers  $A_2B_2$  and  $A_4$ . Often their polarity was very similar to polarity of desired  $A_3B$  isomer. Several chromatographic columns had to be run for every compound but unfortunately MALDI analysis still revealed the presence of the unwanted isomers. Currently all the Pcs are still under purification.



Scheme 4. Four target asymmetric phthalocyanines for synthesis of dyad **5**.



Scheme 5. Synthesis of asymmetric phthalocyanines.

### 5.3 Conclusions

Two different phthalocyanines, hydrophobic and hydrophilic were synthesized, and their behaviour in solid state was investigated by means of UV-Vis spectrometry and SEM microscopy. The two Pcs presenting different polarity do not form mixed aggregates, therefore amphiphilic molecules possessing functionalities of both type were designed and their synthesis was carried on. The first attempt to prepare amphiphilic phthalocyanines, by stoichiometric condensation of two different phthalonitriles, yielded inseparable mixture of products and isomers. Change in design led to “Janus-type” molecule –dyad composed of two asymmetric Pcs, hydrophilic and hydrophobic, joined by triple bond. Currently we are pursuing synthesis of the dyads purifying and characterizing asymmetric Pcs.

### 5.4 Experimental Section

**General:** All commercial reagents were ACS reagent grade and used as received. Solvents were dried and distilled using standard procedures.  $^1\text{H}$  NMR spectra were recorded on a 400 MHz NMR (*Jeol JNM EX-400*) or 270 MHz (*JeolJNM EX-270*) NMR spectrometers. All chemical shifts ( $\delta$ ) were reported in parts per million (ppm) relative to proton resonances resulting from incomplete deuteration of NMR solvents. ESI-MS experiments were performed on a Waters ZMD spectrometer equipped with an electrospray interface.

#### 4,5-dibromobenzene-1,2-diol 5:

To a 250 mL round-bottomed flask 7 mL of bromine (0,136 mol, 2 eq.) solubilised in 10 mL of  $\text{CHCl}_3$  were added by drops over 1,5 hour to brown solution of catechol (7,5 g, 0,068 mol, 1 eq.) in  $\text{CHCl}_3$  at  $0^\circ\text{C}$ . Then the reaction was allowed to warm up to room temperature and was stirred for 18 hours. Upon addition the solution changed colour to orange and a white precipitate was formed. Evolving white fumes has been run through 1 M water solution of NaOH. Upon total consumption of catechol, as evidenced by TLC (95:5 DCM:MeOH), solution has been filtered and washed thoroughly with  $\text{CHCl}_3$  (300 mL) and dried on vacuum pump yielding dibromocatechol (11,66 g, 64 %).

$^1\text{H}$  NMR (400 MHz, Acetone- $d_6$ , 298 K):  $\delta$  (ppm) 7.12 (s, 2H, Ar-H).

#### 1,2-dibromo-4,5-bis(2-(2-(2-methoxyethoxy)ethoxy)ethoxy)benzene 7:

To an oven-dried 50 mL round-bottomed flask charged with **5** (0.5 g, 1.87 mmol, 1 eq.) in dry DMF (20 mL) was added oven-dried  $K_2CO_3$  (1.29 g, 9.34 mmol, 5 eq.). The mixture was stirred at room temperature for 20 min. **6** (1.31 g, 4.1106 mmol, 2.2 eq.) was added and solution was stirred at 80°C for 16 h in Ar atmosphere. Reaction mixture was then cooled to room temperature, solubilised in 40 mL of AcOEt, washed twice with 15 mL of a saturated water solution of  $NH_4Cl$ , 15 mL of water and 10 mL of brine. Organic phase was dried with  $MgSO_4$  and evaporated giving 0.95 g of crude solid which had at least 80% purity (by  $^1H$  NMR) and was used without further purification in the next step.

$^1H$  NMR (400 MHz,  $CDCl_3$ , 298 K):  $\delta$  (ppm) 7.12 (s, 2H, Ar-H), 4.11 (t,  $J=9.8$  Hz, 4H,  $ArOCH_2$ ), 3.82 (t,  $J=5.0$  Hz, 4H,  $ArOCH_2CH_2$ ), 3.70 (m, 4H,  $OCH_2$ ), 3.64 (m, 8H,  $OCH_2$ ), 3.54 (m, 4H,  $OCH_2$ ), 3.36 (s, 6H,  $CH_3$ ).

#### 4,5-bis(2-(2-(2-methoxyethoxy)ethoxy)ethoxy)phthalonitrile **8**:

In an oven-dried 50-mL two-necked round-bottomed flask purged with Ar, a solution of **7** (0.95 g, 1.6956 mmol, 1 eq.) and  $Zn(CN)_2$  (0.24 g, 2.04 mmol, 1.2 eq.) in dry DMF (20 mL) was deoxygenated *via* three freeze-pump-thaw cycles with Ar.  $[Pd(PPh_3)_4]^0$  (0.196 g, 0.1696 mmol, 0.1 eq.) was added and the resulting solution heated at 120°C for 4 h. After cooling to room temperature,  $NH_4OH$  was added. The resulting solution was stirred for 1 h and triple extracted with DCM (3 x 50 mL) in presence of 3 mL of brine. Combined organic phases were washed once with brine (20 mL), dried over  $MgSO_4$  and evaporated. Column chromatography (Cy/AcOEt 1:1) provided the product **8** as a white solid (570 mg, 74%).

$^1H$  NMR (400 MHz,  $CDCl_3$ , 298 K):  $\delta$  (ppm) 7.23 (s, 2H, Ar-H), 4.21 (t,  $J=4.6$  Hz, 4H,  $ArOCH_2$ ), 3.85 (t,  $J=4.6$  Hz, 4H,  $ArOCH_2CH_2$ ), 3.68 (m, 4H,  $OCH_2$ ), 3.60 (m, 8H,  $OCH_2$ ), 3.50 (m, 4H,  $OCH_2$ ), 3.33 (s, 6H,  $CH_3$ ).

$^{13}C$  NMR (100 MHz,  $CDCl_3$ , 298 K):  $\delta$  (ppm) 152.48, 117.15, 115.90, 108.76, 71.97, 71.05, 70.73, 70.64, 69.52, 69.45, 59.08.

#### Hydrophilic Pc, 2,3,9,10,16,17,23,24-octa(2-(2-(2-methoxyethoxy)ethoxy)ethoxy)phthalocyaninato zinc(II) **1**

To an oven-dried 50-mL two-necked round-bottomed flask purged with Ar, a solution of **8** (100 g, 0.22 mmol, 4 eq.) and  $Zn(OAc)_2$  (10 g, 0.05 mmol, 1 eq.) in hexanol (10 mL) was added. The mixture was stirred for 16 h at reflux. After



cooling to room temperature, the solvent was evaporated *in vacuo* and the residue purified by repeated column chromatography preparative TLC (gradient, DCM→DCM/MeOH9:1) providing Pc **1** (10 mg, 10 %).

$^1\text{H}$  NMR (400 MHz,  $\text{CDCl}_3$ , 298 K):  $\delta$  (ppm) 8.90 (s, 8H, Ar-H), 4.73 (t,  $J=4.4$  Hz, 16H,  $\text{ArOCH}_2$ ), 4.16 (t,  $J=5.0$  Hz, 16H,  $\text{ArOCH}_2\text{CH}_2$ ), 3.90 (t,  $J=5.1$  Hz, 16H,  $\text{OCH}_2$ ), 3.75 (t,  $J=4.4$  Hz, 16H,  $\text{OCH}_2$ ), 3.68 (t,  $J=4.9$  Hz, 16H,  $\text{OCH}_2$ ), 3.53 (t,  $J=4.9$  Hz, 16H,  $\text{OCH}_2$ ), 3.32 (s, 24H,  $\text{CH}_3$ ).

MALDI TOF-TOF: calc. for  $[\text{M}]^+$   $\text{C}_{88}\text{H}_{128}\text{N}_8\text{O}_{32}\text{Zn}$   $m/z = 1875.3834$ , found  $[\text{M}]^+$   $m/z = 1875.7668$ .

### 1,2-dibromo-4,5-bis(dodecyloxy)benzene **10**:

To a round-bottomed flask charged with solution of **5** (1 g, 3.73 mmol, 1 eq.) in dry DMF (35 mL), oven-dried  $\text{K}_2\text{CO}_3$  (2.68 g, 18.66 mmol, 5 eq.) was added at room temperature. After 30 min bromododecane (1.99 mL, 8.21 mmol, 2.2 eq.) was added and reaction was completed after 16 h at  $80^\circ\text{C}$  as revealed by TLC (Cy/AcOEt 7:3). Solution was cooled to room temperature and the solvent was evaporated under vacuum. The residue was then solubilised in AcOEt (30 mL), washed with saturated water solution of  $\text{NH}_4\text{Cl}$  (3 x 15 mL) and brine (10 mL), dried with  $\text{MgSO}_4$  and evaporated giving 2.26 g (quantitative yield) of pure product **10**.

$^1\text{H}$  NMR (400 MHz,  $\text{CDCl}_3$ , 298 K):  $\delta$  (ppm) 7.05 (s, 2H, Ar-H), 3.93 (t,  $J=6.6$  Hz, 4H,  $\text{CH}_2\text{OAr}$ ), 1.79 (m, 4H,  $\text{OCH}_2\text{CH}_2$ ), 1.44 (m, 4H,  $\text{O}(\text{CH}_2)_2\text{CH}_2$ ), 1.26 (bs, 32H,  $\text{O}(\text{CH}_2)_3\text{CH}_2$ ), 0.88 (t,  $J=6.7$  Hz, 6H,  $\text{CH}_3$ ).

### 4,5-bis(dodecyloxy)phthalonitrile **11**:

5-mL microwave vial was charged with **10** (605 mg, 1.00 mmol, 1 eq.) and  $\text{Zn}(\text{CN})_2$  (141 mg, 1.20 mmol, 1.2 eq.) in dry and deoxygenated (*via freeze-pump-thaw* cycle once with Ar) DMF (3 mL).  $[\text{Pd}(\text{PPh}_3)_4]^0$  (0.115 g, 0.10 mmol, 0.1 eq.) was added and the resulting mixture was stirred for 2 h under microwave irradiation ( $120^\circ\text{C}$ , 0 bar internal pressure, very high power). After cooling to room temperature,  $\text{NH}_4\text{OH}$  was added and the solution was stirred 1 h followed by extraction with DCM (3 x 50 mL). Combined organic phases were evaporated and purified by column chromatography (gradient Cy/DCM2:1→0:1) provided the desired product **11** as a white solid (373 mg, 75%).

$^1\text{H}$  NMR (400 MHz,  $\text{CDCl}_3$ , 298 K):  $\delta$  (ppm) 7.10 (bs, 2H, Ar-H), 4.02 (bt, 4H,  $\text{CH}_2\text{OAr}$ ), 1.82 (m, 4H,  $\text{OCH}_2\text{CH}_2$ ), 1.43 (bs, 4H,  $\text{O}(\text{CH}_2)_2\text{CH}_2$ ), 1.24 (bs, 32H,  $\text{O}(\text{CH}_2)_3\text{CH}_2$ ), 0.86 (bt, 6H,  $\text{CH}_3$ ).

**Hydrophobic Pc, 2,3,9,10,16,17,23,24-octadodecyloxyphthalocyaninato zinc(II) 2**

Oven-dried 25-mL round-bottomed flask purged with Ar, was charged with **16** (200 g, 0.40 mmol, 4 eq.) and  $\text{Zn}(\text{OAc})_2$  (19 g, 0.10 mmol, 1 eq.) and pentanol (10 mL) at room temperature. The mixture was stirred for 24 h at reflux. After cooling to room temperature, the solvent was evaporated *in vacuo*, the residue solubilized in minimal quantity of dichloromethane and precipitated by addition of EtOH. After 1 h at 5 °C the precipitate was filtrated and subjected to column chromatography (gradient,  $\text{DCM} \rightarrow \text{DCM}/\text{MeOH} 9:1$ ) providing Pc **2** (46 mg, 24%).

$^1\text{H}$  NMR (270 MHz,  $\text{CDCl}_3$ , 298 K):  $\delta$  (ppm) 8.89 (s, 8H, Ar-H), 4.50 (t,  $J=8.8$  Hz, 16H,  $\text{ArOCH}_2$ ), 2.06 (m, 16H,  $\text{OCH}_2\text{CH}_2$ ), 1.63 (m, 16H,  $\text{O}(\text{CH}_2)_2\text{CH}_2$ ), 1.41 (m, 16H,  $\text{O}(\text{CH}_2)_3\text{CH}_2$ ), 1.22 (m, 128H,  $\text{O}(\text{CH}_2)_3\text{CH}_2$ ), 0.82 (bt, 24H,  $\text{CH}_3$ ).

MALDI TOF-TOF: calc. for  $[\text{M}]^+$   $\text{C}_{128}\text{H}_{208}\text{N}_8\text{O}_8\text{Zn}$   $m/z = 2052.4640$ , found  $[\text{M}]^+$   $m/z = 2052.5334$ .

**Amphiphilic Pcs, 2,3,9,10-tetradodecyloxy-16,17,23,24-tetra(2-(2-(2-methoxyethoxy)ethoxy)ethoxy)phthalocyaninato copper(II) 3 and 4**

In an oven-dried 50-mL two-necked round-bottomed flask purged with Ar, a solution of **8** (52 g, 0.115 mmol, 2 eq.), **11** (58 g, 0.115 mmol, 2 eq.) and  $\text{Cu}(\text{OAc})_2$  (10 g, 0.058 mmol, 1 eq.) in pentanol (15 mL) was placed at room temperature. The mixture was stirred for 16 h at reflux. After cooling to room temperature, the solvent was evaporated *in vacuo* and the residue purified by repeated column chromatography and preparative TLC (gradient,  $\text{DCM} \rightarrow \text{DCM}/\text{MeOH} 9:1$ ), yet not providing pure isomers **3** and **4**.

MALDI TOF-TOF: calc. for  $[\text{M}]^+$   $\text{C}_{108}\text{H}_{168}\text{CuN}_8\text{O}_{20}$   $m/z = 1962.0880$ , found  $[\text{M}]^+$   $m/z = 1962.1321$ ; also calc. for  $[\text{M}]^+$   $\text{C}_{88}\text{H}_{128}\text{N}_8\text{O}_{32}\text{Zn}$   $m/z = 1875.3834$ , found  $[\text{M}]^+$   $m/z = 1875.7668$ .

**2,3,9,10,16,17-hexadodecyloxy-23-iodophthalocyaninato zinc(II) 12**

Oven-dried 10-mL schlenk tube purged with Ar, was charged with a solution of **11** (150mg, 0.30mmol, 6 eq.), 4-iodophthalonitrile (13mg, 0.05mmol, 1 eq.) and Zn(OAc)<sub>2</sub> (20 g, 0.10 mmol, 2 eq.) in pentanol (4 mL) at room temperature. The mixture was stirred for 24 h at reflux. Reaction was cooled to room temperature and solvent was evaporated *in vacuo*. Repeated column chromatography (gradient, DCM→DCM/MeOH 9:1) and preparative thin layer chromatography failed to provide the pure product, which is present in the mixture.

MALDI TOF-TOF: calc. for [M]<sup>+</sup> C<sub>104</sub>H<sub>159</sub>IN<sub>8</sub>O<sub>6</sub>Zn m/z = 1809.7215, found [M]<sup>+</sup>m/z = 1809.9827; also A<sub>4</sub> isomer calc. for [M]<sup>+</sup>C<sub>128</sub>H<sub>208</sub>N<sub>8</sub>O<sub>8</sub>Zn m/z = 2052.4640, found m/z = 2052.4330.

### **2,3,9,10,16,17-octa(2-(2-(2-methoxyethoxy)ethoxy)ethoxy)-23-iodophthalocyaninato zinc(II) 15**

In an oven-dried 25-mL two-necked round-bottomed flask purged with Ar, a solution of **8** (137mg, 0.30mmol, 6 eq.), 4-iodophthalonitrile (13mg, 0.05mmol, 1 eq.) and Zn(OAc)<sub>2</sub> (20 g, 0.10 mmol, 2 eq.) in pentanol (4 mL) was placed at room temperature. The mixture was stirred for 60 h at reflux. After cooling to room temperature, solvent was evaporated *in vacuo*. Repeated column chromatography (gradient, DCM/MeOH95:5→8:2) provided mixture where product was present as minor product as demonstrated by MALDI MS experiment.

MALDI TOF-TOF: calc. for [M]<sup>+</sup>C<sub>74</sub>H<sub>99</sub>IN<sub>8</sub>O<sub>24</sub>Zn m/z = 1676.9110, found m/z = 1676.4504; also A<sub>4</sub> isomer calc. for [M]<sup>+</sup>C<sub>88</sub>H<sub>128</sub>N<sub>8</sub>O<sub>32</sub>Zn m/z = 1875.3834, found m/z = 1873.7246.

### **4-((trimethylsilyl)ethynyl)phthalonitrile 17:**

5-mL microwave vial was charged with 4-iodophthalonitrile (200 mg, 0.79 mmol, 1 eq.), trimethylsilylacetylene (0.330 mL, 2.36 mmol, 3.0 eq.), CuI (3 mg, 0.02 mmol, 0.02 eq.) and Pd(PPh<sub>3</sub>)<sub>2</sub>Cl<sub>2</sub> (11 mg, 0.02 mmol, 0.02 eq.) in TEA (3 mL) and was deoxygenated *via freeze-pump-thaw* cycles three times with Ar. Resulting mixture was stirred for 2.5 h under microwave irradiation (50°C, 0 bar internal pressure, very high power). After cooling to room temperature, toluene (10 mL) was added and resulting mixture filtrated through celite and evaporated *in vacuo*. Column chromatography (Cy/AcOEt20:1→9:1) provided the desired product (162 mg, 92 %).

$^1\text{H}$  NMR (400 MHz,  $\text{CDCl}_3$ , 298 K):  $\delta$  (ppm) 7.84 (t,  $J=1.1$ , 1H, Ar-H), 7.74 (dd,  $J=1.1$ , 2H, Ar-H), 0.27 (s, 9H, Si- $\text{CH}_3$ ).

$^{13}\text{C}$  NMR (101 MHz,  $\text{CDCl}_3$ , 298 K): 136.48, 136.05, 133.49, 129.15, 116.26, 115.19, 114.77, 114.65, 103.47, 100.68, -0.39.

### **2,3,9,10,16,17-hexadodecyloxy-23- ((trimethylsilyl)ethynyl)phthalocyaninato zinc(II)18**

Oven-dried 10-mL schlenk tube purged with Ar, was charged with a solution of **11** (220 mg, 0.44 mmol, 6 eq.), **17** (17mg, 0.07mmol, 1 eq.) and  $\text{Zn}(\text{OAc})_2$  (27 g, 0.15 mmol, 2 eq.) in pentanol (4 mL) at room temperature. The mixture was stirred for 24 h at reflux, cooled to room temperature and the solvent was evaporated *in vacuo*. Repeated column chromatography (gradient,  $\text{DCM} \rightarrow \text{DCM}/\text{MeOH}$  9:1) provided mixture of compounds, in which the desired product was present but its isolation was not possible.

MALDI TOF-TOF: calc. for  $[\text{M}]^+ \text{C}_{109}\text{H}_{168}\text{N}_8\text{O}_6\text{SiZn}$   $m/z = 1780.0280$ , found  $[\text{M}]^+ m/z = 1780.1476$ ; also  $\text{A}_4$  isomer calc. for  $[\text{M}]^+ \text{C}_{128}\text{H}_{208}\text{N}_8\text{O}_8\text{Zn}$   $m/z = 2052.4640$ , found  $m/z = 2051.5163$  and  $\text{A}_2\text{B}_2$  isomer calc. for  $[\text{M}]^+ \text{C}_{90}\text{H}_{128}\text{N}_8\text{O}_4\text{Si}_2\text{Zn}$   $m/z = 1507.5920$ , found  $[\text{M}]^+ m/z = 1506.8336$ .

### **2,3,9,10,16,17-octa(2-(2-(2-methoxyethoxy)ethoxy)ethoxy)-23- ((trimethylsilyl)ethynyl)phthalocyaninato zinc(II)19**

Oven-dried 10-mL schlenk tube purged with Ar, was charged with a solution of **8** (200mg, 0.44mmol, 6 eq.), **17** (17mg, 0.07mmol, 1 eq.) and  $\text{Zn}(\text{OAc})_2$  (27 g, 0.15 mmol, 2 eq.) in pentanol (4 mL) at room temperature. The mixture was stirred for 48 h at reflux. Reaction was cooled to room temperature and solvent was evaporated *in vacuo*. Repeated column chromatography and preparative TLC (gradient,  $\text{DCM} \rightarrow \text{DCM}/\text{MeOH}$  8:2) provided some separation but the products were not identified by MALDI.

## **5.5 Acknowledgements**

We would like to thank Prof. Davide Bonifazi from the University of Namur, where all of the synthesis and measurements were carried on. We would like to

further acknowledge Dr. S. Santhosh Babu for guidance during stay of K. M. in Namur and for carrying on self-assembly on surfaces and SEM measurements.

## 5.6 References and notes

1. [http://www.ren21.net/Portals/0/documents/Resources/GSR/2013/GSR2013\\_low\\_res.pdf](http://www.ren21.net/Portals/0/documents/Resources/GSR/2013/GSR2013_low_res.pdf)
2. A. E. Becquerel, *Comptes Rendus De L'Académie Des Sciences*, 1839, **9**, 561.
3. D. M. Chapin, C. S. Fuller, G. L. Pearson *J. Appl. Phys.* 1954, **25**, 674.
4. T. Saga, *NPG Asia Mater*, 2010, **2**, 96-102.
5. W. Shockley and H. J. Queisser, *J. Appl. Phys.*, 1961, **32**, 510-519.
6. M. C. Hanna and A. J. Nozik, *J. Appl. Phys.*, 2006, **100**, 074510 - 074510-8.
7. M. A. Green, K. Emery, Y. Hishikawa, and W. Warta, *Prog. Photovolt: Res. Appl.*, 2009, **17**, 320-326.
8. M. Gratzel, *Nature*, **2001**, *414*, 338-344.
9. M. K. Nazeeruddin, A. Kay, I. Rodicio, R. Humphry-Baker, E. Mueller, P. Liska, N. Vlachopoulos, and M. Graetzel, *J. Am. Chem. Soc.*, **2002**, *115*, 6382-6390.
10. A. de la Escosura, M. V. Martinez-Diaz, P. Thordarson, A. E. Rowan, R. J. M. Nolte and T. Torres, *J. Am. Chem. Soc.*, **2003**, *125*, 12300-12308.
11. P. Peumans, A. Yakimov, and S. R. Forrest, *J. Appl. Phys.*, **2003**, *93*, 3693-3723.
12. M. Muntwiler, Q. Yang, W. A. Tisdale, and X. Y. Zhu, *Phys. Rev. Lett.*, **2008**, *101*, 196403-1-196403-4.
13. B. A. Gregg and M. C. Hanna, *J. Appl. Phys.*, **2003**, *93*, 3605-3613.
14. P. Peumans and S.R. Forrest, *Appl. Phys. Lett.*, **2001**, *79*, 126-128.
15. G. Yu, J. Gao, J. C. Hummelen, F. Wudl, and A. J. Heeger, *Science*, **1995**, *270*, 1789-1791.
16. Y. Shao and Y. Yang, *Adv. Mater.*, **2005**, *17*, 2841-2844.

17. W. A. Luhman and R. J. Holmes, *Appl. Phys. Lett.*, **2009**, *94*, 153304-1–153304-3.
18. B. P. Rand, S. Schols, D. Cheyns, H. Gommans, C. Giroto, J. Genoe, P. Heremans, and J. Poortmans, *Org. Electron.*, **2009**, *10*, 1015–1019.
19. P. Sullivan, S. Heutz, S. M. Schultes, and T. S. Jones, *Appl. Phys. Lett.*, **2004**, *84*, 1210–1212.
20. S. Uchida, J. Xue, B. P. Rand, and S. R. Forrest, *Appl. Phys. Lett.*, **2004**, *84*, 4218–4220.
21. M. Hiramoto, H. Fujiwara, and M. Yokoyama, *Appl. Phys. Lett.*, **1991**, *58*, 1062–1064.
22. J. Xue, B. P. Rand, S. Uchida, and S. R. Forrest, *Adv. Mater.*, **2005**, *17*, 66–71.
23. J. Drechsel, B. Mannig, D. Gebeyehu, M. Pfeiffer, K. Leo, and H. Hoppe, *Org. Electron.*, **2004**, *5*, 175–186.
24. F. Yang, K. Sun, and S. R. Forrest, *Adv. Mater.*, **2007**, *19*, 4166–4171
25. Z. R. Hong, B. Maennig, R. Lessmann, M. Pfeiffer, K. Leo, and P. Simon, *Appl. Phys. Lett.*, **2007**, *90*, 203505-1–203505-3.
26. S. H. Park, A. Roy, S. Beaupr'e, S. Cho, N. Coates, J. S. Moon, D. Moses, M. Leclerc, K. Lee, and A. J. Heeger, *Nature Photon.*, **2009**, *3*, 297–302.
27. P. Peumans, S. Uchida, and S. R. Forrest, *Nature*, **2003**, *425*, 158–162.
28. T. Tsuzuki, Y. Shirota, J. Rostalski, and D. Meissner, *Solar Energy Mater. Solar Cells*, **2000**, *61*, 1–8.
29. B. P. Rand, J. Li, J. Xue, R. J. Holmes, M. E. Thompson, and S. R. Forrest, *Adv. Mater.*, **2005**, *17*, 2714–2718.
30. M. Bronner, A. Opitz, and W. Brutting, *Phys. Stat. Sol. (a)*, **2008**, *205*, 549–563.
31. B. Pradhan and A. J. Pal, *Synth. Met.*, **2005**, *155*, 555–559.
32. L. Chen, Y. Tang, X. Fan, C. Zhang, Z. Chu, D. Wang, and D. Zou, *Org. Electron.*, **2009**, *10*, 724–728.
33. N. Sakai, R. Bhosale, D. Emery, J. Mareda, and S. Matile, *J. Am. Chem. Soc.*, **2010**, *132*, 6923–6925.
34. O. A. Scherman, G. B. W. L. Ligthart, H. Ohkawa, R. P. Sijbesma and E. W. Meijer, *Proc. Natl. Acad. Sci. U.S.A.*, **2006**, *103*, 11850–11855 .

35. O. E. Sielcken, M. M. Van Tilborg, M. F. M. Roks, R. Hendriks, W. Drenth and R. J. M. Nolte, *J. Am. Chem. Soc.*, **1987**, *109*, 4261-4265.
36. C. F. van Nostrum, S. J. Picken, A.-J. Schouten, R. J. M. Nolte, *J. Am. Chem. Soc.*, **1995**, *117*, 9957-9965 .
37. M. Gonidec, D. B. Amabilino , J. Veciana, *Dalton Trans.*, **2012**, *41*, 13632-13639 .
38. E. L. Spitler, W.R. Dichtel, *Nat. Chemistry*, **2010**, *2*, 672-677.





# **Chapter 6**

## **Towards UPY-decorated Terbium Phthalocyanine Double Deckers Single Molecule Magnets**

### **6.1. Introduction**

Single Molecule Magnets (SMMs) are compounds with strong magnetic properties at the molecular level. SMMs can be considered as molecular analogues of classical bulk ferromagnets, therefore they are useful for applications involving the storage and processing of digital information. However, in contrast to bulk magnets currently used for this purpose, such as neodymium–iron boride magnets,<sup>1</sup> the molecular nature of SMMs offers unique attributes that may allow information to be stored with much higher densities, and to be processed at unprecedented speeds.<sup>2</sup> SMMs typically present nanometric dimensions, thus if properly organized on surfaces can reach the ultimate goal of storing 1 bit per molecule.<sup>3</sup>

The origin of unique magnetic properties of SMMs is high spin ground state showing a slow magnetization relaxation rate at low temperatures.<sup>4</sup> It means that SMMs retain magnetization for long periods of time in the absence of an external magnetic field at temperatures lower than magnetic blocking temperatures,  $T_B$ ,<sup>5</sup> leading to magnetic hysteresis. Usually these temperatures are very low, in order of few K, or even below 1K. This poses important problems from technological point of view and there are only two ways to resolve this problem. First is development of applications where low temperatures will not be a problem yet it seems hard to accomplish. Second option is to find SMMs with much higher  $T_B$ , what is main activity of scientist working in the field, and lanthanide phthalocyanines double-deckers (LnDD) seems to be the best among new materials. However, beyond temperature

limitations, a quick development of a *SMM-based technology* is hampered by the intrinsic chemical fragility of most polynuclear SMMs and the evanescence of the SMM behaviour, which make the retention of the molecular magnetic bistability at the nanoscale difficult. The chemical bond between a sulphur functionalized SMM, the tetrairon(III) system ( $\text{Fe}_4$  hereafter), and a gold surface has been recently employed and the typical magnetic hysteresis observed through synchrotron-light based experiments.<sup>6,7</sup> Unfortunately the lability of the Au-S bond<sup>8</sup> cannot guarantee the long term stability required for the development of an SMM-based device. For this reason grafting of SMMs on a particularly attractive inorganic platform, such as silicon wafers, will offer the possibility to make robust and durable devices by forming stable Si-C covalent bonds. Moreover, the possibility of different doping of the silicon substrate can be used to influence the electronic properties of the grafted molecules.<sup>9</sup> Although preliminary promising results have been obtained with  $\text{Fe}_4$  SMMs chemically anchored on silicon,<sup>10</sup> very low temperature was required for the observation of magnetic bistability (i.e. below 1K). Good alternative can be another molecule, i. e. the Terbium(III) bis-phthalocyaninato neutral complex,<sup>11</sup>  $\text{TbPc}_2$ . Slow dynamics in the magnetization reversal is here due to the large activation energy barrier generated by crystal field splitting of the  $J=6.3$  ground multiplet of the highly anisotropic Tb III ion.<sup>12</sup> This results in one of the most promising and investigated SMMs,<sup>13-15</sup> whose insertion in single molecule transport devices has allowed to monitor the quantum dynamics of a single nuclear spins<sup>16</sup> and to observe a novel supramolecular spin valve effect.<sup>17</sup> In general, however, the magnetization dynamics of  $\text{TbPc}_2$  is severely altered in amorphous materials, where the packing of the molecules characterizing the crystalline phase is lost.<sup>18</sup> The origin of the phenomenon remains unclear, although it should be considered that small distortion of the two phthalocyaninato ligands from the perfectly staggered configuration, corresponding to  $D_{4d}$  symmetry, can be very efficient in promoting the tunnel mechanism of relaxation.<sup>18</sup> A similar reduction of the magnetic bistability is observed at the nanoscale: by thermal evaporation of these double-deckers on clean metallic surfaces in Ultra-High Vacuum (UHV) environment, the wide opening of the magnetic hysteresis loop above liquid helium temperature vanishes.<sup>19</sup> The phthalocyaninate ligand appears to efficiently couple the magnetic moment of the Tb ion with the magnetization of substrates as recently shown for submonolayer UHV-prepared deposits of  $\text{TbPc}_2$  on magnetic substrates.<sup>20</sup> The strength of the interaction can be tuned modifying the electronic characteristics of the substrate, though also in these cases no evidences of the SMM character of the pristine molecular system has been observed.

Taking into consideration above mentioned issues, we decided to prepare the silicon surfaces covered with the TbDDs. Although silicon is technologically important substrate, very common in modern electronics for multiple applications, like processors, flash drives, solar cells, sensors, etc. it is not easy surface to work with. Substrate needs to be of high purity, grafting protocol is quite harsh and requires dry box conditions, also wafers cannot be exposed to air and humidity, as this factors cause surface degradation, due to formation of silica, which is insulator and interfere during characterization. Therefore designing of system is challenging as all this factors needs to be taken into consideration.

## 6.2. Results and discussion

### 6.2.1. Design of system

There are two main roads by which TbDD can be successfully grafted on silicon. One is anchoring in non-reversible way by formation of covalent bonds. For this way TbDD needs to be functionalized with terminal double bonds to apply photografting protocol, successfully reported by our group for grafting of cavitands on silicon. This task was undertaken by other PhD student from our group, Federico Bertani. The other way for formation of monolayers of SMMs on silicon can be achieved in reversible, non-covalent way exploiting strong H-bonding motifs. To test our idea we decided to functionalize surface and TbDD with NAPY and UPY groups, respectively, forming strong hydrogen bonding heterodimer.<sup>21</sup>

Silicon surface decorated with NAPY was reported by our group previously.<sup>22</sup> Meanwhile, synthesis of TbDD functionalized with UPY has not been published in the literature until now. As will be presented later, synthesis is challenging, due to harsh conditions of formation of both, phthalocyanines and double-deckers, and as a consequence unpredictable side-reactions of intermediates, as well as difficulties with characterization of products by both NMR and MALDI.

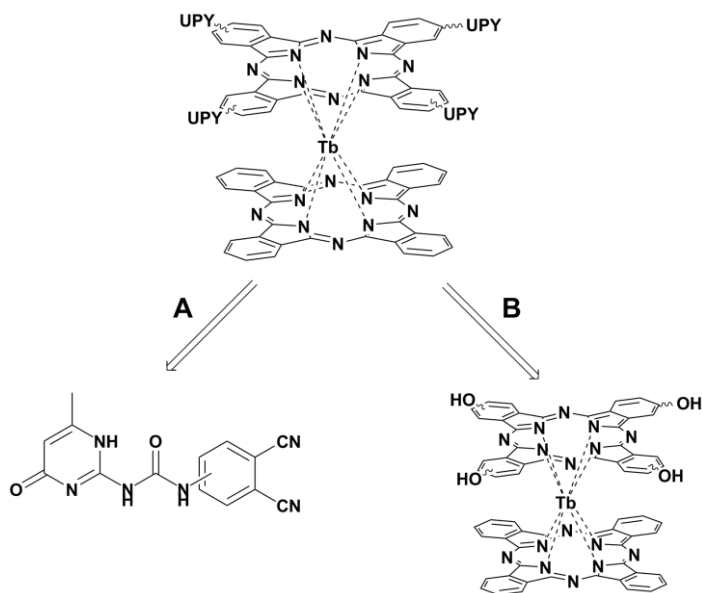
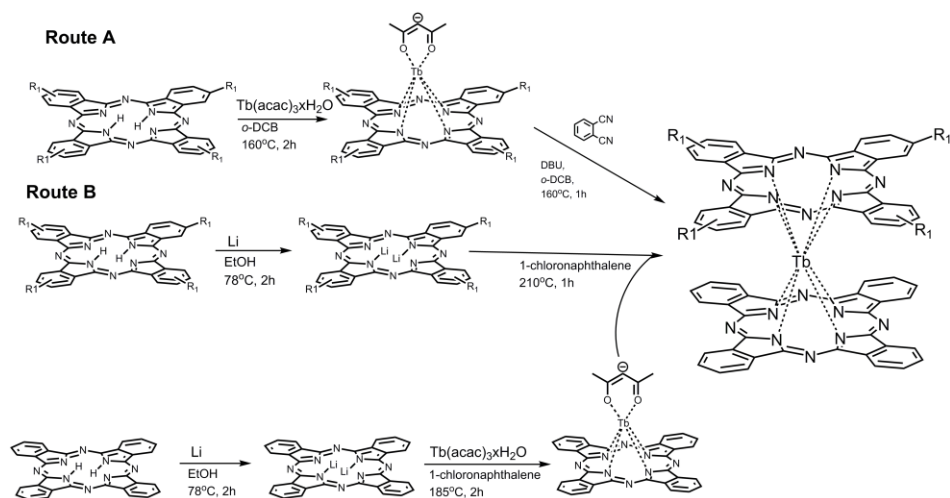


Chart 1. Two ways for grafting UPY isocyanate on TbDD. A) by functionalization of monomer; B) by post-functionalization of TbDD with free hydroxyl groups.

The structure of the target molecule, TbDD functionalized with UPY, is presented in Chart 1. The molecule is functionalized with four UPY units, all attached to one Pc, one for each monomer subunit. The target molecule is mixture of constitutional isomers sharing the same physical properties. The Pc can be in turn synthesized in two ways: 1) functionalization of phthalonitrile with UPY, followed by cyclization to Pc and complexation of Tb to form double decker; 2) formation of TbDD with reactive functional group, which in next step is used as anchoring site. The first road should be much faster and more straightforward, but as will be shown later, we were forced to take longer, second road due to problems mentioned before.

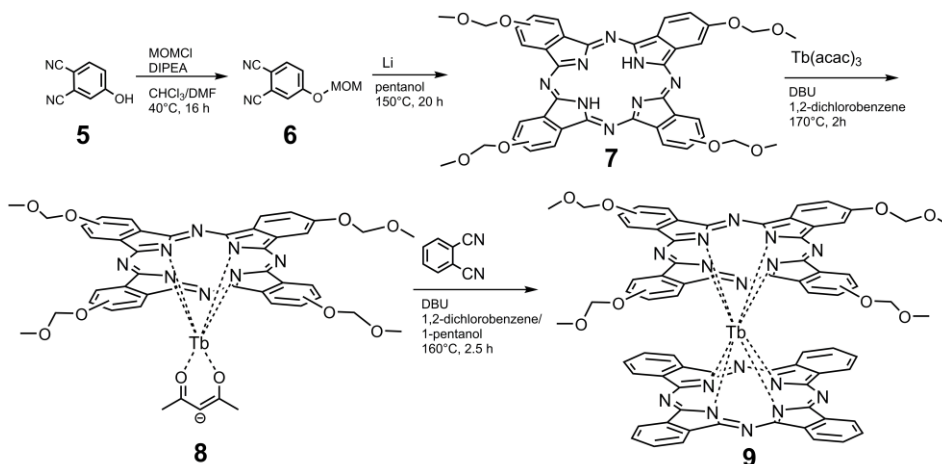


## 6.2.3. TbDD post-functionalization



Scheme 2. Synthetic pathways for synthesis of heteroleptic terbium double deckers.

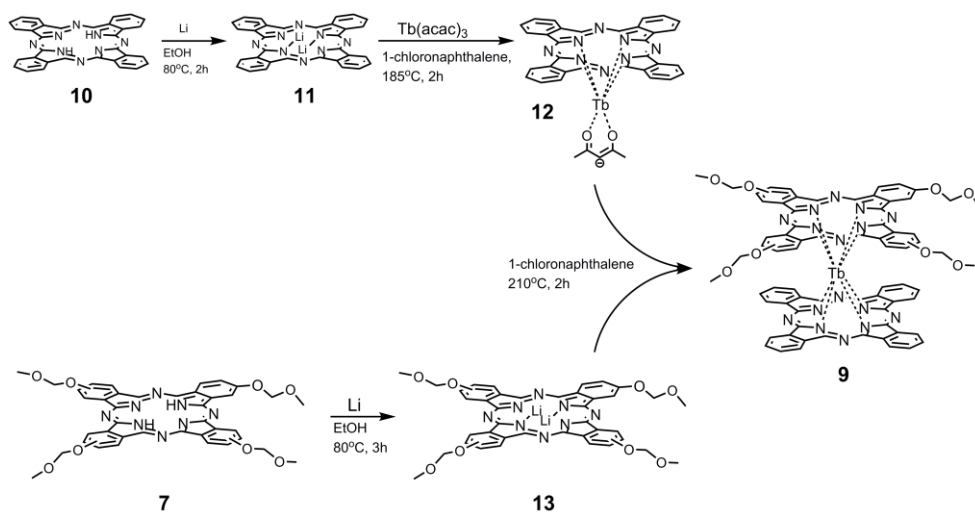
Like in previous case, for grafting of UPY on TbDD we decided to employ isocyanate chemistry and formation of carbamate bonds. This required functionalization of TbDDs with free OH or primary amines. In Scheme 2 are presented two most common pathways for synthesis of heteroleptic double deckers. Route A<sup>23</sup> goes through synthesis of metal-free Pc and formation of half-sandwich complex with Tb salts (here Tb(acac)<sub>3</sub>) in presence of base. Synthesis of second macrocycle is carried during the reaction, where Tb complex has the function of a template. Route B<sup>24</sup> is very similar to route A, but instead of synthesis of second Pc, lithiated compound is used. In this case two extra steps are needed but reaction is cleaner and usually the final step has better yields; however global yields are lower. Certain disadvantage might be also formation of homoleptic complexes, which often are hard to separate from heteroleptic complexes. One can notice that in both cases conditions are very harsh and many functional groups can undergo degradation.



Scheme 3. Synthesis of heteroleptic TbDD **9** from 4-hydroxyphthalonitrile.

On Scheme 3 is depicted synthesis of TbDD **9** following route A. As starting monomer we decided to use commercially available 4-hydroxyphthalonitrile. We introduced protecting group because our initial trials revealed, that use of monomer with free phenolic OH prevent formation of macrocycle. We decided to use MOM protecting group which is easily introduced in presence of base, and easily cleaved under acidic conditions. However, MOMCl has to be handled with care because fumes are hazardous and may cause cancer. Phthalocyanine was obtained in moderate yield (20%) as a mixture of constitutional isomers and used in this form. Pc was complexed with Tb salt in presence of DBU in *o*-dichlorobenzene at 170°C. During formation of TbDD **9** all starting material **8** was consumed, as revealed by TLC, unfortunately MALDI TOF-TOF analysis of all separated fractions did not confirm presence of product.

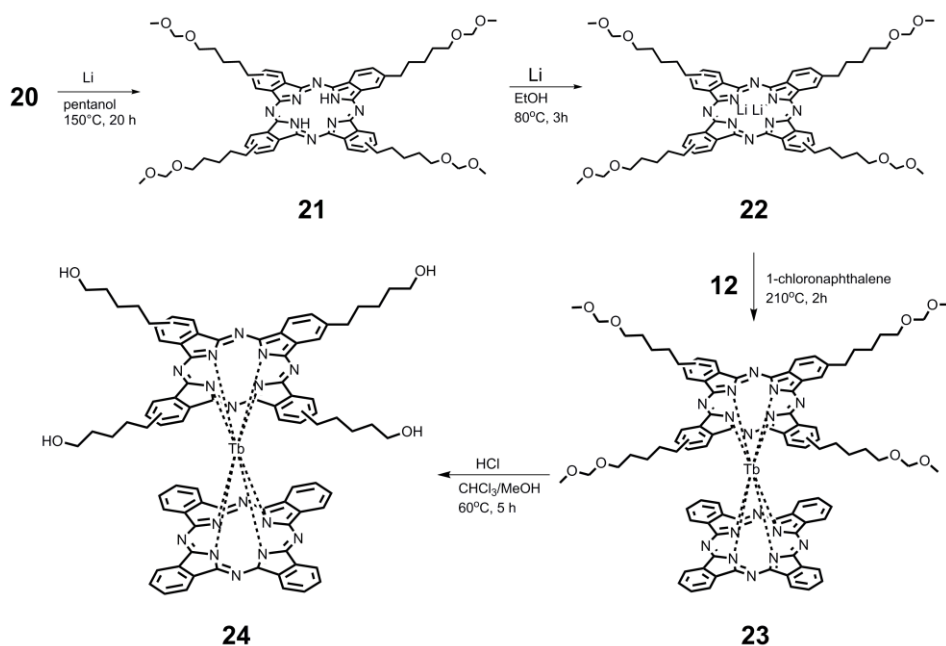
Therefore, we decided to follow route B towards the same TbDD **9**, depicted on Scheme 4. Pc **10** has been synthesised in one step from commercial phthalonitrile, and subsequently lithiated with Li in refluxing ethanol (**11**). Half-sandwich complex **12** was obtained in reaction with Tb(acac)<sub>3</sub> in high-boiling solvent. In next step, carried in the same flask, lithiated Pc **13** was added and reaction mixture was refluxed for 2 hours. After purification we were able to isolate product **9**, confirmed by MALDI TOF-TOF experiment.

Scheme 4. Synthesis of TbDD **9** by route B.

Next steps (Scheme 4) comprehended deprotection of MOM and reaction with UPY isocyanate (**15**). TbDD with 4 free phenolic OH, **14**, was obtained in reaction of **9** with HCl in mixture of methanol and chloroform, added in order to increase solubility of **9** and decrease solubility of **14**, therefore push the equilibrium towards products. Reaction of **14** with excess of isocyanate **15**, in presence of catalyst DABCO, was carried for prolonged period of time in elevated temperature, until all starting material disappeared in TLC. We were not able to isolate pure product, and MALDI experiment of mixture did not reveal peaks corresponding to four substituted product **16** neither partially substituted intermediates, the only evident peaks belonged to starting compound. We assumed that one of the reasons why compound **16** does not form was low reactivity of phenolic OH in reaction with isocyanate. The other possibility was fragmentation of final product upon ionization during MALDI experiment.





Scheme 7. Synthesis of TbDD **24**.

In order to obtain molecule **24** we followed route B for synthesis of double deckers. Cyclization of monomer **20** was accomplished in similar fashion as before, and Pc **21** was obtained in good yield (30%). Further lithilation (**22**) and complexation with half-sandwich **12** gave TbDD **23** in good yield (62%). Formation of this complex was confirmed by MALDI TO-TOF. Subsequent deprotection in the same conditions as before, gave TbDD with free alkylic OH **24**, again confirmed by MALDI experiment. Again, reaction of **24** with isocyanate **15** in the same conditions as previously did not lead to the product. Although the reaction was run for prolonged period of time, the only peaks in mass spectra which can be identified belong to starting material and MOM-deprotected Pc **21**. We think that the problem lays in the MALDI TOF-TOF characterization. The next step will be analysing the reaction of **24** with UPY on Orbitrap MS instrument.

### 6.3. Conclusions

A TbDD equipped with UPY units for non-covalent grafting on silicon wafers was designed. So far difficulties during synthesis and time frame did not permit us obtain satisfactory results. The limited amount of analytical tools available for

paramagnetic TbDD downsized only to MS, is also a bottleneck. Purification of this kind of compounds is challenging and often leads to losses of product. Though, we were able to synthesize TbDD with free hydroxyl and phenolic groups, **24** and **14** respectively, which can be used as building blocks for further functionalization. From our results we are not able to undoubtedly state whether we failed to obtain target molecule or only characterize it.

## 6.4. Experimental section

**General:** All commercial reagents were ACS reagent grade and used as received. Solvents were dried and distilled using standard procedures. <sup>1</sup>H NMR spectra were recorded on Bruker Avance 400 (400MHz) and Bruker Avance 300 (300 MHz) NMR spectrometers. All chemical shifts (δ) were reported in parts per million (ppm) relative to proton resonances resulting from incomplete deuteration of NMR solvents. ESI-MS experiments were performed on a Waters ZMD spectrometer equipped with an electrospray interface.

### 4-hexyloxyhydroxyphthalonitrile **2**

In an oven-dried 50-mL two-necked round-bottomed flask purged with Ar, a solution of 4-hydroxyphthalonitrile (300 mg, 2.083 mmol, 1 eq.) and K<sub>2</sub>CO<sub>3</sub> (0.72 g, 5.210 mmol, 2.5 eq.) in dry DMF (10 mL) was placed at RT for 10 min. 6-bromohexanol (0.33 mL, 2.500 mmol, 1.2 eq.) was added at once and the mixture was stirred for 16 h at 80°C. After cooling to room temperature suspension was filtered through celite plug and washed with DCM. Solvent was evaporated and residue subjected to column chromatography (DCM/MeOH 95:5) affording white powder (415 mg, y=81%).

<sup>1</sup>H NMR (400 MHz, CDCl<sub>3</sub>, 298 K): 7.69 (d, *J*=8.8 Hz, 1H, Ar-H), 7.25 (d, *J*=2.5 Hz, 1H, Ar-H), 7.18 (dd, *J*<sub>1</sub>=2.5 Hz, *J*<sub>2</sub>=8.8 Hz, 1H, Ar-H), 4.05 (t, *J*=6.4 Hz, 2H, ArO-CH<sub>2</sub>), 3.63 (t, *J*=6.4 Hz, 2H, HO-CH<sub>2</sub>), 1.83 (m, 2H, ArOCH<sub>2</sub>-CH<sub>2</sub>), 1.57 (m, 2H, CH<sub>2</sub>-CH<sub>2</sub>-OH), 1.45 (m, 4H, -CH<sub>2</sub>-).

### UPY-phthalonitrile **3**

To a round-bottomed flask charged with solution of hexylhydroxyphthalonitrile **2** (150 mg, 0.615 mmol, 1 eq.) in dry CHCl<sub>3</sub> (10 mL), UPY-isocyanate (236 mg,

0.800 mmol, 1.3 eq.) was added at RT. Reaction was stirred at 67°C for 16 h. Solvent was evaporated and the residue subjected to column chromatography (9:1 DCM:EtOH) yielding 14 mg (trace) of pure compound.

<sup>1</sup>H NMR (400 MHz, CDCl<sub>3</sub>, 298 K): 13.15 (bs, 1H, C-NH-C), 11.87 (bs, 1H, C-NH-CO), 10.16 (bs, 1H, CO-NH-CH<sub>2</sub>), 7.71 (d, *J*=8.8 Hz, 1H, Ar-H), 7.25 (d, *J*=2.5 Hz, 1H, Ar-H), 7.18 (dd, *J*<sub>1</sub>=2.5 Hz, *J*<sub>2</sub>=8.8 Hz, 1H, Ar-H), 5.86 (s, 1H, C-CH-CO), 4.89 (bs, 1H, CH<sub>2</sub>-NH-CO), 4.05 (m, 4H, ArO-CH<sub>2</sub>, COOCH<sub>2</sub>CH<sub>2</sub>), 3.27 (q, *J*=6.7 Hz, 2H, CH<sub>2</sub>-CH<sub>2</sub>-NHCOO), 3.17 (q, *J*=6.3 Hz, 2H, NHCONH-CH<sub>2</sub>-CH<sub>2</sub>), 2.25 (s, 3H, C-CH<sub>3</sub>), 1.85 (m, 2H, ArOCH<sub>2</sub>-CH<sub>2</sub>), 1.68-1.20 (m, 14H, -CH<sub>2</sub>-).

ESI-MS: calc. [M+Na]<sup>+</sup>=560.60, found *m/z*=560.3.

#### Pc-UPY 4

In a dry round-bottomed flask, UPY-phthalonitrile **3** (14 mg, 0.026 mmol, 1 eq.) was added to a solution of DBU (2 μL, 0.010 mmol, 0.4 eq.) in pentanol (3 mL) at RT. The resulting mixture was stirred for 10 h at 138°C, when TLC (CHCl<sub>3</sub>/MeOH 9:1) show the disappearance of phthalonitrile. Solvent was evaporated and the residue subjected to preparative TLC. Unfortunately, the mixture contained at least 6 green-colored fractions, which were probably phthalocyanines and it was impossible to separate them.

#### MOM-protected 4-hydroxyphthalonitrile 6

In a dry round-bottomed flask, MOMCl (0.95 mL, 12.5 mmol, 6 eq.) was added dropwise to a solution of 4-hydroxyphthalonitrile (300 mg, 2.08 mmol, 1 eq.) and DIPEA (3.45 mL, 19.76 mmol, 9.5 eq.) in mixture of DMF (4 mL) and CHCl<sub>3</sub> (4 mL) at 0°C. The resulting mixture was stirred for 16 h at 40°C. Then the reaction mixture was cooled down to RT and the solvent was evaporated. The residue was solubilized in DCM and filtrated through short silica plug affording pure product (*m*=370 mg) in excellent yield (95%).

<sup>1</sup>H NMR (400 MHz, CDCl<sub>3</sub>, 298 K): 7.70 (d, *J*=8.8 Hz, 1H, Ar-H), 7.43 (d, *J*=2.5 Hz, 1H, Ar-H), 7.34 (dd, *J*<sub>1</sub>=2.5 Hz, *J*<sub>2</sub>=8.8 Hz 1H, Ar-H), 5.26 (s, 2H, CH<sub>2</sub>), 3.48 (s, 3H, CH<sub>3</sub>).

**H<sub>2</sub>Pc(OMOM)<sub>4</sub> 7**

In an oven-dried 25-mL two-necked round-bottomed flask purged with Ar, a solution of MOM-hydroxyphthalonitrile **6** (320 mg, 1.70 mmol, 1 eq.) and metallic Li (70 mg, 10.20 mmol, 6 eq.) in pentanol (15 mL) was placed at RT. The mixture was stirred for 16 h at 138°C. After cooling to room temperature, the solvent was evaporated and residue solubilized in MeOH (20 mL) and 2 mL of CH<sub>3</sub>COOH. After 2 h in fridge a green precipitate was collected and subjected to column chromatography (CH<sub>2</sub>Cl<sub>2</sub>/MeOH 95:5) affording 80 mg (25%) of green solid, as a mixture of constitutional isomers.

<sup>1</sup>H NMR (400 MHz, CDCl<sub>3</sub>, 298 K): 8.30-8.10 (m, 4H, Ar-H), 8.07-7.84 (m, 4H, Ar-H), 7.43-7.24 (m, 4H, Ar-H), 5.60 (m, 8H, CH<sub>2</sub>), 3.81 (s, 12H, CH<sub>3</sub>).

**TbPc(OMOM)<sub>4</sub> 8**

To a vigorously stirred solution of H<sub>2</sub>Pc(OMOM)<sub>4</sub> **7** (50 mg, 0.066 mmol, 1eq.) in dry *ortho*-dichlorobenzene (2 mL), Tb(acac)<sub>3</sub> (27 mg, 0.080 mmol, 1.2eq.) and 1 drop of DBU were added at the RT. The resulting mixture was stirred for 1.5 h at 170°C under constant flow of Ar. After cooling to RT, solvent was evaporated and residue washed with hexane. The solid was used as recovered in next step.

**TbPcPc(OMOM)<sub>4</sub> 9a**

In an oven-dried 50-mL two-necked round-bottomed flask purged with Ar, a solution of TbPc(OMOM)<sub>4</sub> **8** (65 mg, 0.060 mmol, 1 eq.) in mixture of pentanol (2 mL) and dry *ortho*-dichlorobenzene(2 mL), phthalonitrile (33 mg, 0.261 mmol, 4.3 eq.) and 1 drop of DBU were added and resulting mixture was stirred for 2.5 h at 160°C. After cooling to room temperature, the solvent was evaporated and the residue was subjected to preparative TLC (CHCl<sub>3</sub>/MeOH 9:1). Unfortunately, using <sup>1</sup>H NMR and MALDI, it was impossible to evaluate if one of 4 separated fractions was the desired product.

**Li<sub>2</sub>Pc(OMOM)<sub>4</sub> 13**

In a dry round-bottomed flask,  $\text{H}_2\text{Pc}(\text{OMOM})_4$  (30 mg, 0.04 mmol, 1 eq.) was added to a solution of metallic Li (1 mg, 0.16 mmol, 4 eq.) in absolute EtOH (5 mL) at RT. The resulting mixture was stirred for 2h at 80°C. After cooling to RT solvent was removed *in vacuo*. The residue was solubilized in acetone, filtrated and dried with  $\text{Na}_2\text{SO}_4$ , to give a green solid (30 mg, quant.). In  $^1\text{H}$  NMR no presence of aromatic peaks.

$^1\text{H}$  NMR (400 MHz, Acetone- $d_6$ , 298 K): 5.68 (m, 8H,  $\text{CH}_2$ ), 3.71 (s, 12H,  $\text{CH}_3$ ).

### **TbPcPc(OMOM) $_4$ 9b**

In an oven-dried 25-mL two-necked round-bottomed flask purged with Ar, a solution of **11**<sup>22</sup> (33 mg, 0.063 mmol, 1.2 eq.) and  $\text{Tb}(\text{OAc})_3$  (21 mg, 0.063 mmol, 1.2 eq.) in 1-chloronaphthalene (5 mL) was stirred for 1 h at 185°C. After cooling to room temperature,  $\text{Li}_2\text{Pc}(\text{OMOM})_4$  **13** (40 mg, 0.052 mmol, 1.0 eq.) was added and reaction was stirred for 1 h at 210°C. After cooling to RT solvent reaction mixture was subjected to column chromatography with hexane to get rid of solvent, then washed with DCM to recover the product. Repeated column chromatography (gradient DCM/Hex 8:2->DCM->DCM/MeOH 8:2) gave **9b** as pure product (30 mg, 25%).

MALDI TOF-TOF: calc.  $\text{C}_{72}\text{H}_{48}\text{N}_{16}\text{O}_8\text{Tb}$   $[\text{M}]^+ = 1423.31$ , found  $[\text{M}]^+ = 1423.329$

### **TbPcPc(OH) $_4$ 14**

To a vigorously stirred solution of  $\text{TbPcPc}(\text{OMOM})_4$  **9b** (20 mg, 0.014 mmol, 1 eq.) in in mixture of  $\text{CHCl}_3$  (4 mL) and MeOH (4 mL), 0.5 mL of HCl was added at RT. After 5 h at 60°C reaction was cooled to RT and solvent was removed on rotavapor. Residue was sonicated with  $\text{H}_2\text{O}$ , filtrated and washed extensively with  $\text{H}_2\text{O}$  in order to remove HCl, resulting in 20 mg (quant.) of product after drying on vacuum pump.

ESI-MS: calc.  $\text{C}_{64}\text{H}_{33}\text{N}_{16}\text{O}_4\text{Tb}$   $[\text{M}+\text{H}]^+ = 1247.97$ , found  $[\text{M}+\text{H}]^+ = 1248.6$ .

### **TbPcPc(OH) $_4$ – UPY 16**

In an oven-dried 50-mL two-necked round-bottomed flask purged with Ar, to a solution of UPY isocyanate (17 mg, 0.056 mmol, 7 eq.) in dry  $\text{CHCl}_3$  (5 mL)

TbPcPc(OH)<sub>4</sub> **14** (10 mg, 0.008 mmol, 1 eq.) was added. The solution was stirred at 67°C for 4 h. After this time 1 spoon of DABCO was added and temperature was maintained for another 2 days until disappearance of starting **14**. The reaction mixture was cooled down to RT, the solvent was evaporated and residue subjected to column chromatography (gradient, CH<sub>2</sub>Cl<sub>2</sub>/EtOH 99:1 - > 9:1). MALDI TOF-TOF of separated fractions did not reveal any peaks originating from four times functionalized product, neither intermediates. The only identified peak belonged to Pc(OH)<sub>4</sub>.

### 5-(3,4-diisocyanophenyl)pent-4-yn-1-ol **18**

In an oven-dried 25-mL two-necked round-bottomed flask purged with Ar, to a solution of 4-iodophthalonitrile (300 mg, 1.18 mmol, 1 eq.) in dry DMF (1 mL) and TEA (5 mL), CuI (60 mg, 0.31 mmol, 0.26 eq.) and 1 spoon of [Pd(PPh<sub>3</sub>)<sub>4</sub>]<sup>0</sup> were added at RT. 4-pentyn-1-ol (0.23 mL, 2.48 mmol, 2.1 eq.) was added and the resulting solution stirred at RT for 5 h. The reaction mixture was diluted with 20 mL of DCM and washed with H<sub>2</sub>O (3 x 10 mL), 0.5 M HCl (10 mL), dried over MgSO<sub>4</sub>, and the solvent evaporated *in vacuo*. **18** was purified by column chromatography (AcOEt/Hex 6:4) (250 mg, quant.).

<sup>1</sup>H NMR (300 MHz, CDCl<sub>3</sub>, 298 K): 7.76-7.62 (m, 3H, Ar-H), 3.75 (t, *J*=6.1 Hz, 2H, CH<sub>2</sub>-OH), 2.57 (t, *J*=7.1 Hz, 2H, C-CH<sub>2</sub>), 1.84 (m, 2H, CH<sub>2</sub>-CH<sub>2</sub>-CH<sub>2</sub>).

### 5-(3,4-diisocyanophenyl)pentan-1-ol **19**

In a dry round-bottomed flask, 1 spoon of Pd/C was added to a solution of 5-(3,4-diisocyanophenyl)pent-4-yn-1-ol **18** (240 mg, 1.14 mmol) in AcOEt (15 mL) at RT. The resulting mixture was stirred in the atmosphere of H<sub>2</sub> for 16 h at RT. Reaction was filtered on celite PAD and washed with AcOEt, giving pure compound (235 mg, quant.) after removal of the solvent.

<sup>1</sup>H NMR (300 MHz, CDCl<sub>3</sub>, 298 K): 7.69 (d, *J*=7.8 Hz, 1H, Ar-H), 7.60 (s, 1H, Ar-H), 7.53 (dd, *J*=7.8 Hz, *J*=8.1 Hz, 1H, Ar-H), 3.59 (t, *J*=6.6 Hz, 2H, CH<sub>2</sub>-OH), 2.71 (t, *J*=7.5 Hz, 2H, Ar-CH<sub>2</sub>), 1.65 (m, 2H, CH<sub>2</sub>-CH<sub>2</sub>OH), 1.53 (m, 2H, ArCH<sub>2</sub>-CH<sub>2</sub>), 1.38 (m, 2H, CH<sub>2</sub>).

### 1,2-diisocyno-4-(5-(methoxymethoxy)pentyl)benzene **20**

In a dry round-bottomed flask, MOMCl (0.45 mL, 6.0 mmol, 6 eq.) was added dropwise to a solution of 5-(3,4-diisocyanophenyl)pentan-1-ol **19** (215 mg, 1.00 mmol, 1 eq.) and excess of DIPEA (3.0 mL) in ACN (10 mL) at 0°C. The resulting mixture was stirred for 16 h at 50°C. Then reaction mixture was cooled down to RT and the solvent was evaporated. The residue was solubilized in DCM, filtrated through short silica plug and washed with acetone, affording **20** as pure product (200 mg, 78%).

<sup>1</sup>H NMR (300 MHz, CDCl<sub>3</sub>, 298 K): 7.69 (d, *J*=7.8 Hz, 1H, Ar-H), 7.60 (s, 1H, Ar-H), 7.53 (dd, *J*=7.8 Hz, *J*=8.1 Hz, 1H, Ar-H), 4.59 (s, 2H, O-CH<sub>2</sub>-O), 3.50 (t, *J*=6.6 Hz, 2H, CH<sub>2</sub>CH<sub>2</sub>-O), 3.33 (s, 3H, O-CH<sub>3</sub>), 2.73 (t, *J*=7.5 Hz, 2H, Ar-CH<sub>2</sub>), 1.64 (m, 4H, CH<sub>2</sub>-CH<sub>2</sub>OH, Ar-CH<sub>2</sub>CH<sub>2</sub>), 1.42 (m, 2H, -CH<sub>2</sub>-).

### H<sub>2</sub>Pc(C<sub>6</sub>H<sub>12</sub>OMOM)<sub>4</sub> **21**

In an oven-dried 25-mL two-necked round-bottomed flask purged with Ar, a metallic Li (23 mg, 3.25 mmol, 6 eq.) was placed in pentanol (5 mL) at RT and stirred for 15 min at 80°C. Solution of 1,2-diisocyno-4-(5-(methoxymethoxy)pentyl)benzene **20** (140 mg, 0.54 mmol, 1 eq.) in pentanol (5 mL) was added and mixture was stirred for 5 h at 138°C. After cooling to room temperature, the solvent was evaporated and residue solubilized in mixture of MeOH (20 mL) and of CH<sub>3</sub>COOH (3 mL). After 16 h in freezer a blue precipitate was separated from the green solution. The liquid phase was evaporated and subjected to column chromatography (CH<sub>2</sub>Cl<sub>2</sub>/MeOH 95:5) affording 60 mg (43%) of green solid, which was mixture of constitutional isomers of **21**.

<sup>1</sup>H NMR (400 MHz, CDCl<sub>3</sub>, 298 K): 7.73 (d, *J*=10.4 Hz, 4H, Ar-H), 7.65 (s, 4H, Ar-H), 7.52 (d, *J*=10.0 Hz, 4H, Ar-H), 4.60 (s, 8H, O-CH<sub>2</sub>-O), 3.51 (t, *J*=8.4 Hz, 8H, CH<sub>2</sub>CH<sub>2</sub>-O), 3.34 (s, 12H, O-CH<sub>3</sub>), 2.74 (m, 8H, Ar-CH<sub>2</sub>), 1.65 (m, 16H, CH<sub>2</sub>-CH<sub>2</sub>O, Ar-CH<sub>2</sub>CH<sub>2</sub>), 1.42 (m, 8H, -CH<sub>2</sub>-).

MALDI TOF-TOF: calc. for C<sub>60</sub>H<sub>75</sub>N<sub>8</sub>O<sub>8</sub>, [M+H]<sup>+</sup> 1035.5707, found 1035.5538.

### Li<sub>2</sub>Pc(C<sub>6</sub>H<sub>12</sub>OMOM)<sub>4</sub> **22**

To a vigorously stirred solution of metallic Li (1 mg, 0.12 mmol, 3 eq.) in absolute EtOH (10 mL), H<sub>2</sub>Pc(C<sub>6</sub>H<sub>12</sub>OMOM)<sub>4</sub> **21** (40 mg, 0.04 mmol, 1 eq.) was added and the reaction was kept for 2 h at 80°C. The solvent was removed on



rotavapor, the residue was solved in acetone and filtrated. Evaporation of the liquid phase yielded a solid used in next step without further purification.

### TbPcPc(C<sub>6</sub>H<sub>12</sub>OMOM)<sub>4</sub> **23**

Li<sub>2</sub>Pc(C<sub>6</sub>H<sub>12</sub>OMOM)<sub>4</sub> **22** (40 mg, 0.039 mmol, 1 eq.) and Tb(acac)<sub>3</sub> (18 mg, 0.039 mmol, 1 eq.) were solubilized in 1-chloronaphtalene (5mL) at RT and then heated at 185°C for 5 h, until disappearance of starting material on TLC (DCM/MeOH 9:1). The reaction mixture was cooled down to RT, Li<sub>2</sub>Pc **11** (22 mg, 0.039 mmol, 1 eq.) was added and temperature was maintained at 210°C for 1 h. Purification with column chromatography gave first 1-chloronaphtalene eluted with hexane, later using gradient DCM/MeOH 10:0->9:1 product **23** was obtained (40 mg, 62%).

MALDI TOF-TOF: calc. for C<sub>92</sub>H<sub>88</sub>N<sub>16</sub>O<sub>8</sub>Tb, [M]<sup>+</sup> 1703.6225, found 1703.5581.

### TbPcPc(C<sub>6</sub>H<sub>12</sub>OH)<sub>4</sub> **24**

TbPcPc(C<sub>6</sub>H<sub>12</sub>OMOM)<sub>4</sub> **23** (20 mg, 0.012 mmol) was placed in mixture of MeOH (2 mL) and CHCl<sub>3</sub> (2 mL) at RT giving clear green solution, to which was added 0.5 mL of HCl. After 7 h at 50°C reaction was finished, as indicated by TLC (DCM/MeOH 8:2). The solvent was evaporated and the residue used as recovered in next step.

MALDI TOF-TOF: calc. for C<sub>84</sub>H<sub>73</sub>N<sub>16</sub>O<sub>4</sub>Tb, [M+H]<sup>+</sup> 1528.5254, found 1528.4411.

### TbPcPc(C<sub>6</sub>H<sub>12</sub>OH)<sub>4</sub> – UPY **25**

In an oven-dried 50-mL two-necked round-bottomed flask purged with Ar, to a solution of UPY isocyanate (10 mg, 0.032 mmol, 5 eq.) and 1 spoon of DABCO in dry DMF (5 mL) was added TbPcPc(C<sub>6</sub>H<sub>12</sub>OH)<sub>4</sub> **24** (10 mg, 0.006 mmol, 1 eq.). The solution was stirred at 50°C for 16 h. No substrate **24** was observed by TLC after this time, so reaction mixture was cooled down to RT and the solvent was evaporated. MALDI TOF-TOF of crude did not reveal any peaks originating from four times functionalized product, neither intermediates. The only identified peak belonged to starting TbPcPc(C<sub>6</sub>H<sub>12</sub>OH)<sub>4</sub> **24** and Pc(OH)<sub>4</sub> (probably product of fragmentation of **24** during MALDI analysis).

## 6.5. Acknowledgements

We would like to acknowledge Centro Interdipartimentale Misura “G. Casnati” of the University of Parma for the use of NMR and MALDI TOF-TOF facilities. And special thanks are going to Dr. Daniela Menozzi and Federico Bertani for help and good advices during the project.

## 6.6. References and notes

1. S. V. Eliseeva, J.-C. G. Bünzli, *New J. Chem.* **2011**, *35*, 1165-1176.
2. M. N. Leuenberger, D. Loss, *Nature* **2001**, *410*, 789-796.
3. M. Cavallini, J. Gomez-Segura, D. Ruiz-Molina, M. Massi, C. Albonetti, C. Rovira, J. Veciana, F. Biscarini, *Angew. Chem. Int. Ed.* **2005**, *44*, 888-892.
4. D. Gatteschi, R. Sessoli, J. Villain, *Molecular Nanomagnets*, **2006**, Oxford University Press, USA.
5. R. Sessoli, D. Gatteschi, A. Caneschi, M. A. Novak, *Nature* **1993**, *365*, 141-143.
6. M. Mannini, F. Pineider, P. Sainctavit, C. Danieli, E. Otero, C. Sciancalepore, A. M. Talarico, M.-A. Arrio, A. Cornia, D. Gatteschi, R. Sessoli, *Nat. Mater.* **2009**, *8*, 194–197.
7. M. Mannini, M. Mannini, F. Pineider, C. Danieli, F. Totti, L. Sorace, P. Sainctavit, M. A. Arrio, E. Otero, L. Joly, J. C. Cezar, A. Cornia and R. Sessoli, *Nature* **2010**, *468*, 417–421.
8. J. B. Schlenoff, M. H. Li, *J. Am. Chem. Soc.* **1995**, *117*, 12528–12536.
9. D. N. Woodruff, R. E. P. Winpenny, R. A. Layfield, *Chem. Rev.* **2013**, *113*, 5110–5148.
10. G. G. Condorelli, A. Motta, I. L. Fragalà, F. Giannazzo, V. Raineri, A. Caneschi, D. Gatteschi, *Angew. Chem. Int. Ed.* **2004**, *43*, 4081–4084.
11. N. Ishikawa, M. Sugita, T. Ishikawa, S.-Y. Koshihara, Y. Kaizu, *J. Am. Chem. Soc.* **2003**, *125*, 8694–8695.

12. N. Ishikawa, M. Sugita, T. Okubo, N. Tanaka, T. Iino, Y. Kaizu, *Inorg. Chem.* **2003**, *42*, 2440-2446.
13. K. Katoh, Y. Yoshida, M. Yamashita, H. Miyasaka, B. K. Breedlove, T. Kajiwara, S. Takaishi, N. Ishikawa, H. Isshiki, Y. F. Zhang, T. Komeda, M. Yamagishi, J. Takeya, *J. Am. Chem. Soc.* **2009**, *131*, 9967-9976.
14. T. Komeda, H. Isshiki, J. Liu, Y. Zhang, N. Lorente, K. Katoh, B. K. Breedlove, M. Yamashita, *Nat. Commun.* **2011**, *2*, 217-222.
15. M. Gonidec, R. Biagi, V. Corradini, F. Moro, V. De Renzi, U. del Pennino, D. Summa, L. Muccioli, C. Zannoni, D. Amabilino, J. Veciana, *J. Am. Chem. Soc.* **2010**, *133*, 6603-6612.
16. R. Vincent, S. Klyatskaya, M. Ruben, W. Wernsdorfer, F. Balestro, *Nature* **2012**, *488*, 357-360.
17. M. Urdampilleta, S. Klyatskaya, J.-P. Cleuziou, M. Ruben, W. Wernsdorfer, *Nat. Mater.* **2011**, *10*, 502-506.
18. L. Malavolti, M. Mannini, P.-E. Car, G. Campo, F. Pineider, R. Sessoli, *J. Mater. Chem. C*, **2013**, *1*, 2935-2942.
19. L. Margheriti, D. Chiappe, M. Mannini, P.-E. Car, Ph. Saintavrit, M.-A. Arrio, F. B. de Mongeot, J. C. Cezar, F. M. Piras, A. Magnani, E. Otero, A. Caneschi, R. Sessoli, *Adv. Mater.*, **2010**, *22*, 5488-5493.
20. A. Lodi Rizzini, C. Krull, T. Balashov, A. Mugarza, C. Nistor, F. Yakhov, V. Sessi, S. Klyatskaya, M. Ruben, S. Stepanow, P. Gambardella, *Nano Lett.* **2012**, *12*, 5703-5707.
21. O. A. Scherman, G. B. W. L. Ligthart, H. Ohkawa, R. P. Sijbesma, E. W. Meijer, *Proc. Natl. Acad. Sci. U.S.A.* **2006**, *103*, 11850-11855
22. F. Tancini, D. Genovese, M. Montalti, L. Cristofolini, L. Nasi, L. Prodi, E. Dalcanale, *J. Am. Chem. Soc.* **2010**, *132*, 4781-4789.
23. B. Ballesteros, G. de la Torre, A. Shearer, A. Hausmann, M. Herranz, D. Guldi, T. Torres, *Chem. Eur. J.* **2010**, *16*, 114-125.
24. S. Kyatskaya, J.R.G. Mascarós, L. Bogani, F. Hennrich, M. Kappes, W. Wernsdorfer, M. Ruben, *J. Am. Chem. Soc.* **2009**, *131*, 15143-15151



# Chapter 7

## Application of tetraphosphonate cavitands in OECT sensors

### 7.1. Introduction

The field of organic electronics has grown significantly in the past 20 years largely due to the many desirable properties of organic semiconductors such as low cost, ease of processing and tunability through synthetic chemistry which open many possibilities to use these materials in different applications such as lighting (OLED),<sup>1,2</sup> photovoltaic<sup>3</sup> and sensing.<sup>4,5</sup>

Among these devices, organic thin film transistors (OTFTs) have attracted considerable interest for their application in printed electronics.<sup>6, 7</sup> Within the subset of OTFTs, organic electrochemical transistors (OECTs) have distinguished themselves in recent years given their simple fabrication and low voltage operation.<sup>8-10</sup> The ability to operate in aqueous environments and the integration with microfluidics make OECTs excellent candidates for a variety of applications, especially in the area of biosensing.<sup>11</sup> OECTs were first demonstrated by White et al., where the conductivity of a poly(pyrrole) film was modulated by the application of a gate voltage through an electrolyte.<sup>12</sup> Many groups have followed and demonstrated other materials and applications of OECTs.<sup>4,13-15</sup> In these devices a gate voltage is applied through an electrolyte and the conductivity of an organic semiconductor film is modulated due to the motion of ions between the electrolyte and the organic film. Being “soft” materials, organic semiconductors allow significant ionic motion within their films and are particularly suited for the effects exploited in OECTs. The preferred material used in this devices is poly(3,4-ethylenedioxythiophene) doped with poly(styrenesulfonate) (PEDOT:PSS); the mixture is commercially available and stable under a variety of conditions. PEDOT:PSS is a degenerately doped p-type semiconductor (commonly referred to as a conducting polymer), where holes on the PEDOT are compensated by acceptors ( $\text{SO}_3^{2-}$ ) on the PSS. Organic ECTs (OECT) have been studied as

chemical and biological sensors, in particular as glucose sensors,<sup>16, 17</sup> gas sensors,<sup>18</sup> pH sensors,<sup>19</sup> and biological species detection.<sup>20</sup>

In our group we are involved in fabrication of systems for evaluations of biologically and environmentally relevant species, particularly sarcosine,<sup>21</sup> drugs, alcohols,<sup>22</sup> explosives, BTEX etc.<sup>23,24</sup> As a result we took part in the development of devices exploiting our host molecules, particularly tetrakisphosphonate and tetraquinoline bridged cavitands, for surface functionalization and as preconcentrators and sensors. OECTs are a transduction platform which provides fast response time, simple setup, biocompatibility, acting in aqueous media and low cost.

Incorporation of specific hosts into semiconducting polymer of OECTs can bring many advantages, as was already shown by e.g. Ivaska et al.<sup>25</sup> The idea was to use functionalized resorcinarenes and calixarenes as electrolytes instead of PSS. Response of device towards some of the ions, which interact specifically with supramolecular hosts, has been improved with respect to standard systems. In typical OECT device ions present in solution form layers on the semiconductor changing its electrical conductivity. In OECT doped with host molecules, guest ions penetrate deeper into material, their interactions are stronger, and consequently response of device should be higher. Based on this premise we doped semiconductor with tetrakisphosphonate cavitands which are much better hosts for cations than both resorcinarenes and calixarenes.

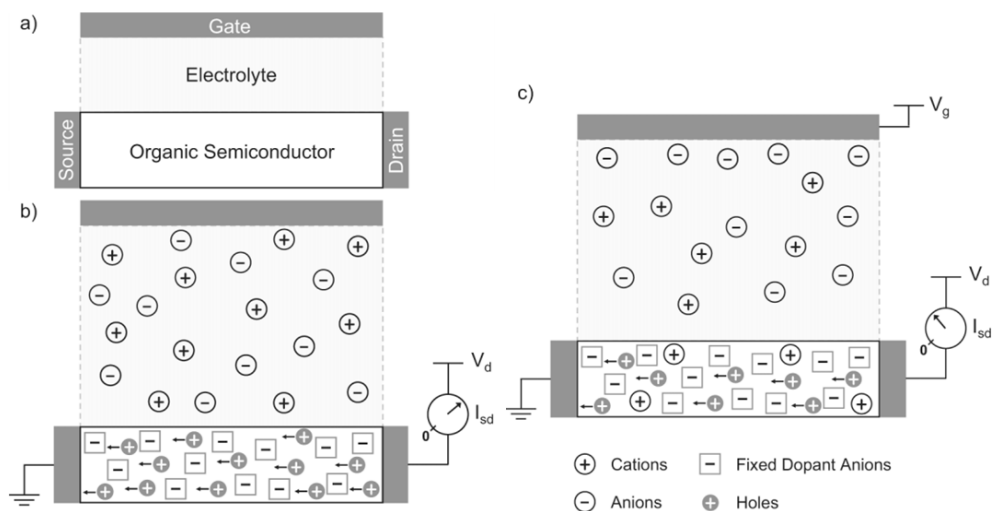


Figure 1. Qualitative representation of OECT behavior. a) OECT labeled with appropriate naming conventions. b) OECT without gate voltage applied. Current is determined by the intrinsic conductance of the organic

semiconductor. c) OECT with gate voltage ( $V_g$ ) applied. Current is determined by the extent to which the organic semiconductor is de-doped

A picture illustrating typical OECT is shown in Figure 1 (from Ref.26). The essential components are an organic semiconductor film with source and drain contacts, an electrolyte, and a gate electrode. Because the majority of organics used for OECTs are hole transporters, the nomenclature of this analysis refers to p-type doping (mobile holes and spatially fixed acceptor ions), but it is trivial to repeat the analysis for electron transporting materials. As a convention, the source contact is grounded and a voltage is applied to the drain contact ( $V_d$ ) relative to ground. The current that passes through the organic semiconductor ( $I_{sd}$ ) can be monitored as a function of the applied gate voltage ( $V_g$ ). Upon the application of a positive gate voltage ( $V_g$ ) relative to ground, cations from the electrolyte are injected into the organic semiconductor film. This in turn de-dopes the organic semiconductor and thus decreases the source-drain current ( $I_{sd}$ ). The transport of ions from the electrolyte into the organic semiconductor film is fundamental to the behavior of OECTs.

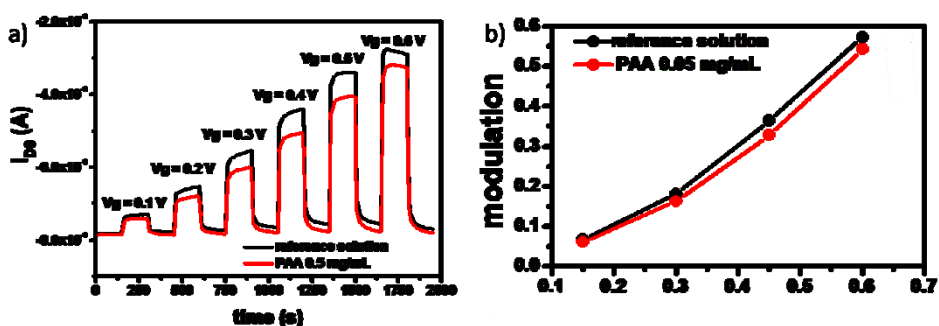


Figure 2. Typical response of OECT device used in this chapter. Solution containing poly(acrylic acid) sodium salt (PAA), 0.05 mg/mL. (from Ref. 27)

The OECTs response is determined by the kinetic curve that represents the electrical behavior of the devices interacting with the solutions<sup>17</sup> and is presented on Fig. 2. In this curve, the difference of the drain current in the *on* and in the *off* state, depends on the used electrolytes and their concentration, similarly to what happens to the standard electrodes used in electrochemistry. As can be observed on the Fig. 2, difference in response between reference and sample increases with increase of applied gate voltage  $V_g$ . The modulation is determined by the ratio  $|I_{on}-I_{off}|/I_{off}$  as a function of the gate voltage applied  $V_g$ , with  $I_{on}$  the current when  $V_g$  is on and  $I_{off}$  the current when  $V_g$  is off. As

shown on Fig. 2b modulation for PAA solution is much lower than in the case of reference sample. Performing experiments with known solutions, concentration or type of unknown samples can be evaluated.

## 7.2. Results and discussion

### 7.2.1. Simple approach

Our device is based on PEDOT:PSS and is easily fabricated applying concepts of ink-jet printing: desired structure is drawn on the glass slide using an automatic syringe and a micro-positioning system. Commercially available PEDOT:PSS solution in water, from Sigma Aldrich, is fluid enough to be deposited in this way. Therefore simplest and cheapest approach, which could allow fabrication of many devices in short time, was to suspend tetraphosphonate cavitands in this solution and fabricate device in standard way. 9 parts of commercial solution containing ~1.5% w/w PEDOT:PSS in water was diluted with 1 part of ethylene glycol and 1 part of methanol. To this solution 2% by weight, with respect to PEDOT:PSS, of tetraphosphonate cavitands  $Tiiii[C_3H_7, CH_3, Ph]$  was added and solution was stirred for one hour at room temperature. In the next step the solution was deposited on the pretreated glass surface following the procedure described in the experimental section and used in the experiment.

To measure current modulation in drain-source electrode we used the setup presented in Ref. 27. Through drain-source electrode was running small current (-0.1 V) which was kept constant all the time. To the gate was applied positive  $V_g$  in the range from 0.1 V to 0.5 V, always for 150 s periods, with 0 V in between, also for 150 s. Device chamber was filled with solution of analyte. Reference solution was  $10^{-2}M$  water solution of LiCl (LiCl+water). Concentration of methylbutylammonium chloride (MBACl) was  $10^{-3}M$  in water containing  $10^{-2}M$  water solution of LiCl (MBACl+water). In order to give more reliable data, for each device experiments were repeated few times, indicated by number in curve name.



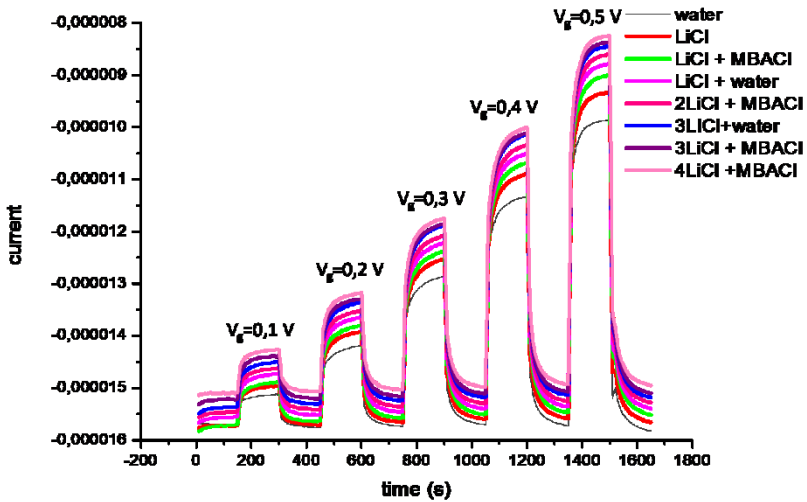


Figure 3. Kinetic curve for MBACI measurements of cavitand doped PEDOT:PSS. LiCl  $10^{-2}$ M, MBACI  $10^{-3}$ M, water solutions.

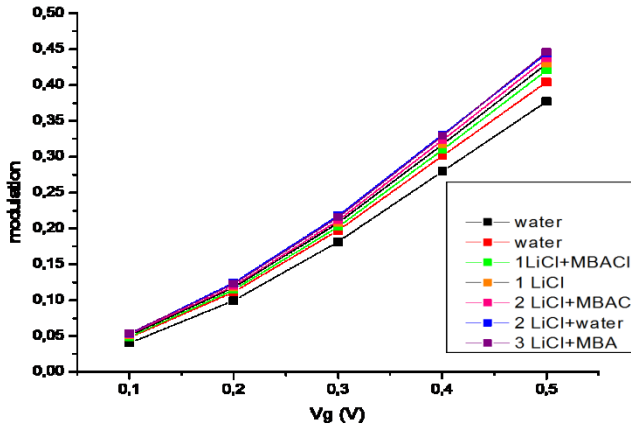


Figure 4. Modulation curve for MBACI measurements for cavitand doped PEDOT:PSS.

Modulations, calculated according to the before mentioned equation, are presented on Fig. 4. Analysis of the graph clearly reveals small differences in modulations between samples containing both MBACI and LiCl and only LiCl.

Such a small varieties are within experimental error and can be rather attributed to slightly increased concentration of ions in mixture MBACl+LiCl.

Lack of specific response of device towards guest molecules inspired us to design of system with better communication between cavitands and semiconductor, higher homogeneity and better control of material composition.

### 7.2.2. Formation of covalently bound 4PO-PEDOT

Synthesis of PEDOT functionalized with tetraphosphonate cavitands was carried out by electropolymerization. The molecular structure of monomers **1** and **2** and the resulting copolymer are depicted in Chart 1. Monomers **1** and **2** were both obtained in one step via esterification reactions from commercially available EDOT-carboxylic acid, in particular **1** by Steglich esterification from monohydroxy-footed tetraphosphonate cavitand,<sup>28</sup> **2** by Fisher esterification from methanol.

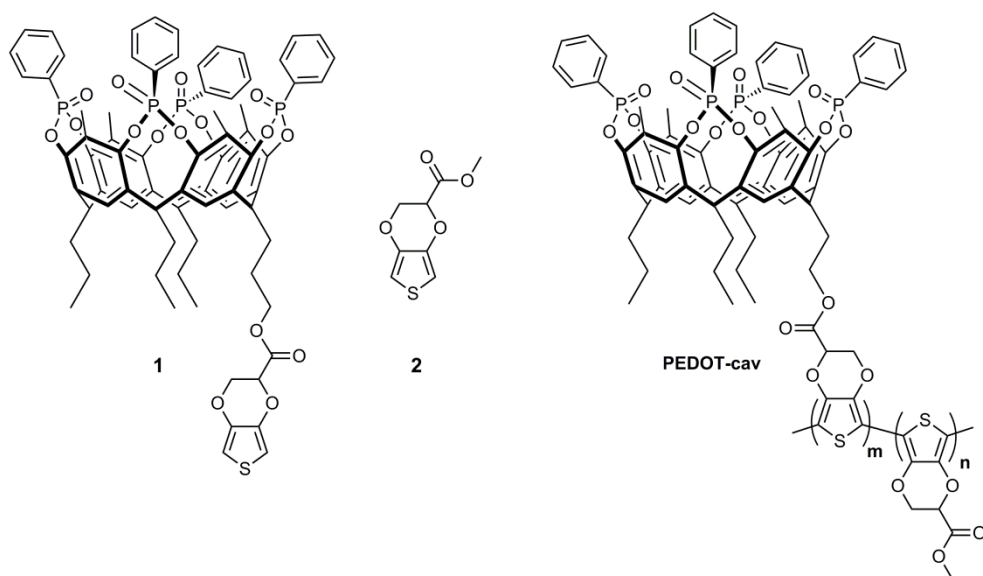


Chart 1. Structure of monomers **1** and **2** for electropolymerization, and copolymer **PEDOT-cav**.

**PEDOT-cav** was prepared by electropolymerization using Cyclic Voltammetry. In solution of dry acetonitrile:dichloromethane 9:1, **1** and **2** were solubilised in molar ratio 1:8, and concentration was  $10^{-2}$  mol/L fixed on **2** in presence of supporting electrolyte  $\text{LiClO}_4$   $10^{-1}$  mol/L. Gold disk presented on

Figure 1 ( $d=20$  mm) was acting as working electrode; in the system were also present glassy carbon counter electrode and Ag/AgCl in 3 M KCl reference electrode. Solution was first purged with  $N_2$  for 100 s and then 25 scans from -1.0 V to +1.5 V were run with scan rate 0.1 V/s. Cyclic voltammetry curve of initial scans is presented in Fig. 5.

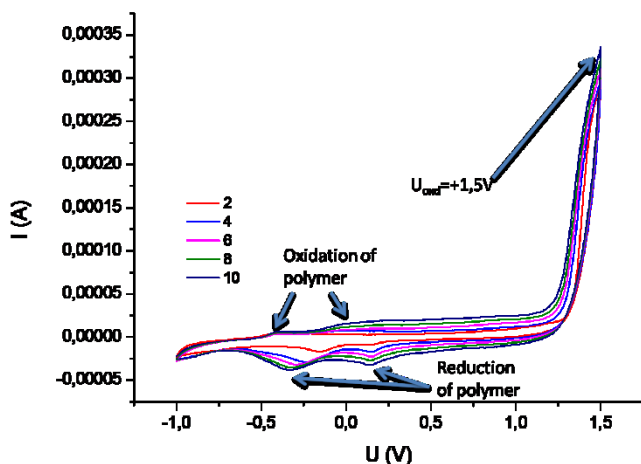


Figure 5. Initial scans of electropolymerization of monomers **1** and **2** in ratio 1:8, range -1.0 V to +1.5 V, scan rate 0.1 V/s.

The prepared sample (Figure 5) was subjected to XPS analysis. The sample was divided in three zones based on coverage thickness evaluated by naked eye.

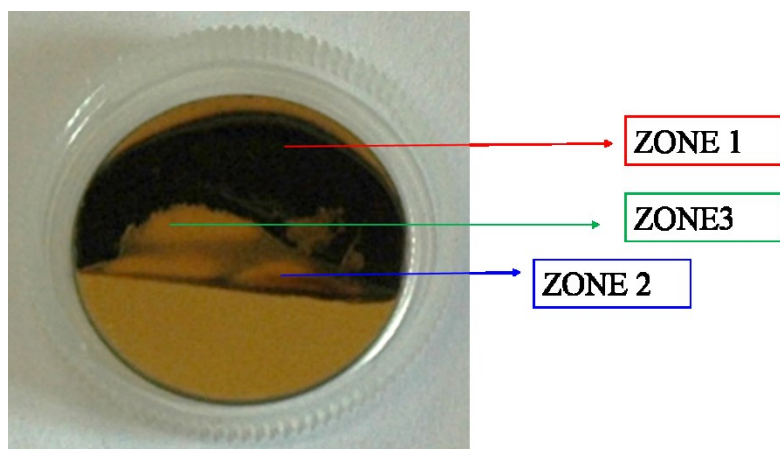


Figure 5. Gold surface covered by electropolymerization of mixture of compounds **1** and **2** and division by zones according to level of deposition.

Survey spectra of sample with partial attribution of peaks, for all three zones are reported in Fig. 6. The XPS data confirm the presence of all important elements on the gold surface and show some difference between separated three zones.

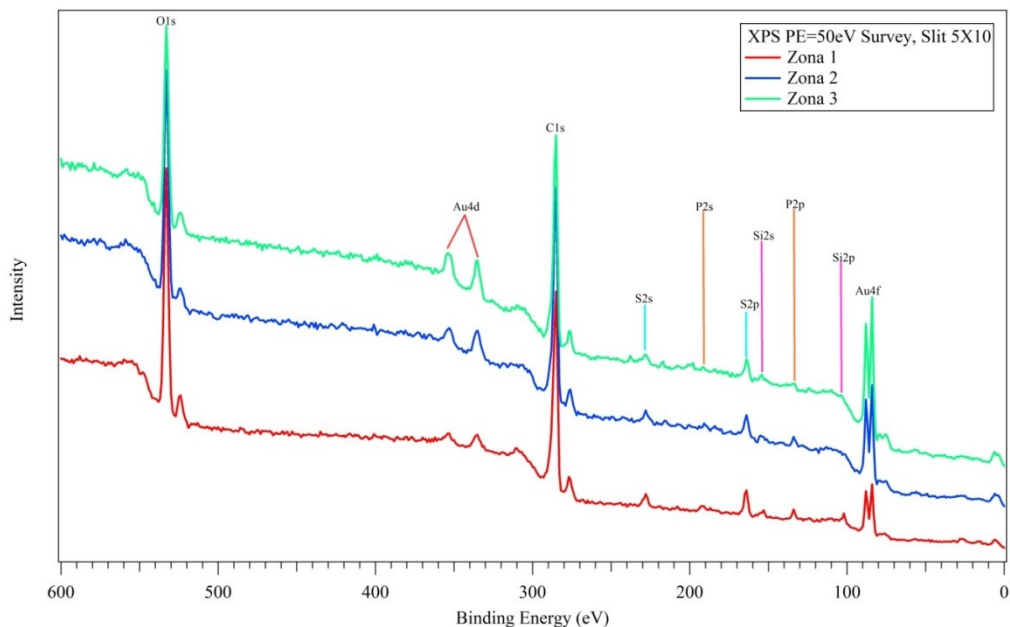


Figure 6. XPS survey spectra with partial attribution of peaks.

Quantitative analysis determined atomic composition of three zones of sample surface and results are presented in Table 1. The ratio between elements and theoretical values calculated for ideal monomers (**1:2**) ratio 1:8 is presented in Table 2 for all three zones. This data confirm lack of other elements on the surface apart of C, O, P, S and Au and show lack of homogeneity of surface coverage, in line with naked eye observations, expressed in differences in stoichiometry.

Table 1. Atomic composition of sample in all three zones.

Atomic composition on sample surface					
	%C	%O	%P	%S	%Au
ZONA 1	68.1	23.5	2.1	4.7	1.5
ZONA 2	69.0	21.8	1.7	4.5	2.9
ZONA 3	70.7	20.2	2.5	2.6	3.9

Table 2. Ratio between elements calculated for ideal monomers (**1:2**) ratio 1:8.

	theoretical	Zone 1	Zone 2	Zone 3
C/O	2.9	2.9	3.2	3.5
C/P	34.7	31.7	40.1	27.8
C/S	15.4	14.3	15.2	26.8
S/P	2.2	2.2	2.6	1.0

Zone 1 seems to be completely covered by copolymer due to black colour of surface. Indeed copolymer provides good coverage and molar ratio between monomers **1** and **2**, as evaluated from ratios between C/P, C/S and S/P, are close to theoretical values. In zone 2 the coverage seems to be partial, and data confirm it, as percentage of Au in respect to C is much bigger than for zone 1. Bigger values of ratios between C/P, C/S and S/P also suggest that ratio between monomers **1** and **2** is higher than in previous case in favour of **2**. Instead in case of zone 3, which seems to be transparent, ratio between Au/C (Table 1) is the biggest from all zones, yet all elements are present on the surface. Ratios between elements suggest much higher percentage of monomer **1** in this area than in other two. At this moment we are not able to explain differences in coverage thickness and composition of the copolymer.

The OECT device consists of two electrodes from semiconductor deposited on an insulating surface immersed in an analyte solution. Therefore for our purposes we need to electropolymerize mixture of monomers **1** and **2** on glass surface in controlled manner. It is challenging task, as electropolymerization can be only carried on metallic conductors. Proper OECT device require only drain-source electrode functionalized with host molecules, as gate electrode does not interact with solutions. Our idea was to deposit only one electrode consisting of **PEDOT-cav** by electropolymerization, and gate electrode would be later one deposited next to it, as described earlier. New drain-source electrode might arise during polymerization between two gold electrodes, if distance between

them would not be too big. Later both gold electrodes could be erased from glass surface leaving **PEDOT-cav** deposited on the surface.

Unfortunately, this approach was not successful. We were able to cover glass between electrodes, when we ran electropolymerization with only **2**, but experiment repeated in the same conditions in mixture of **1** and **2** in 1:8 ratio, just like before on gold disc, was not successful. Decreasing distance between gold lines was not possible, as it would cause many problems during removing of gold, and amount of semiconductor would be probably too small for stable functioning.

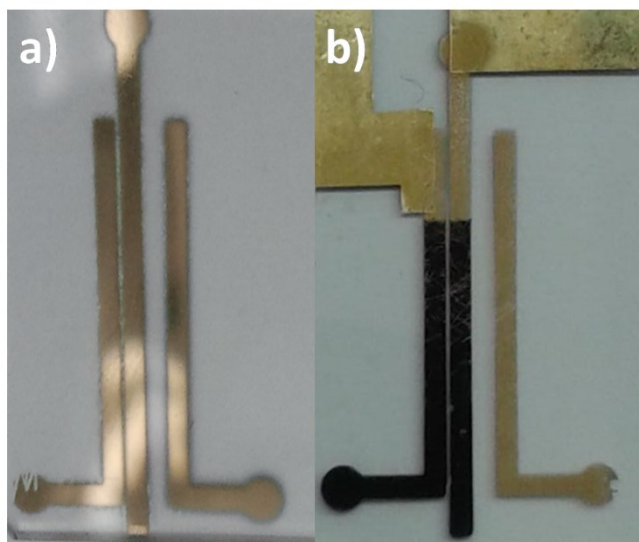


Figure 7. Gold electrodes on glass before (a) and after (b) electropolymerization.

### 7.3. Conclusions

We were able to functionalize EDOT with tetraphosphonate cavitands and at the same time avoid strong non specific interactions. Reactivity of methyl ester EDOT derivative, as well as of receptor functionalized molecule, in the course of electropolymerization was shown to be lower than of simple EDOT, requiring much higher polymerization potential, which can also lead to some kind of degradation of formed polymer in case of pristine material.

We were able to cover gold surface with layer of functionalized PEDOT in good stoichiometric ratio between monomers by cyclic voltammetry and this

was confirmed by XPS experiments. Unfortunately device cannot be fabricated with use of conducting support because all electric current should run through gold due to lack of energy barrier in this material. Change of geometry of the device did not solve the problem.

## 7.4. Experimental section

**General:** All commercial reagents were ACS reagent grade and used as received. Solvents were dried and distilled using standard procedures.  $^1\text{H}$  NMR spectra were recorded on Bruker Avance 400 (400MHz) and Bruker Avance 300 (300 MHz) NMR spectrometers. All chemical shifts ( $\delta$ ) were reported in parts per million (ppm) relative to proton resonances resulting from incomplete deuteration of NMR solvents. ESI-MS experiments were performed on a Waters ZMD spectrometer equipped with an electrospray interface. Monohydroxy footed cavitand was prepared according to literature procedure.<sup>28</sup>

**Tetraphosphonate cavitand EDOT ester, 1:** In an oven-dried 25-mL two-necked round-bottomed flask purged with Ar, a solution of 2,3-dihydrothieno[3,4-*b*][1,4]dioxine-2-carboxylic acid (10 mg, 0.054 mmol, 1 eq.), DMAP (1 mg, 0.008 mmol, 0.15 eq.) and monohydroxy footed tetraphosphonate cavitand (66 mg, 0.054 mmol, 1 eq.) in dry  $\text{CH}_2\text{Cl}_2$  (10 mL) was placed at  $0^\circ\text{C}$ . After 10 min DCC (11 mg, 0.054 mmol, 1 eq.) was added and reaction was stirred for 3 h at room temperature until complete disappearance of **3** by TLC (9:1 DCM:MeOH). White precipitate (urea) was filtrated off and liquid phase, diluted with 20 mL of DCM, was washed twice with 0.5 M aqueous HCl (15 mL), once with  $\text{NaHCO}_3$  saturated  $\text{H}_2\text{O}$  solution (15 mL) and evaporated *in vacuo*. Column chromatography (DCM/MeOH 1:1, 2%  $\text{CH}_3\text{COOH}$ ), followed by evaporation, solubilization in DCM and filtration off silica provided product (45 mg, 60%).

ESI-MS: calc.  $\text{C}_{75}\text{H}_{71}\text{O}_{16}\text{P}_4\text{SNa}$ =1407.3,  $[\text{M}+\text{Na}]^+$   $m/z$ =1407.4.

$^1\text{H}$  NMR (400 MHz,  $\text{CDCl}_3$ , 298 K): 8.07 (m, 8H, PAr-H), 7.67 (t,  $J$ = 6.9 Hz, 4H, PAr-H), 7.56 (m, 8H, PAr-H), 7.28-7.22 (m, 4H, Ar-H), 6.42 (d,  $J$ = 3.6 Hz, 1H, Th), 6.21 (d,  $J$ = 3.6 Hz, 1H, Th), 4.90-4.70 (m, 5H,  $\text{Ar}_3\text{-CH}$ , O-CH), 4.40 (m, 1H, O- $\text{CH}_2$ ), 4.29 (m, 1H, O- $\text{CH}_2$ ), 2.35 (m, 8H,  $\text{CH}_2$ ), 2.18 (s, 9H, Ar- $\text{CH}_3$ ), 2.11 (s, 3H, Ar- $\text{CH}_3$ ), 1.90 (bs, 4H,  $\text{CH}_2$ ), 1.77 (m, 2H,  $\text{CH}_2$ ), 1.43 (m, 6H,  $\text{CH}_2$ ), 1.43 (t,  $J$ = 7.2 Hz, 9H,  $\text{CH}_3$ ).

$^{31}\text{P}$  NMR (160 MHz,  $\text{CDCl}_3$ , 298 K): 8.86 (s, 1P), 8.04 (s, 3P).

**Methyl 2,3-Dihydrothieno[3,4-*b*][1,4]dioxine-2-ester, 2:** To a round-bottomed flask, equipped with Dean-Stark, charged with solution of 2,3-dihydrothieno[3,4-*b*][1,4]dioxine-2-carboxylic acid ( 50 mg, 0.269 mmol, 1 eq.) in toluene (20 mL), MeOH (0.11 mL, 2.688 mmol, 10 eq.) and 3 drops of 12 M HCl were added at room temperature. The reaction was stirred for 3 h at 130°C and then cool down to room temperature. The resulting solution was evaporated, residue solubilized in DCM (15 mL) and washed with H<sub>2</sub>O triple (3x15 mL). The organic phase was run through short plug silica and washed with DCM affording 47 mg (86%) of pure product.

ESI-MS: calc. C<sub>8</sub>H<sub>8</sub>O<sub>4</sub>SNa=223.2, [M+Na]<sup>+</sup> m/z=222.9.

<sup>1</sup>H NMR (400 MHz, CDCl<sub>3</sub>, 298 K): 6.46 (d, *J*= 4.8 Hz, 1H, Th), 6.36 (d, *J*= 4.8 Hz, 1H, Th), 4.79 (t, *J*= 5.2 Hz, 1H, O-CH), 4.35 (d, *J*= 5.0 Hz, 2H, O-CH<sub>2</sub>), 3.82 (s, 3H, CH<sub>3</sub>).

**Fabrication of the OECT device:** The apparatus used for ink-jet printing is based on X, Y, Z servo motors controlled by a computer and an automatic micro-syringe providing a reduced solution flow up to 1 μl/min. While X and Y axes are used to draw the devices the Z axis is used to position the needle of the syringe at right distance respect to the glass slides. A motion-controlling program (Motion Assistant, National Instruments) is used to implement the movements of the three axes and to draw the devices. The combination of needle size, flow rate and solution/substrate wettability determines the smallest line width; to obtain large size lines we performed multiple passages of the needle one close to the other. In the present case the typical thickness of a single passage line is between 150 and 200 μm. The drain–source electrode is made with one or at least two overlapped passages to increase the conductivity if needed. The gate electrode width was about 0.8–1 mm corresponding to 6 adjacent lines. The distance between the two electrodes is about 250 μm. The inset in Fig. 1 shows a picture of the final result. The optimal adhesion of the polymer to the glass slide is maximized controlling the glass surface properties in terms of wettability and roughness and optimizing the drawing speed and the flux of the polymeric solution. It is important to have optimal adhesion to prevent the detachment of the polymer due to the mechanical stress when the solution is inserted in the vessel or removed from it. The last step is a curing treatment at 150 °C in oven for 2 h. Finally all the devices are characterized in terms of their electrodes resistance.

A vessel made of PDMS is attached to the glass slide to create a water resistant chamber containing the electrolyte solution in contact to the



electrodes. The geometry of the vessel was designed to maximize the exposure of the electrodes to the solution and their sensitivity. A homemade Labview (National Instruments) program was written to pilot the two electrometers (Keithley 2400 and Keithley 6417) used to apply the voltage and to read the current at the electrodes. Typically the drain–source current modulation was collected at different gate voltages applied, to obtain a kinetic curve. The potential applied to the drain electrode was set negative (-0.1 V) and was kept constant during the experiment. The potential applied to the gate was set positive and was increased during the experiment from 0 up to 0.5 V with steps of 0.1 V amplitude and 150 s period. The gate is turned off for the same period of time before each increasing step.

**Cyclic voltammetry:** Experiments were carried using Autolab PG Stat 20 or  $\mu$ Autolab 3 Type 3, both produced by EcoChemi Utrecht, Netherlands, both equipped with polarographic head Merolm 663 VA Stand and customised software GPES (General Purpose Electropolymerization Software).

## 7.5. Acknowledgements

We would like to thank Prof. Salvatore Iannotta from IMEM CNR Parma and Dr. Tullio Toccoli from IMEM CNR Trento for developing this project together. Dr. Toccoli and Elisa Borga are acknowledged for formation of device and measurements of its properties. Also we would like to thank Dr. Marco Giannetto for the use of electropolymerization facilities and help with the experiments. Centro Interdipartimentale Misure “G. Casnati” of the University of Parma is acknowledged for the use of NMR and HR ESI-MS facilities.

## 7.6. References and Notes

1. R. Capelli, S. Toffanin, G. Generali, H. Usta, A. Facchetti, M. Muccini, *Nat. Mat.* **2010**, *9*, 496-503.
2. J.-H. Jou, C.-P. Wang, M.-H. Wu, H.-W. Lin, H. C. Pan, B.-H. Liu, *J. Mat. Chem.* **2010**, *20*, 6626-6629.
3. B. P. Rand, J. Genoe, P. Heremans, J. Poortmans, *Prog. Photovolt: Res. Appl.* **2007**, *15*, 659-676.
4. J. T. Mabeck, G. G. Malliaras, *Anal. Bioanal. Chem.* **2006**, *384*, 343-353.
5. L. Torsi, A. Dodabalapur, *Anal. Chem.* **2005**, 381-387.

6. C. D. Dimitrakopoulos, P. R. L. Malenfant, *Adv. Mater.* **2002**, *14*, 99-117
7. L. Torsi, M. Magliulo, K. Manoli, G. Palazzo *Chem. Soc. Rev.* **2013**, *42*, 8612-8628.
8. R. M. Owens, G. G. Malliaras, *MRS Bull.* **2010**, *35*, 449-456.
9. G. Mattana, P. Cosseddu, B. Fraboni, G. G. Malliaras, J. P. Hinstroza, A. Bonfiglio, *Org. Electron.* **2011**, *12*, 2033-2039.
10. M. Hamedi, R. Forchheimer, O. Inganas, *Nat. Mater.* **2007**, *6*, 357-362.
11. P. Lin, F. Yan, *Adv. Mater.* **2012**, *24*, 34-51.
12. H. S. White, G. P. Kittlesen, M. S. Wrighton, *J. Am. Chem. Soc.* **1984**, *106*, 5375-5377.
13. V. Subramanian, J. Chang, and F. Liao, in *Applications of Organic and Printed Electronics*, ed. E. Cantatore, Springer, US, Boston, MA, **2013**, pp. 157-177.
14. D. Khodagholy, T. Doublet, P. Quilichini, M. Gurfinkel, P. Leleux, A. Ghestem, E. Ismailova, T. Herve, S. Sanaur, C. Bernard, G. G. Malliaras, *Nat. Commun.* **2013**, *4*, 1575.
15. M. Irimia-Vladu *Chem. Soc. Rev.* **2014**, *43*, 588-610.
16. D. J. Macaya, M. Nikolou, S. Takamatsu, J. T. Mabeck, R. M. Owens, G. G. Malliaras, *Sens. Actuators B*, **2007**, *123*, 374-378.
17. G. Tant, F. Yan, P. Lin, J. Xu, H. L. W. Chan, *Adv. Funct. Mat.* **2011**, *21*, 2264-2272.
18. L. Torsi, G.M. Farinola, M. C. Tanese, O. Hassan Omar, L. Valli, F. Babudri, F. Palmisano, P. G. Zambonin, F. Naso, *Nat. Mat.* **2008**, *7*, 412-417.
19. M.-J. Spijkman, J. J. Brondijk, T. C. T. Geuns, E. C. P. Smits, T. Cramer, F. Zerbetto, P. Stolar, F. Biscarini, P. W. M. Blom, D. M. de Leeuw, *Adv. Funct. Mat.* **2010**, *20*, 898-905.
20. K. J. Fräsera, S. Y. Yangb, F. Cicoira, V. F. Curtoa, R. Byrnea, F. Benito-Lopez, D. Khodagholyd, R. M. Owensd, G. G. Malliaras, D. Diamond, *Chem. Comm.* **2010**, *46*, 7972-7974.

21. E. Biavardi, C. Tudisco, F. Maffei, A. Motta, C. Massera, G. G. Condorelli, E. Dalcanale *Proc. Natl. Acad. Sci. U.S.A.* **2012**, *109*, 2263–2268.
22. F. Maffei, P. Betti, D. Genovese, M. Montalti, L. Prodi, R. De Zorzi, S. Geremia, E. Dalcanale *Angew. Chem. Int. Ed.* **2011**, *50*, 4654–4657.
23. G.G. Condorelli, A. Motta, M. Favazza, E. Gurrieri, P. Betti, E. Dalcanale *Chem. Commun.* **2010**, *46*, 288–290.
24. R. Pinalli, E. Dalcanale *Acc. Chem. Res.* **2013**, *46*, 399–411.
25. M. Vázquez, J. Bobacka, M. Luostarinen, K. Rissanen, A. Lewenstam, A. Ivaska *J. Solid State Electrochem.* **2005**, 312–319.
26. D. A. Bernards, G. G. Malliaras, *Adv. Funct. Mater.* **2007**, *17*, 3538–3544
27. T. Toccoli, E. Borga, H. Blond, D. Maniglio, L. Minati, C. Fasoli, M. Pola, C. Corradi, S. Iannotta, *Org. Electron.*, **2012**, *13*, 1716–1721.
28. F. Tancini, D. Genovese, M. Montalti, L. Cristofolini, L. Nasi, L. Prodi, E. Dalcanale, *J. Am. Chem. Soc.* **2010**, *132*, 4781–4789.



# ***Appendix A***

## ***Additional information for***

### ***Ch. 3***

*NMR spectra*

Appendix A

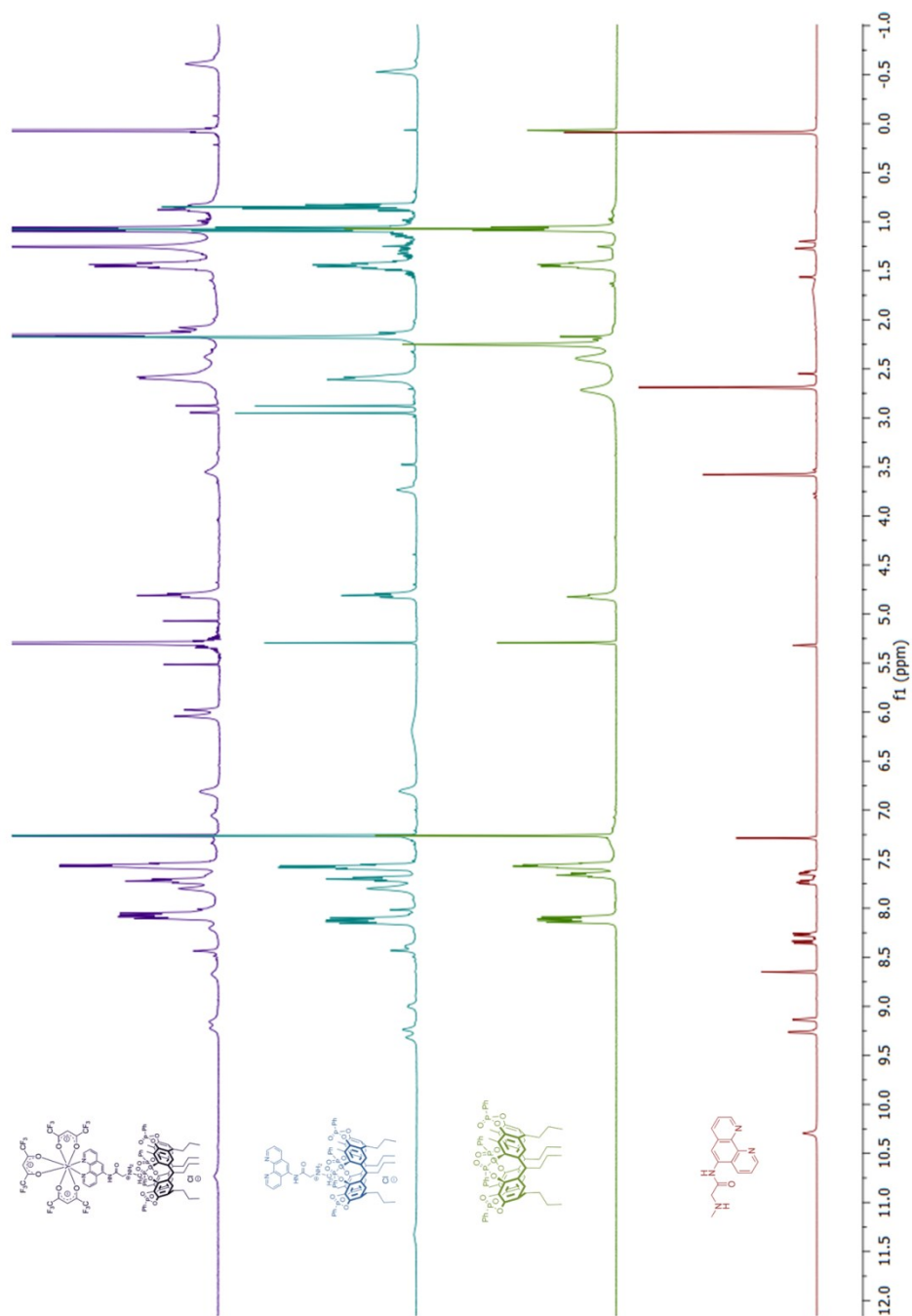


Fig. S1.  $^1\text{H}$  NMR of **1**, **Ti(III)-A**, **Ti(III)-A•1** and **Ti(III)-A•1•3** formation in  $\text{CDCl}_3$ .

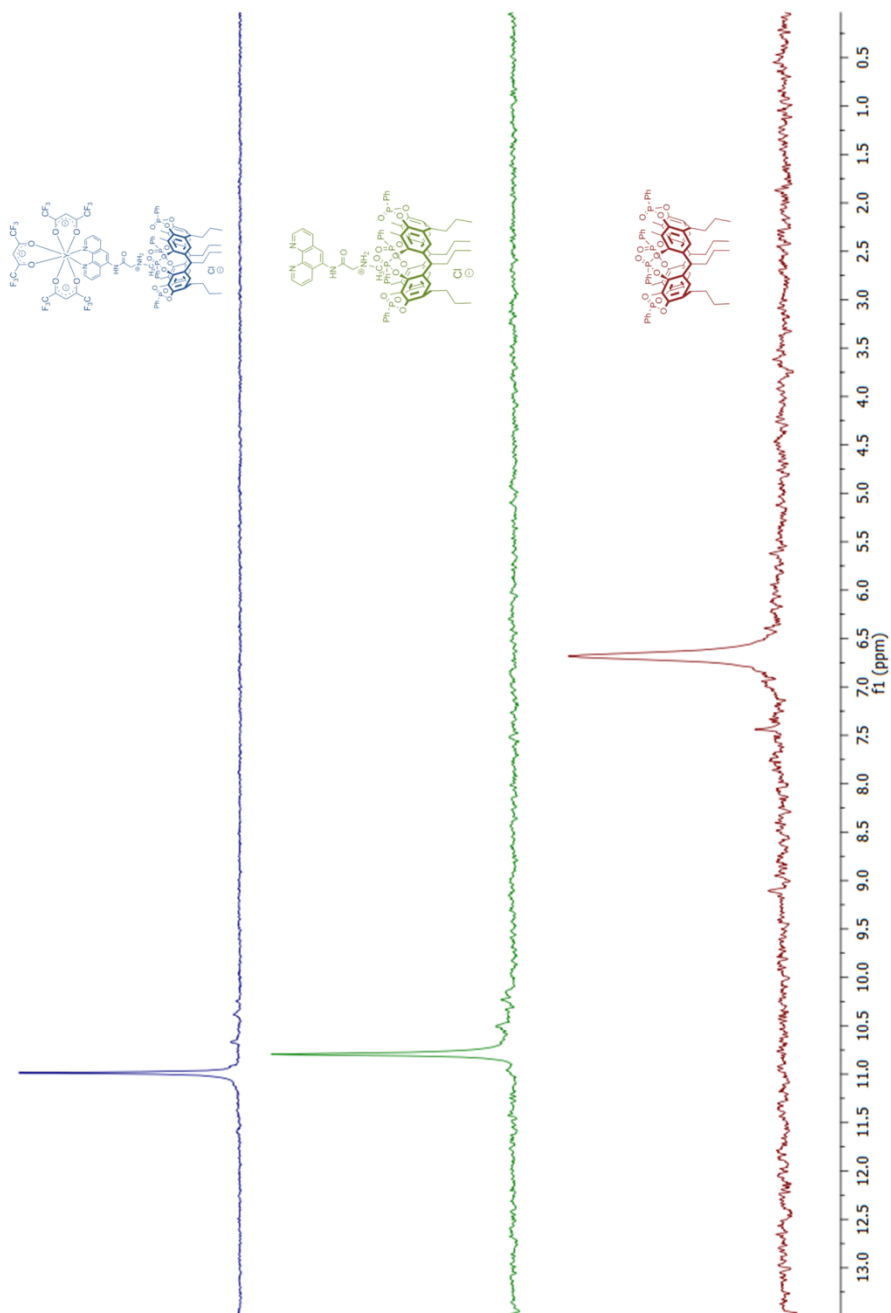


Fig. S2.  $^{31}\text{P}$  NMR of **Ti(III)-A**, **Ti(III)-A•1** and **Ti(III)-A•1•3** formation in  $\text{CDCl}_3$ .

Appendix A

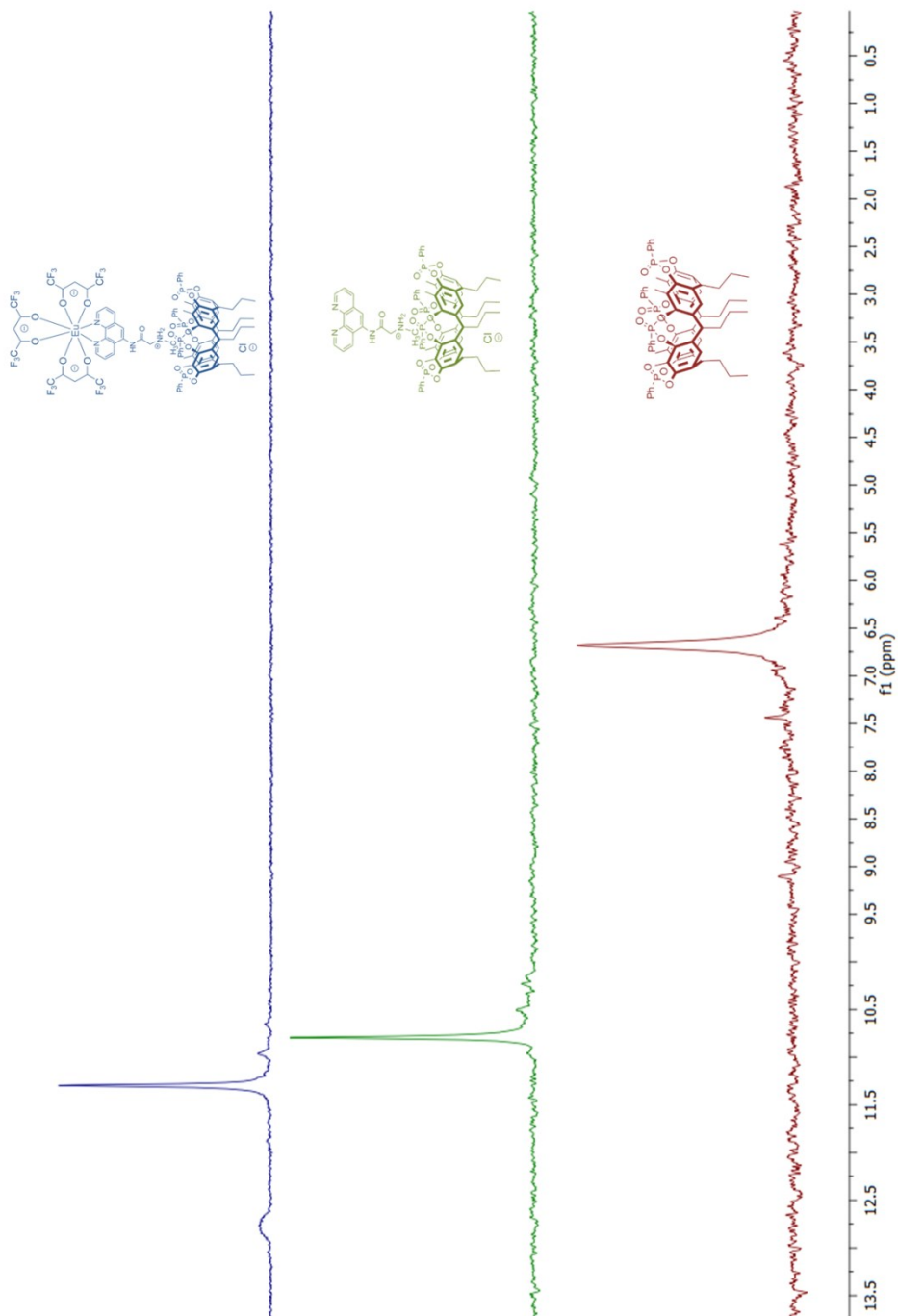


Fig. S3.  $^{31}\text{P}$  NMR of **TiIII-A**, **TiIII-A•1** and **TiIII-A•1•2** changes in  $\text{CDCl}_3$ .



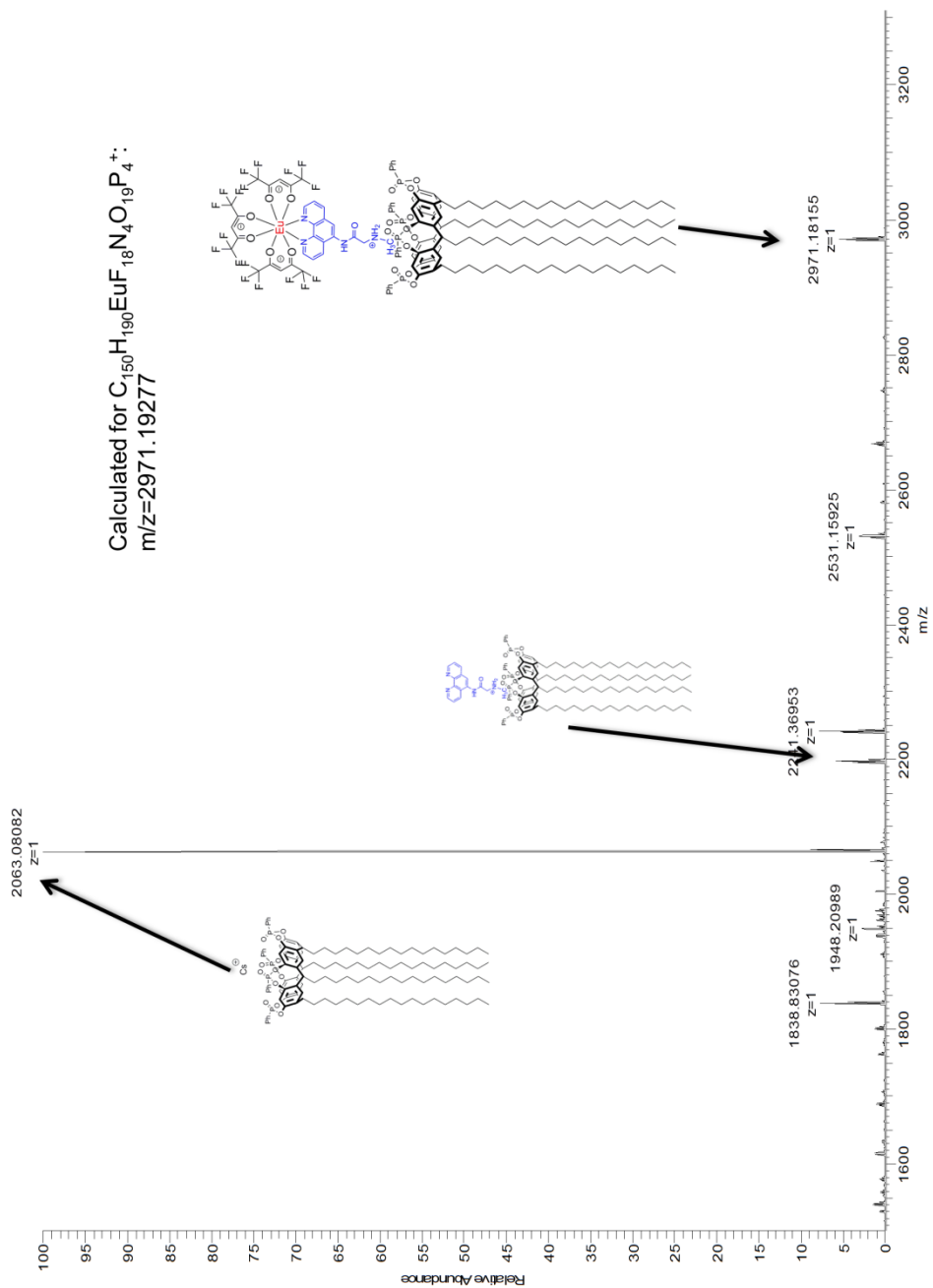


Fig. S4. HR-MS spectra of Tiii-C•1•2.

## Photochemical measurements in solution

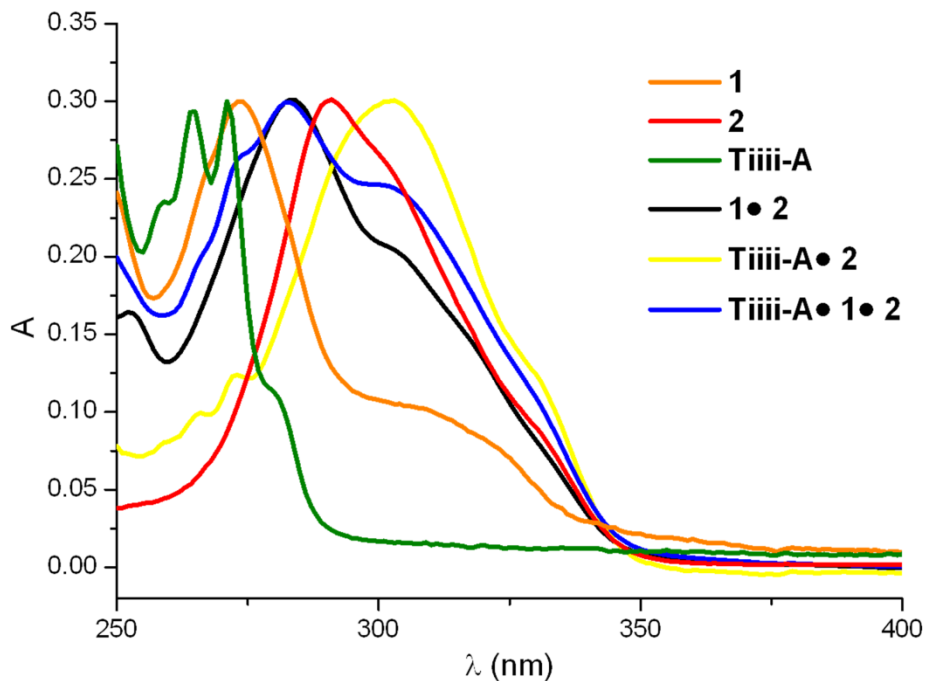


Fig. S5. Normalized absorption spectra\* of europium derivatives in dichloromethane.

\*Absorption spectra were normalized because limited solubility unabled quantitative measurement of extinction coefficient values.

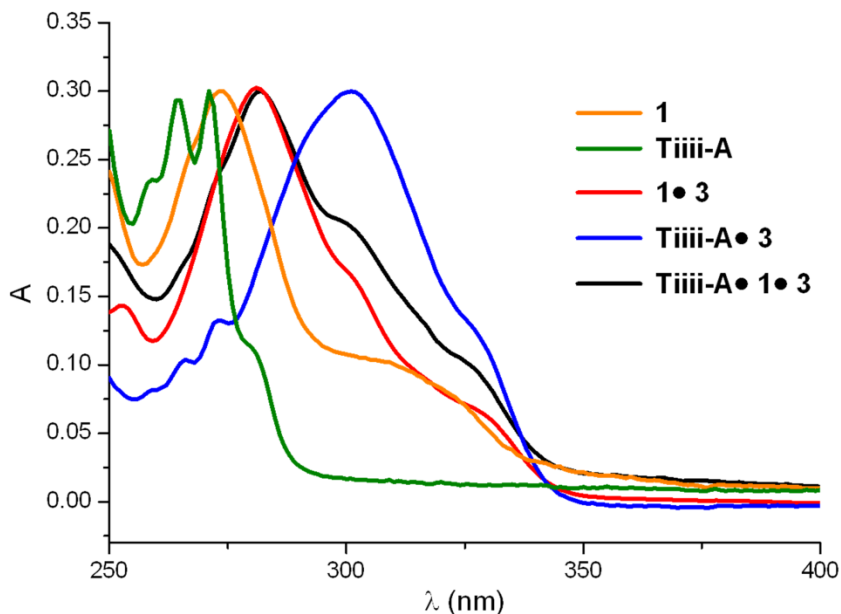


Fig. S6. Normalized absorption spectra\* of yttrium derivatives in dichloromethane.

\*Absorption spectra were normalized because limited solubility unabled quantitative measurement of extinction coefficient values.

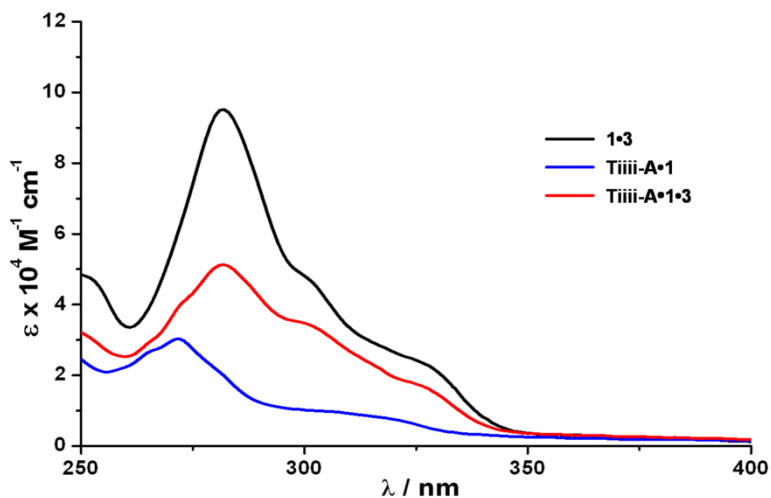


Fig. S7. Absorption spectra of yttrium complexes in dichloromethane.

## XPS analysis

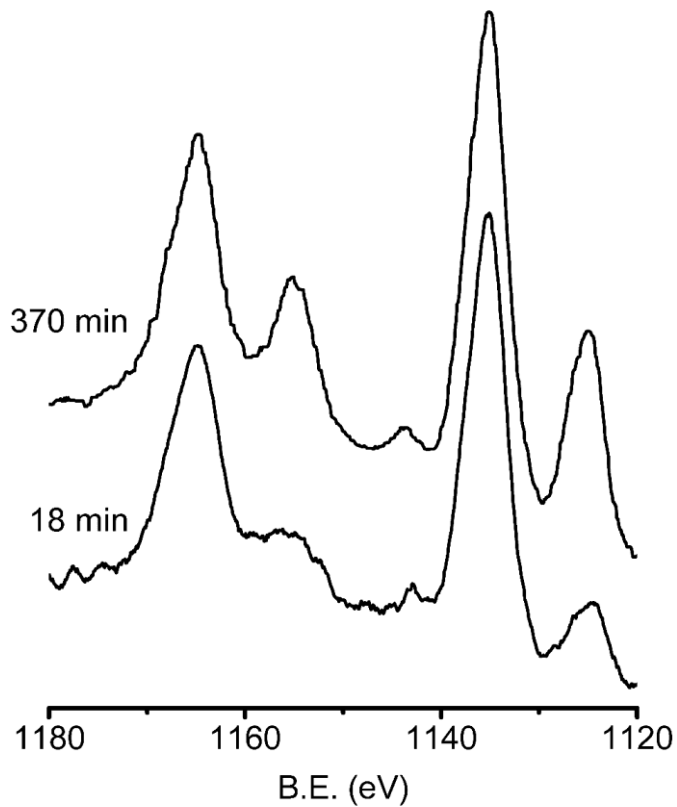


Fig S8. Eu 3d XPS region of **Si-Ti<sub>iii</sub>-B•1•2** after 18 minutes (upper spectra) and 370 minutes (bottom spectra) of acquisition time.



# *Curriculum*

## *Vitae*

- 30/12/1985 Born, Lublin, Poland.
- 06/2004 Maria Skłodowska-Curie High School  
N° 5, Lublin, Poland.
- 07/2009 Master in Chemistry, Specialist in  
Chemistry, Military University of  
Technology, Warsaw, Poland.
- 09/2006-05/2007 Student exchange program, University  
of Oulu, Oulu, Finland.
- 01/2010-12/2010 Post-Graduate Research, University of  
Parma, Italy. Advisor: Prof. E.  
Dalcanale.
- 01/2011-12/2013 Doctoral Research with Prof. E.  
Dalcanale University of Parma, Italy.
- 09/2011 Research Exchange with Prof. K.  
Neyts, University of Ghent, Ghent,  
Belgium.
- 02/2013-07/2013 Research Exchange with Prof. D.  
Bonifazi, University of Namur, Namur,  
Belgium

Parma, January 2014

*Kasjan Misztal*



## Acknowledgements

*Here we are, in the end of my stay in Dalcanale's group. These were amazing four years, I think the most intense years in my life, which taught me more than I could imagine and which offered me even more possibilities.*

*Oczywiście nie było by to możliwe bez wsparcia moich rodziców, za co jestem Wam bardzo wdzięczny. Zawsze mogę na Was liczyć, i bardzo Wam za to dziękuję. Też was kocham!*

*Inna, Tobie też dziękuję za wsparcie i miłość, którymi mnie obdarzasz każdego dnia. I za znoszenie trudów pisania tej pracy i za cały wkład w jej ulepszanie.*

*This whole adventure started over 4 years ago and I am very happy that I could do it. And even more I am pleased with the outcome. Of course it would not be possible, if not faith of few people in me, this mentioned above and below, and their time devoted for me. I learnt a lot, I had a lot of fun, I got new friends and I really enjoyed it!*

*So it all wouldn't be possible without capo, and I would like to thank Professor Enrico Dalcanale for giving me opportunity to spend these amazing four years in his group; for faith, that person with such a background like mine can succeed in organic synthesis and supramolecular chemistry. I hope hopes did not rest unfilled. I am also very grateful for his enthusiasm which I could see in everyday life and faith in projects against all odds.*

*I would like to thank all my lab mates who influenced my life in the lab and outside, introducing me to the Italian style of life. Sarto for guiding me in my first months, showing me good way of doing science, teaching Italian during making column and helping in hard times ;) Marco, who knows about chemists, dead or alive, and their reactions, constantly believe in Milan and taught me "most important words" in Italian. Daniela, who is either happy, laughing loudly, or in panic, running around with word on "c" on her mouth. And who helped me a LOOOOOT with Italian bureaucracy and took me to the first parties here. I still owe you a dinner. Federico, who took my social life to the next level and had advices regarding everything. Kuba who always know which application we need to fill, where to send it and till when. And for possibility to speak Polish every day (in the end more Polenglish with some Italian words ;) ) Daniele for constant laugh and non te ne frega. Ely, master of Office and Photoshop, for good advices and help. Robby for all the sweets and advices. Tahnee for*

*constant will to teach me some French. Pedros, my first student (Fede, calm down ☺), for constant interest in chemistry. Bedini, our best salumiere ever. Veronica for laugh and smile from “dusk till dawn”. Maffy for super dinners! I would like to thank also the others who passed through the lab these last four years and made my stay better: Guiduz, Monica, Giulia, Sonia, Sanna, Alfonso, Riccardo, and others, which I probably missed, due to haste ☺*

*I would also like to thank people who spent time with me within FINELUMEN and made progress meetings not only presentations and “science talks”. Thanks to Federica, Bea, Nitin, Joanna, Oksana, Suraj, and Anand.*

*And of course I would like to thank Professor Davide Bonifazi for giving me opportunity to stay in his group for half a year, doing interesting chemistry. Of course my stay there would not be so nice without people which I met there, especially Federica, Silvia, Laurie-Ellie, Irene, Dario and Dima.*

*THANK YOU ALL once again!!!*

*To już jest koniec, nie ma już nic!  
Jesteśmy wolni, możemy już iść...*

*Kasjan*